AN EXPERIMENTAL STUDY INTO THE IGNITION OF METHANE AND ETHANE BLENDS IN A NEW SHOCK-TUBE FACILITY

A Thesis

by

CHRISTOPHER JOSEPH ERIK AUL

Submitted to the Office of Graduate Studies of
Texas A&M University
in partial fulfillment of the requirements for the degree of

MASTER OF SCIENCE

December 2009

Major Subject: Mechanical Engineering

AN EXPERIMENTAL STUDY INTO THE IGNITION OF METHANE AND ETHANE BLENDS IN A NEW SHOCK-TUBE FACILITY

A Thesis

by

CHRISTOPHER JOSEPH ERIK AUL

Submitted to the Office of Graduate Studies of
Texas A&M University
in partial fulfillment of the requirements for the degree of

MASTER OF SCIENCE

Approved by:

Chair of Committee,	Eric Petersen
Committee Members,	Kalyan Annamalai
	Kenneth Hall
Head of Department,	Dennis O'Neal

December 2009

Major Subject: Mechanical Engineering

ABSTRACT

An Experimental Study into the Ignition of Methane and Ethane Blends in a New Shock-Tube Facility. (December 2009)

Christopher Joseph Erik Aul, B.S., University of Central Florida

Chair of Advisory Committee: Dr. Eric L. Petersen

A new shock tube targeting low temperature, high pressure, and long test times was designed and installed at the Turbomachinery Laboratory in December of 2008. The single-pulse shock tube uses either lexan diaphragms or die-scored aluminum disks of up to 4 mm in thickness. The modular design of the tube allows for optimum operation over a large range of thermodynamic conditions from 1 to 100 atm and between 600-4000 K behind the reflected shock wave. The new facility allows for ignition delay time, chemical kinetics, high-temperature spectroscopy, vaporization, atomization, and solid particulate experiments.

An example series of ignition delay time experiments was made on mixtures of $CH_4/C_2H_6/O_2/Ar$ at pressures from 1 to 30.7 atm, intermediate temperatures from 1082 to 2248 K, varying dilutions (between 75 and 98% diluent), and equivalence ratios ranging from fuel lean (0.5) to fuel rich (2.0) in this new facility. The percentage by volume variation and equivalence ratios for the mixtures studied were chosen to cover a wide parameter space not previously well studied. Results are then used to validate and improve a detailed kinetics mechanism which models the oxidation and ignition of

methane and other higher order hydrocarbons, through C_4, with interest in further developing reactions important to methane- and ethane-related chemistry.

DEDICATION

I dedicate this work to both my Mother and my Father for all of their support and encouragement. I wouldn't have made it this far without them.

ACKNOWLEDGMENTS

I would like to thank my Advisor and Committee Chair, Dr. Eric Petersen, for all of the help and guidance along the course of my graduate career and this work. I would also like to thank Dr. Kalyan Annamalai and Dr. Kenneth Hall for their involvement on my graduate committee.

I would like to express gratitude toward my fellow colleagues, Jaap de Vries, Brandon Rotavera, Alexander Barrett, and Brian Walker, who have all contributed in a major way to the construction of this facility and the completion of my research. I would also like to thank the National Science Foundation for funding this extensive project. Lastly I would like to acknowledge the help of Nicole Donato for her help with recording some of the final data obtained in this study.

NOMENCLATURE

Variables

A	constant, reaction rate pre-exponential factor, or τ_{ign} correlation constant
E_a	activation energy
k_i	reaction rate coefficient of species i
MW	molecular weight
n	temperature dependence exponent in Arrhenius equation
P	static pressure
R	ideal gas constant (R_u/MW)
R_u	universal gas constant, 8.314 kJ/mol-K
R^2	correlation coefficient
t	time
T	static temperature
x	τ_{ign} correlation constant, fuel concentration exponent
y	τ_{ign} correlation constant, oxygen concentration exponent
ϕ	equivalence ratio
τ_{ign}	ignition delay time
[A]	concentration of some species A, $X_A P/RT$

Subscripts

1	driven section of shock tube at t = 0
2	behind the incident shock wave

3	behind contact surface and expansion wave in driver section
4	driver section at time zero
5	behind the reflected shock wave

Abbreviations

BP	backing pump for driven section
DP	driver pump for driver section
GRI	Gas Research Institute
NTC	negative temperature coefficient
PT	pressure transducer
RCM	rapid compression machine
RMS	root-mean square
RP	roughing pump for driven section
TP	turbomolecular pump for driven section

TABLE OF CONTENTS

Page

LIST OF FIGURES

Page

Page

Page

LIST OF TABLES

Page

CHAPTER I

INTRODUCTION

Combustion makes up a large portion of the way we generate energy sources for use in various fields of science and industry. In 2008, almost 80% of our energy usage in the residential, commercial, industrial, and transportation industries came from combustion-related sources (Energy Information Administration, 2008). With nuclear and renewable sources of energy production seeing signs of only mild growth and increasing demand for cleaner-burning technology, it is imperative to have a detailed understanding of the fuels we'll be using well into the future.

Reaction physics has been heavily researched over the past few decades although there still exists a need for study of particular fuels at conditions similar to those found in engines in use today. Turbines for use in both aerospace propulsion and land-based power generation possess combustors which can see pressures of 20 atm and higher, a significant design consideration. Interests in fuel flexibility and reduction of harmful emissions also add complexity to the design process when looking at different fuel sources available.

High-pressure reaction chemistry in a laboratory setting can be facilitated by an experiment called a shock tube. By analyzing the production and depletion of various species in the reaction zone behind the reflected-shock region found in the shock tube it

---

This thesis follows the style of *Combustion Science and Technology*.

is possible to quantify and effectively model similar reactions in traditional applications. Reaction rates and spectroscopic data resolved from the shock-tube experiment are used to validate complex chemical kinetics mechanisms which are then used in the design and understanding of all combustion-related outlets.

Measurements in a Shock Tube

Figure 1 shows a typical pressure-driven shock tube and an associated x-t diagram which shows regions of interest numerated with commonplace nomenclature (Gayden and Hurle, 1963). Rupture of a diaphragm introduces a shock wave that propagates through a given medium of interest, usually a fuel and oxidizer mixture, at some initial pressure (P_1) and temperature (T_1). The step increase in temperature and pressure (T_2, P_2) behind the incident shock wave are further compounded by the shock wave which is reflected from the endwall region of the shock tube (T_5, P_5). It is within this region 5 where conditions are quiescent, and reaction of the driven gas is allowed to take place. The arrival of an expansion wave from the diaphragm rupture or interaction of the reflected shock with the contact surface causes a decrease in pressure which ends the time of relatively constant thermodynamic properties.

For the test mixture under study, the driver medium and initial conditions all play a pivotal role in the formation of the exact dynamics behind each shock. In **Figure 1**, the interaction of the reflected shock and the fast-approaching contact surface, as well as the arrival of the expansion wave, can be fine tuned to exhibit a desired test time. It is often an experimental imperative to cover a broad range of available conditions when designing such a facility; this has been taken under consideration through the bulk of this

work. As necessary, work with colder reaction zones (T < 1000K) can present unique challenges as ignition times increase with decreasing temperature.

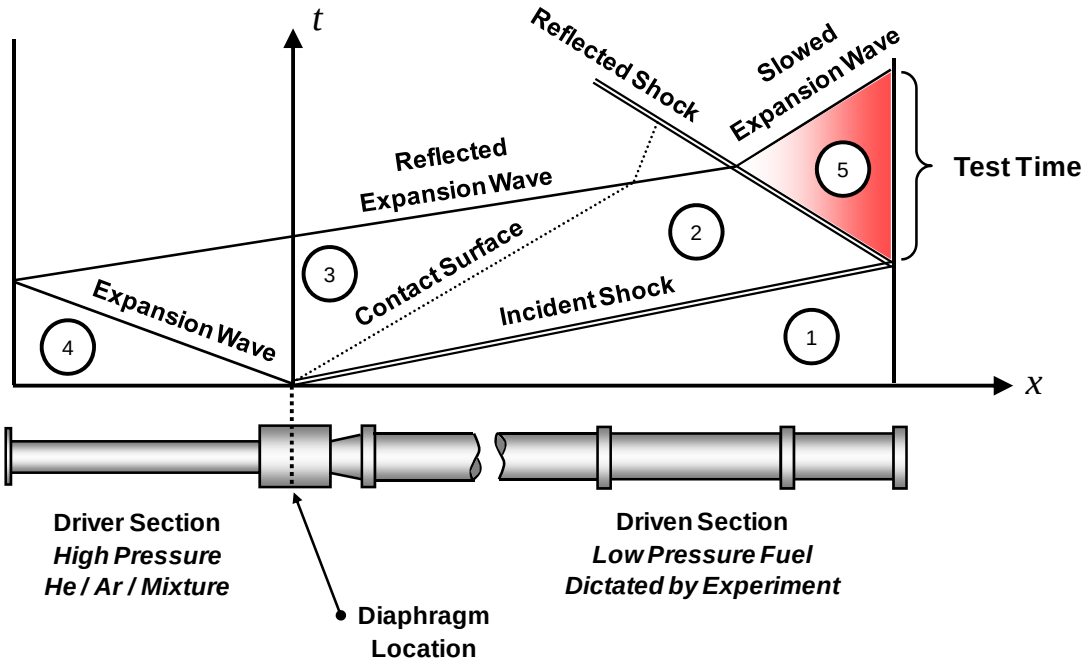

Figure 1. Shock-tube diagram outlining traditional gas dynamic effects

Given the relatively short time period behind the reflected shock wave, on the order of a few milliseconds, it is necessary to utilize diagnostics with quick response times to accurately catch the fast-acting dynamics of the shock-tube experiment. Along with appropriate measurement techniques, a keen understanding of the nonideal gas dynamic effects, such as shock attenuation which can lead to uncertainty in temperature measurement, is required. The severities of such nonideal effects depend heavily on the diameter of the shock tube, mixture accuracy, and the overall measurement time.

Conditions behind the reflected shock are derived from vibrationally equilibrated chemistry and one-dimensional shock relations. For this determination, the input conditions, such as pressure and temperature of the section 1 outlined in **Figure 1**, and the incident shock velocity are needed. P_5 and T_5 are associated with measurements of ignition delay, species profiles, and other unobtrusive diagnostics for reaction analysis.

Methane and Ethane Chemistry

Natural gas, which is mostly comprised of methane, continues to be important for use in propulsion and power generation. Its popularity as well as the applicability of pure methane has been a driver for research of this particular fuel and decades of experiments have taught us a great deal about this seemingly simple hydrocarbon. Ethane, also found within natural gas, has also drawn attention for its tendency for faster reaction when compared with methane. Long since have studies been conducted on mixtures of methane and ethane mirroring compositions typically found in natural gas, with levels of C_2H_6 less than 10%, although there remains to be a lack of autoignition data of methane with increasing levels of ethane.

As mentioned previously the addition of ethane, as well as other higher-order hydrocarbons, tends to speed up ignition, affect emissions, and change flame dynamics. Natural gas components can vary significantly due to location and extraction techniques, but is commonly between 82-96% methane and 1-16% ethane along with smaller levels of higher hydrocarbons (C_3 and greater), hydrogen, and carbon monoxide (Spadaccini and Colket, 1994). Coming from the widespread applicability of natural gas in all forms

of energy consumption, it is necessary to understand the unique characteristics of its reaction at high temperature and pressure.

The drive for the research presented herein is not to better understand natural gas but to thoroughly validate the kinetics of lower-order hydrocarbons as they are fundamental to the combustion of larger hydrocarbons. The chemistry of ethane is studied in this work to understand its role in reaction processes and is not being proposed as a fuel source or alternative to other conventional fuels, such as natural gas. The introduction of methane and ethane and their role in natural gas only serves as a reminder that a majority of the work performed on mixtures of only methane and ethane to this point reflect that of what is found within natural gas sources.

Thesis Organization

This thesis centers around the planning, design, and fabrication of a shock tube capable of reaching the pressures similar to those found in the aforementioned cases. The work detailed herein can be categorized into two distinct parts: 1) Shock-tube construction and 2) methane and ethane chemistry.

Chapter II outlines the shock-tube design and details the specific attributes of the present facility. Capabilities are summarized, and each part of the experiment is explained in detail. It is in this chapter where the adverse and nonideal effects are highlighted as well as how the current design choices help to alleviate such uncertainties. Materials used, equipment chosen, and diagrams of how each part interacts within the whole are described here.

Chapter III gives the approach for an investigation into the reaction of methane and ethane blends with oxygen. A broad parameter space was chosen to cover regions of low, intermediate, and higher pressures; varying stoichiometries; and dilutions. An associated kinetics model is also shown to have areas of needed improvement with such an extensive dataset.

Chapter IV presents the results found for the study outlined in Chapter III. Comparisons to various chemical kinetics models are shown for all cases presented. A correlation for different fuel blend ratios are presented with excellent goodness of fit for all data recorded, which occur well before known negative temperature coefficient (NTC) regimes at lower temperatures.

An overview of the primary findings from this study is presented in Chapter V. Recommendations for future work are also summarized in this chapter. Appendix A catalogues all of the schematics drawn up for the shock tube, including the driver, diaphragm, and driven sections.

CHAPTER II

HIGH-PRESSURE SHOCK-TUBE FACILITY

Fundamental data such as characteristic times and species time histories at practical conditions are invaluable for the improvement and extension of chemical kinetics models to the region of interest for practical applications. The sharply risen interest in fuel flexibility issues concerning land-based power generation gas turbines over the past decade confirms the need for an apparatus capable of testing fundamental combustion properties of a large variety of fuels. Practical concerns among power generation gas turbines include autoignition in premixed systems (de Vries and Petersen, 2007), flash back, blow out, and combustion instability (Lieuwen et al., 2006). Shock tubes are ideal for such measurements and have been utilized extensively in providing measurements of rate coefficients for specific reactions, ignition delay times, and for the validation and improvement of entire mechanisms. Shock-tube ignition data at higher pressures and low-to-intermediate temperatures are scarce but are required for the validation of chemical kinetics models which are, as a consequence, tuned primarily with higher-temperature and lower-pressure data. Ignition data at lower temperatures however require longer test times since the chemistry occurs more slowly.

Amadio et al. have shown that shock-tube test times can be extended by the use of unconventional driver gases, such as CO_2/He mixtures (Amadio et al., 2006). Similar techniques were used for the investigation of automotive fuel blends such as the work by Ciezki and Adomeit (1993), Fieweger et al.(1997), Herzler et al. (2004, 2005), and

Zhukov et al. (2005). From these studies, it is evident that in the lower-temperature regime the ignition behavior often deviates away from linearity when presented on an Arrhenius plot. Such behavior can even lead to NTC behavior as found by Fieweger et al. for n-heptane mixtures (Fieweger et al., 1997). Lower-temperature (< 1000 K), longer test time shock-tube experimental data are relatively sparse especially for gas turbine fuel blends. A more conventional way of measuring the auto-ignition time in this regime is done with rapid compression machines (RCM's). It has been noticed recently that shock-tube experiments can in some cases disagree significantly with RCM data, especially for methane-based fuel blends (Petersen et al., 2009). Numerous suggestions have been given for this disagreement including heat transfer effects, reflected-shock bifurcation with the boundary layer, wall effects, diaphragm particle contaminants, or incident-shock chemical 'priming' prior to reflected shock arrival (Petersen et al., 2007a and Goy et al., 2001). Several experiments have been performed including the usage of schlieren optics and/or high-speed photography (Herzler et al., 2004 and Goy et al., 2001). The facility described herein allows the study of these phenomena with a large (> 15 cm), polished inside diameter which has been specifically designed for these conditions. Optical access throughout the driven section allows for absorption experiments to investigate the incident-wave-induced chemistry.

In addition to ignition delay time measurements in gas-phase mixtures, a shock tube can be utilized for heterogeneous combustion processes and for shock and detonation waves through aerosol-laden mixtures. The near instantly obtained test conditions of temperatures between 600-4000 K and pressures between 1 to 100 atm are

accomplished within a controlled environment. Extended test time conditions allow for lower-temperature experiments and liquid-spray or atomization studies (Rotavera and Petersen, 2007).

Overall Experimental Setup

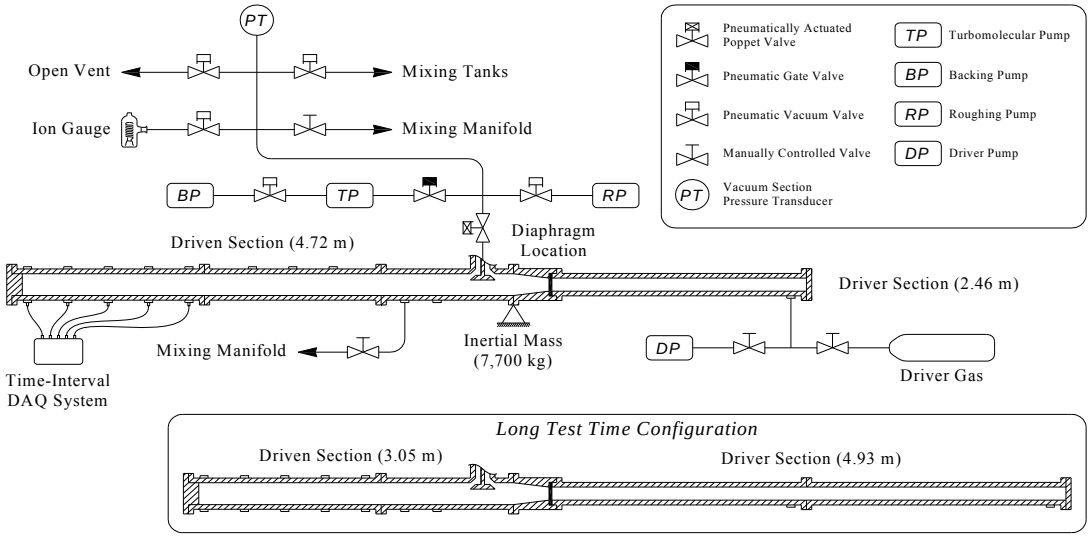

Figure 2. Shock tube facility with two available configurations shown

The total facility consists of the shock-tube hardware, control system, data acquisition system, vacuum section, and the velocity detection system. A schematic of the gas handling and the shock tube in both the conventional and long test time configuration is given in **Figure 2**.

The geometry of the shock tube presented in **Figure 2** can be mapped out according to the diagram shown in **Figure 1**. Region 1 is the driven section of the shock tube before diaphragm rupture. The gas handling system is in place to make accurate mixtures, fill the experiment, and subsequently vacuum down the test region to low pressures between experiments. Region 4 exists in the driver section prior to breaking of the diaphragm. Changing the configuration of the shock tube yields varying gas dynamic effects which enable the experimenter to study longer test times.

The particular configuration where the driver section is lengthened and driven section shortened can delay the arrival of the expansion wave through the driver medium. It is also attractive when long test times are desirable to use a driver medium of specific molecular weight (Amadio et al., 2006).

Figure 2 also shows the presence of a large poppet valve directly after the diaphragm section on the driven side of the experiment which allows for large area access to the shock tube between experiments. This feature enables the quick turnaround of experimental parameters and is precision machined to not affect the formation of the incident shock. The vacuum section is comprised primarily of two pumping systems rated for use at both atmospheric and high-vacuum pressures. The roughing pump (RP) enables reduction of gases at pressures around 1 atm down to the region where the turbo pump (TP) can overtake and continue down to a higher-purity vacuum. Appropriate measurement equipment, such as the pressure transducer and ion gauge shown in **Figure 2**, allow for accurate determination of between-experiment pressure values. A 7700-kg inertial mass is permanently attached to the driven section to minimize shock-induced

vibration of the complete assembly, particularly any displacement in the axial direction. A description of each key component is given herein.

Both the driver and driven sections of the shock tube are made of 304 stainless steel. The driver section has an ID of 7.62 cm with a 1.27-cm wall thickness. The driven section has an ID of 15.24 cm also with a 1.27-cm wall thickness. The inside of the driven section is polished to a surface finish of 1 μm RMS or better. In the conventional configuration, the driver length is 2.46 m, and the driven length is 4.72 m. When long test times are needed for low-temperature experiments, the shock tube can be reconfigured to have a 4.93-m driver section and a 3.05-m driven length. All driven connections are weldless and designed for high pressure, easy removal, and minimum flow/shock perturbations between sections. The design for the driven connection is similar to that described by Petersen et al. (2005) and is detailed in both **Figure 3** and **Figure 4**.

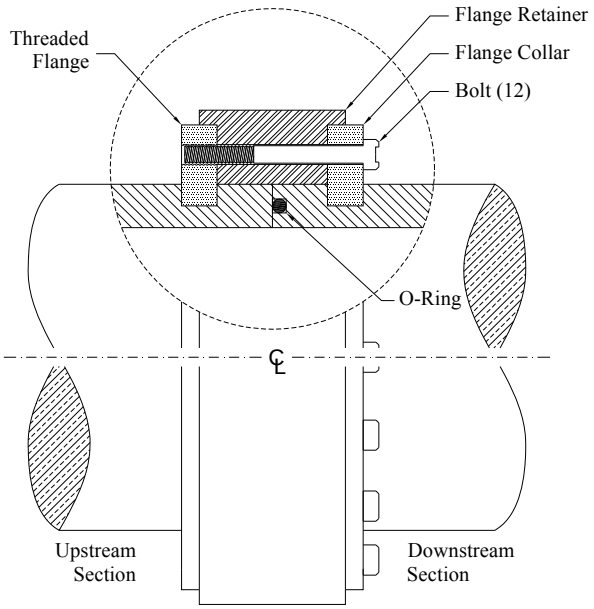

Figure 3. Cutaway view of weldless flange design for the driven section

The use of a weldless flange design is favorable over welded options due to the warping of the welding medium when subjected to local zones of high temperature. The overall compression-style fitting is shown schematically in **Figure 3**. A series of twelve, 5.7-cm bolts are distributed circumferentially through two coupling flanges that fit into grooves machined directly into the shock tube. Between the two grooves, sits a collar piece that ensures stability and offers a buffer for the two adjoining shock-tube sections to line up concentrically. A convention is taken for the shock-tube sections to have an interior o-ring groove for placement of a Parker 2-260 o-ring on the downstream section. An exploded view of such a connection is shown in **Figure 4**.

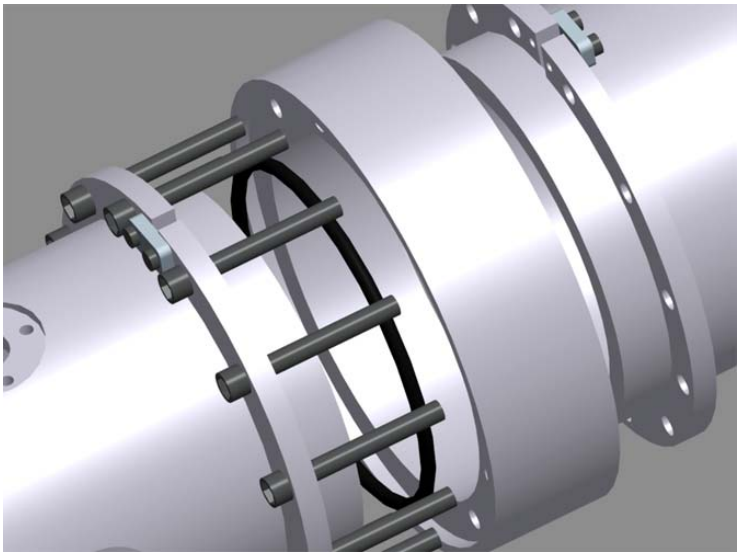

Figure 4. 3-D model of weldess flange design between two portions of the driven section

Pressure transducer and viewing window access is provided through 25 ports located along the tube. The protrusions on the ports are given curvature to match the inside diameter of the tube, as seen in **Figure 5**, to minimize flow and shock obstructions in the test section. The pressure in the tube is constantly monitored by a Setra GCT-225 200-atm pressure transducer. Wave speed and test pressure conditions are measured through five PCB P113A piezoelectric pressure transducers alongside the tube and one PCB 134A located at the endwall.

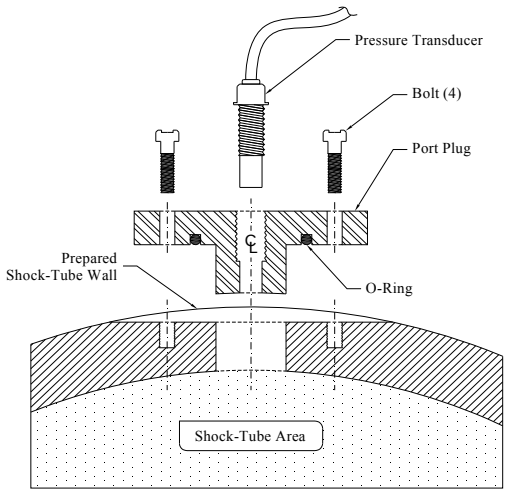

Figure 5. Port housing for pressure transducer having access to the shock-tube test section

Post reflected-shock conditions are obtained by using the incident wave speed and the initial condition in the driven tube. Five equally spaced pressure transducers offer four velocities that are then curve fitted to give the incident wave speed at the endwall location. The transducers are applied to the shock tube in ports, an example of one can be found in **Figure 5**, and the signal is sent to four Fluke PM-6666 counter boxes which record the time for the shock wave to travel from one known location to the next. It is shown by Petersen at al. that this technique can maintain the uncertainty below 10 K (2005). The ports used in **Figure 5** utilize a Parker 2-122 sized o-ring groove on the port itself necessary for obtaining high vacuum pressures.

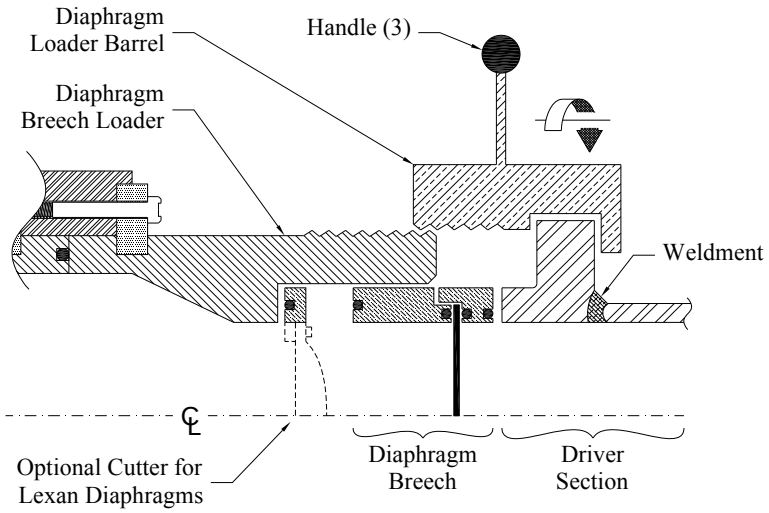

Figure 6. Cutaway view of the diaphragm loading section of the shock tube

The breech-loaded assembly allows for both lexan and aluminum diaphragms (see **Figure 6**). Lexan diaphragms are used for test pressures up to about 10 atm, and pre-scored aluminum diaphragms are used for pressures up to 100 atm. When lexan diaphragms are used, a special cutter is utilized to facilitate breakage of the diaphragm and prevent diaphragm fragments from tearing off. The diaphragms are loaded into a diaphragm breech which has an appropriate number of Parker 2-239 sized o-rings that create an air-tight seal. The basic operation of replacing a diaphragm between experiments is illustrated in **Figure 7**.

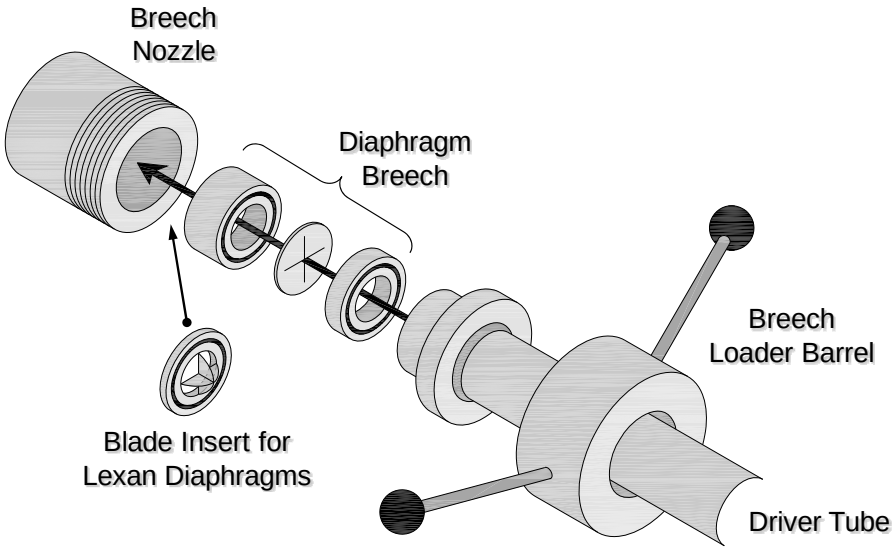

Figure 7. An isometric view of the diaphragm loading section of the shock tube

Test mixtures are created in three different mixing tanks of 1.22 m, 1.83 m, and 3.05 m length made from 304 stainless steel tubing with a 15.24-cm ID and a 1.27-cm wall thickness. The pressure in the mixing tanks is measured using three Setra GCT-225 pressure transducers (2 x 0-17 atm and 1 x 0-34 atm). All mixing tanks are connected to the vacuum system and can be pumped down to pressures below 1×10^{-6} Torr. Different gases are passed through a perforated stinger in the center of each mixing tank to allow for turbulent mixing.

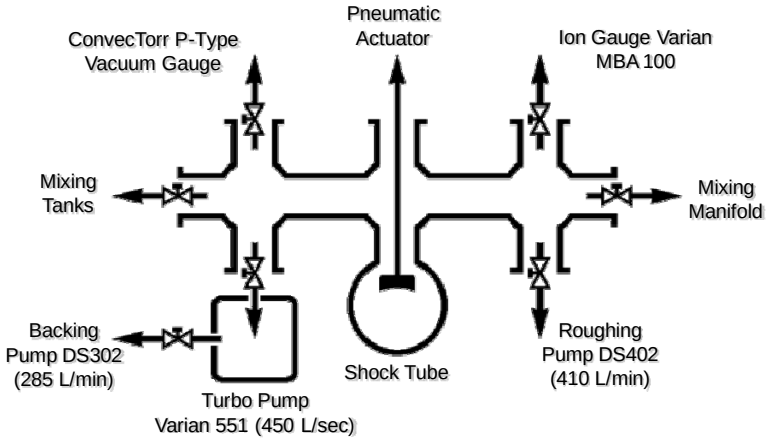

Figure 8. Diagram illustrating the advanced staged pumping system and its interface with the shock-tube test section

A high-vacuum system has been designed to create high-purity mixtures and is shown schematically in **Figure 8**. The driven section is first pumped down to about 50 mTorr using a Varian DS402 (410 L/min) roughing pump. At approximately 50 mTorr, a Varian 551 (450 L/sec with He) Turbo-molecular pump with a Varian DS302 (285 L/min) backing pump takes over which can pump the entire system down to 1×10^{-6} Torr or better. The pressure is measured using two MKS Baratron model 626A capacitance manometers (0-1000 Torr and 0-10 Torr) and an ion gauge for high vacuums. A pneumatically driven poppet valve matching the inside diameter of the driven section is used to separate the tube from the vacuum system. This poppet-valve design allows for a 7.62-cm passage between the vacuum cross section and the driven tube. The driver tube is evacuated by a separate Varian DS102 vacuum pump (114 L/min). A thorough set of design drawings and schematics for the entire shock tube are given in Appendix A for reference.

CHAPTER III

APPROACH

The use of various fuels in gas turbines for both the aerospace and power generation industries has shown that there is a need for research into the production of these fuels from different sources. As energy concerns continue to mount over the availability of fuels typically used in power generation and automotive applications, there has been a push to study the effects that chemical composition have on reaction characteristics. Natural gas is one of the many popular fuel types being developed for these specific purposes. The use of natural gas is common among land-based gas turbines for power generation (Lefebvre, 1999). Different production methods of natural gases have led to an overall composition which is mostly methane with other constituents, percentages of which vary from one source to another (Lamourex and Paillard, 2003). Alongside methane, there tends to exist various amounts of ethane within most forms of natural gas (< 10%) and alternative fuels, which rely on hydrocarbons for their calorific value. For this reason, it is important to see how the oxidation of these two components, methane and ethane, affects the combustion characteristics of these widely used fuels.

However, the main impetus for the present study is the need for fundamental kinetics data for mixtures of methane and ethane that span the entire range from 100% methane to 100% ethane as opposed to mixtures that are more like natural gas. In this way, a better understanding of the chemistry of such blends can be gained, ultimately

leading to kinetics models of greater utility. An observation from the literature is that data exist for pure methane and methane/ethane blends with relatively small levels of ethane, but no data exist that span the entire range, particularly at elevated pressures. For example, studies have been performed on many blends of methane/oxygen and ethane/oxygen reactions such as the work performed by Cooke and Williams (1975) which outlines how ethane typically decomposes much faster than methane in separate reactions. The study by de Vries et al. (2007) took a look at specific ethane mixtures with oxygen highly diluted in argon in a shock-tube study that identified key reactions for ethane oxidation chemistry. There has also been work on blends of methane/ethane with concentrations of each being similar to those found in natural gas. Petersen et al. (2007b) show how lean methane-based fuels react with varying levels of other components such as ethane, propane, and hydrogen at engine pressures. This study shows that ethane, in combination with methane, tends to accelerate the overall reaction rate over a wide variety of temperatures and pressures extending out into negative temperature coefficients (NTC). Research by Huang and Bushe (2006) describes the pathways taken by both methane and ethane during combustion and shows how each of them differ with temperature and pressure. Lamoureux and Paillard (2003) have studied methane and ethane blends diluted in 95-97% argon with ethane levels of up to 8% in a shock-tube study that looked at the general differences between natural gas compositions from various known sources around the world.

The utility of natural gas has facilitated a need for further investigation into methane-based fuel blends. A study with these types of fuels with respect to

autoignition, a potentially damaging event in gas turbines, has been carried out by de Vries and Petersen (2007) to better understand fuel performance characteristics at a wide range of pressures and temperatures. Research into ignition chemistry and flame characteristics for more compositions of "natural gas" with significant levels of heavier hydrocarbons, with methane ranging from 81% to 62% and ethane at 10% to 20% (along with other hydrocarbons) was conducted by Bourque et al. (2008) at undiluted conditions and at elevated pressures. Also deserving mention is the comprehensive and classically recognized study by Spadaccini and Colket (1994), which provides an in-depth look into methane ignition delay time with other hydrocarbons, including ethane, for diluted conditions. Although research has been performed with percentages of ethane typically found in raw natural gas and related blends (3~30%), there has been little research performed which specifically looks at a wider ranges of methane and ethane blends with the intent of constructing a model that is valid from 100% methane to 100% ethane.

The absence of such experimental kinetics data has prompted the authors to conduct the study herein. Shock-tube experiments were performed to determine ignition delay time characteristics at a wide assortment of conditions for varying levels of methane and ethane. These combustion data were used in comparison with several well-researched kinetics models to identify areas in need of improvement.

Experiment Parameters

This study describes blends of methane/ethane from equivalence ratios of 0.5 to 2.0 at pressures of 1, 10, and 25 atm. The mixtures are diluted in argon at 75, 95, and

98% with blend ratios of, between methane and ethane, 100/0, 75/25, 50/50, 25/75, and 0/100 by volume. To cover the wide range of parameters suggested above, a test matrix was chosen in a similar style as the methods described by Petersen and de Vries (2005). This approach allows for a general comprehensive analysis which can be used to better the associated model utilized herein. The overall set of 19 mixtures chosen is shown in **Table 1**. All mixtures were diluted only with argon and reacted with oxygen.

Table 1. Mixture compositions diluted in argon and target pressures

Mixture	Blend (CH_4/C_2H_6)	Dilution (%)	Φ	Pressure (atm)
1	75 / 25	98	0.5	1
2	50 / 50	98	0.5	1
3	25 / 75	98	1.0	1
4	100 / 0	98	1.0	1
5	75 / 25	75	1.0	1
6	50 / 50	75	1.0	1
7	25 / 75	75	0.5	1
8	100 / 0	75	0.5	1
9	0 / 100	75	1.0	1
10	0 / 100	75	0.5	1
11	75 / 25	95	1.0	10
12	50 / 50	95	1.0	10
13	25 / 75	95	0.5	10
14	25 / 75	95	2.0	10
15	75 / 25	85	2.0	25
16	50 / 50	85	2.0	10
17	100 / 0	85	1.0	10
18	0 / 100	85	1.0	10
19	0 / 100	85	0.5	10

Ignition Delay Time Determination

Ignition behind the reflected-shock region of the shock tube is determined by way of chemiluminescence emission of excited radicals and pressure traces at both the

endwall and sidewall locations. The sidewall measurement diagnostics are located at a plane distanced 1.6 cm away from the endwall of the shock tube. The overall optical access for the test region of the shock tube is shown schematically in **Figure 9**.

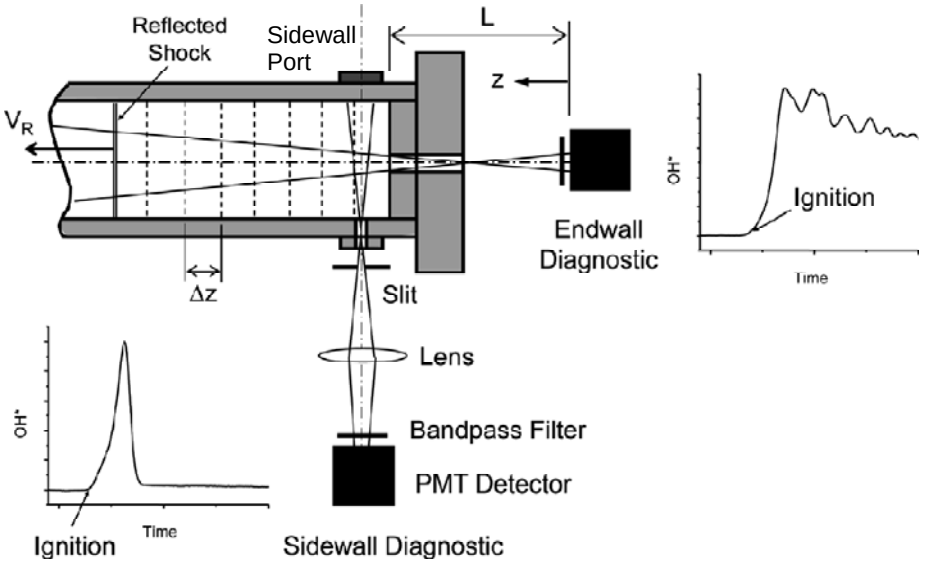

Figure 9. Emission diagnostics schematic for measuring chemiluminescence of various species at both the endwall and sidewall locations of the shock tube (Petersen, 2009)

Ideal ignition within the shock tube originates at the endwall of the shock tube and continues upstream. It is because of this ideal case that autoignition data are measured from the endwall location by monitoring pressure and emission. It has been found by Petersen (2009) that ignition of highly dilute mixtures, where pressure does not rise, that endwall emission can lead to artificially longer ignition times due to the presence of pre-ignition radicals formed axially along the shock tube. For these cases, it is necessary to use a method of ignition delay time determination from the sidewall

location diagnostics like that shown in **Figure 9**. A representative plot of ignition for the first 10 mixtures studied from **Table 1** is shown in **Figure 10**. The strong pressure rise from both the incident and reflected shocks is noted, with the arrival of the reflected shock at the sidewall location indicating the beginning of recorded ignition time. The inference of ignition from sidewall emission is shown as the intersection of the steepest recorded slope with the baseline of the emission signal.

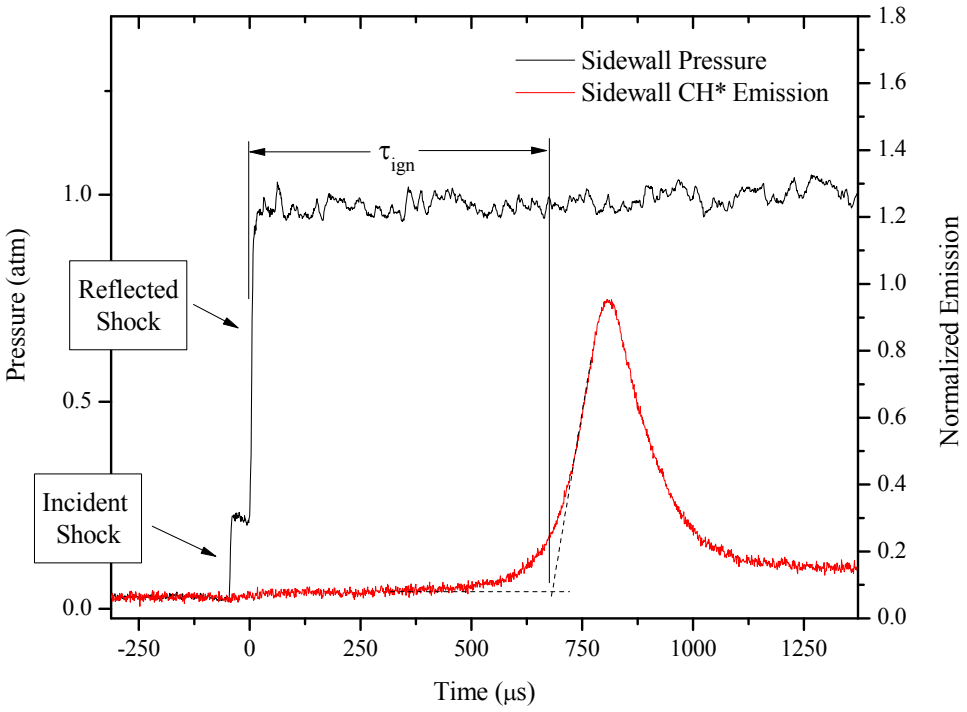

Figure 10. Representative emission and pressure trace for highly dilute ignition from mixture 1 of the present study

For mixtures where ignition is abrupt and shows a drastic rise in pressure, as is the case for lower percentages of diluent, it is necessary to infer ignition from said pressure rise. An example plot which represents the whole of data obtained in this style is shown in **Figure 11**. For less-diluted conditions, mixtures 11 through 19 in **Table 1**, ignition is recorded from the rise of pressure at the endwall due to the arrival of the incident shock to the distinct rise in both pressure and emission. This method of autoignition determination is described in detail by Petersen (2009).

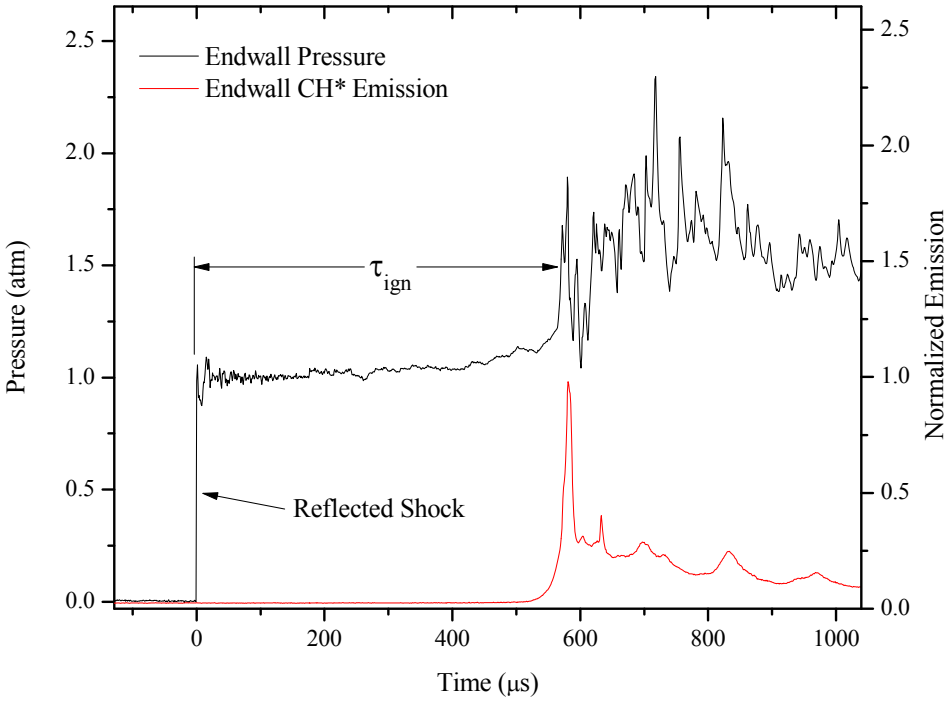

Figure 11. Representative emission and pressure trace for less dilute ignition from mixture 6 of the present study

Conditions behind the reflected shock are determined by way of measuring incident shock velocity for use with the Rankine-Hugoniot one dimensional shock relations. As mentioned previously in Chapter II this method has an uncertainty in temperature measurement of ±10 K (Petersen et al., 2005).

Kinetics Modeling

Chemical kinetics modeling was performed for CH* time histories of the given mixtures by way of the GRI-Mech 3.0 (Smith et al., 2008), RAMEC (Petersen et al., 1999), and the recent C4 model (version 46, Healy et al., 2008) for oxidation and ignition of methane and other higher order hydrocarbons, through C4, developed by Healy and coworkers for which the rate constants and transport properties can be found on the National University of Ireland Galway Combustion Chemistry Centre website at http://www.nuigalway.ie/chem/c3/mechanisms.html (2008). This model represents a kinetics mechanism built from the ground up, starting with hydrogen and methane validation, followed by the C2, C3, and C4 chemistry. It is an evolving mechanism that has been under development for the past few years as new ignition data from rapid compression machine and shock-tube experiments become available in the authors' laboratories. The basic C4 mechanism has been shown in recent publications to predict the ignition times of methane-based fuel blends containing ethane and propane at pressures up to 30 atm or more and a wide range of stoichiometries from fuel-lean to – rich (0.5 to 2.0) (Bourque et al., 2008 and Petersen et al., 2007a). This model will be referred to as the current model for the remainder of this work. Calculations with the current mechanism were made by way of the HCT program (Lund and Chase, 1995) and

the Chemkin 4.1.1 software (Kee et al., 2004) at constant-volume and constant internal energy conditions.

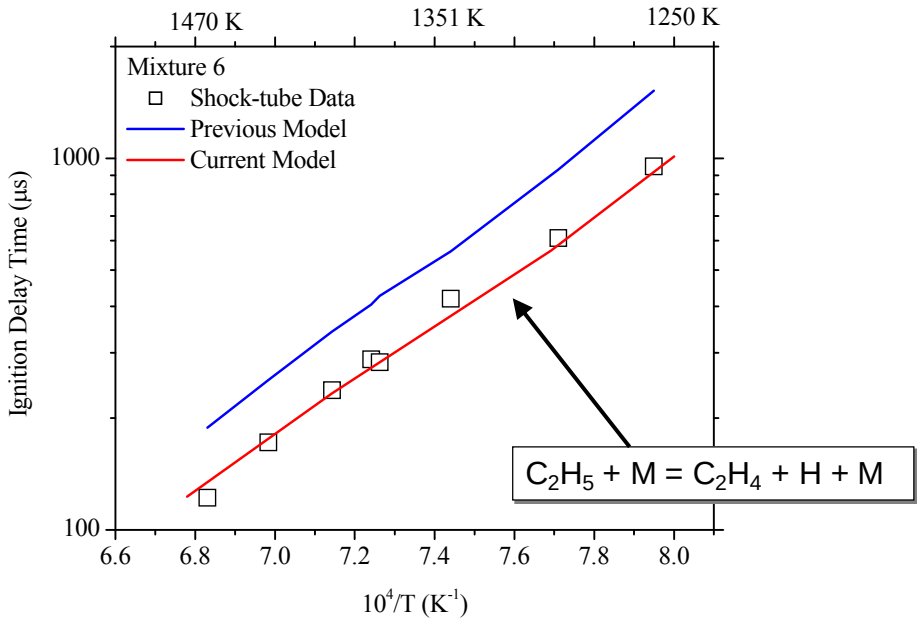

Figure 12. Data comparison to various incarnations of the model used in this study

Figure 12 highlights a typical Arrhenius plot of ignition delay time on an inverse temperature axis. Noted is a set of predicted results from two different forms of the model detailed previously; the data in **Figure 12** are shown in this section for the purpose of describing the modeling and are covered in more detail in the following chapter. The previous modeled results are predicting much slower ignition delay times over the temperatures presented. The current model, modified with the results presented in this work, does much better to capture the autoiginition data for these conditions. This

significant change in the model was a result of increasing the pre-exponential factor of the ethyl decomposition reaction, a traditionally important reaction in methane and ethane chemistry, by a factor of two. The reaction rate coefficient is defined within a mechanism by way of the following expression:

$$k_i = AT^n \exp\left(-\frac{E_a}{RT}\right)$$

where k_i is the reaction rate of some elementary species i, A, n and E_a are all constants, the gas constant R, and temperature T. A is referred to as the pre-exponential factor. Any mechanism in use is made up of many of these reaction rate expressions for different species of interest.

All other models were employed with the Chemkin 4.1.1 software at relevant conditions. Both the GRI-Mech 3.0 and current mechanisms were used for each mixture, while the RAMEC was only used to model mixtures 4 and 8 as it was not generated for use with ethane combustion and is only accurate for cases with 100% methane. Although GRI 3.0 was also constructed around mostly methane data, it is widely employed and deserves attention.

CHAPTER IV

RESULTS

For each of the nineteen mixtures presented in **Table 1**, an extensive set of ignition delay time experiments was performed. The values for ignition delay time were then compared with those predicted by several models outlined in the previous chapter to distinguish where current inaccuracies from the model(s) can be improved upon. For kinetics modeling, the experimental values for pressure and temperature recorded from the ignition delay time measurements were used. Results for mixtures 1 through 10 were initially presented by Walker (2007) and are briefly reviewed in this work for completeness. Following the initial ten mixtures, all recorded with the average pressure of 1 atm, higher-pressure datasets are presented for mixtures 11 through 19. The inclusion of all mixtures of this entire study was essential in deriving the correlation results that are presented at the end of this chapter. The ignition times for all mixtures presented in this chapter are plotted on a base 10 logarithmic scale with the inverse temperature along the x-axis.

Experimental and Modeled Results

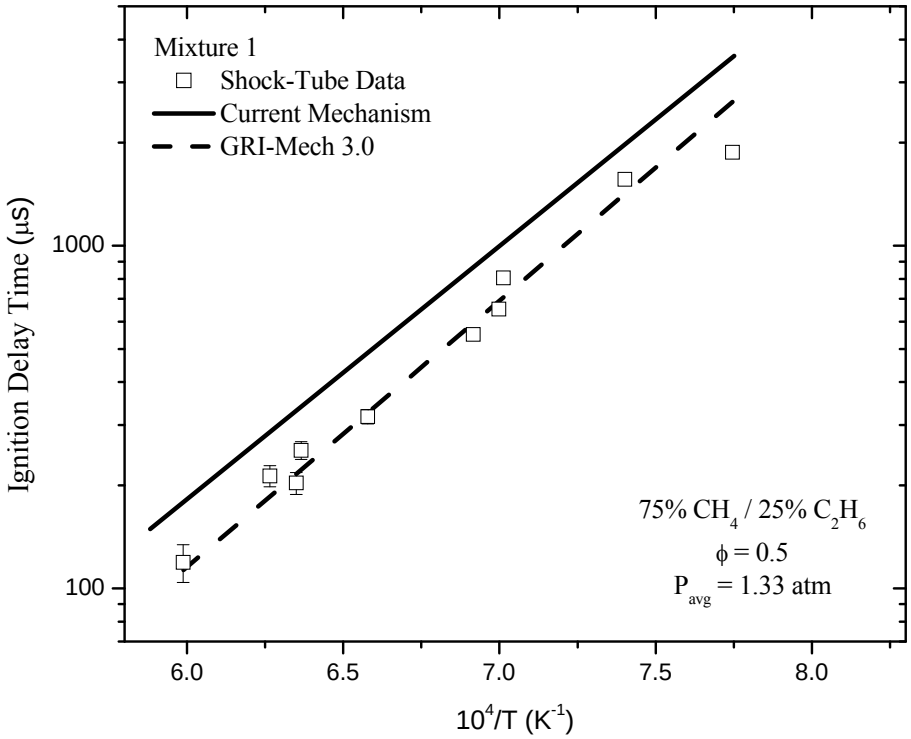

Figure 13. Experimental and modeled ignition data for mixture 1, diluted in 98% argon

Ignition delay time data are presented with regards to inverse temperature in **Figure 13**. Mixture 1 is a fuel-lean blend of 75% methane and 25% ethane with oxygen at an equivalence ratio of 0.5 diluted in 98% by volume of argon. For mixture 1 it is shown that predictions from the GRI-Mech 3.0 are slightly more accurate than the ones obtained from the current mechanism. There is a tendency for the current model to over predict ignition delay by a constant offset, but shows good agreement with the overall

slope suggesting that the predicted activation energy is accurate. An observed ignition time uncertainty of ±15 ms is shown in **Figure 13** by way of error bars. Due to the logarithmic plot of ignition times the error for higher temperatures appears higher, with decreasing uncertainty heading to lower temperatures. This uncertainty in ignition delay time is typical of all results presented herein and is shown in **Figure 13** as an example for the rest of this study.

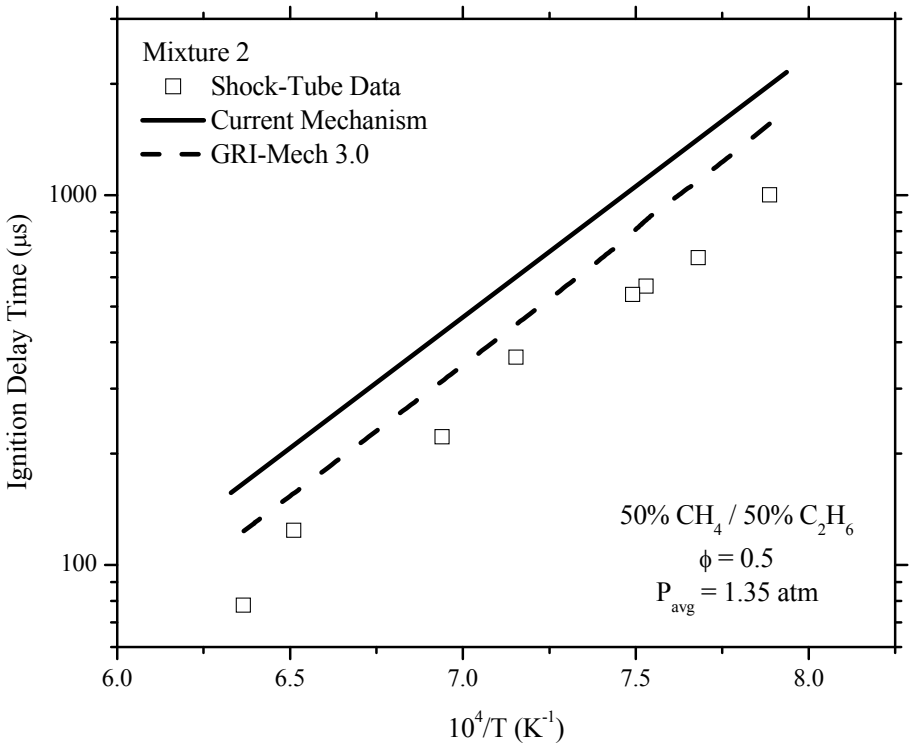

Figure 14. Experimental and modeled ignition data for mixture 2, diluted in 98% argon

Autoignition data for mixture 2 are presented in **Figure 14**. This mixture is fuel lean ($\phi = 0.5$) with a blend of 50% methane and 50% ethane with oxygen diluted in 98%

argon. The average pressure for this mixture is 1.35 atm, and both models predict slightly higher ignition delay times with similar slopes. There is no change in activation energy throughout the given range of temperatures between 1268 and 1571 K.

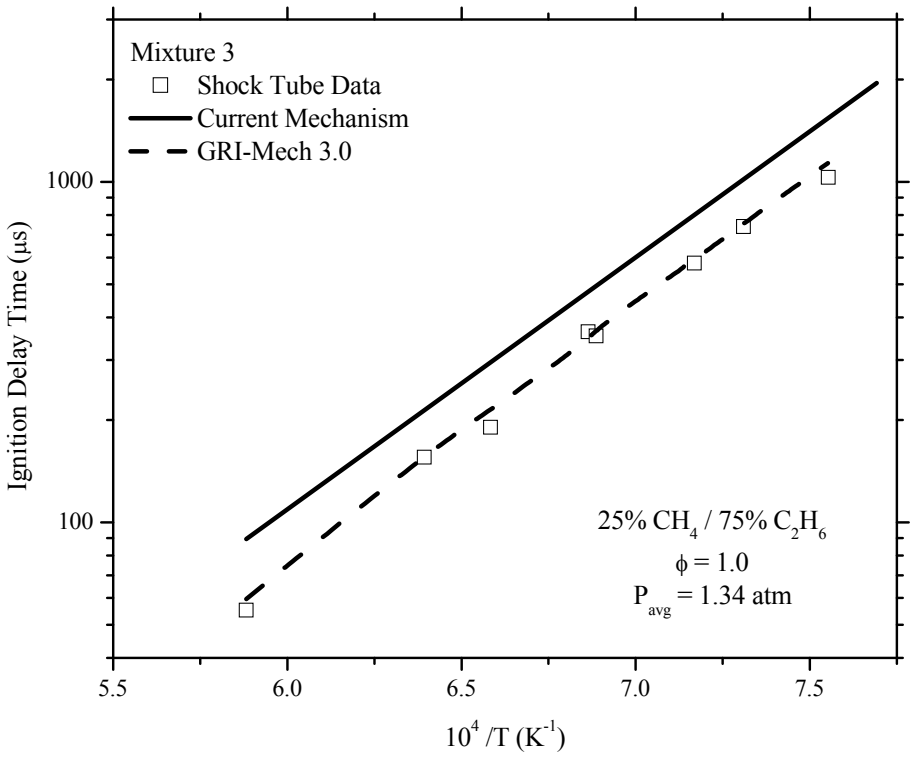

Figure 15. Experimental and modeled ignition data for mixture 3, diluted in 98% argon

Figure 15 presents the ignition delay time data for mixture 3. Data for this mixture were taken at pressures around 1.34 atm and consisted of a 25% methane and 75% ethane blend of fuel with oxygen in an overall dilution of 98% argon. It is shown that the GRI-Mech 3.0 model tends to agree much more so with the recorded data as the

current mechanism predicts higher ignition delay times for the full range of temperatures, 1324 – 1700 K. The slope of the data, as was noticed in the previous mixtures, agrees with the predicted results from both models. The over prediction noticed from the current mechanism in mixtures 1 through 3 suggest that there are areas of possible improvement for these highly diluted conditions.

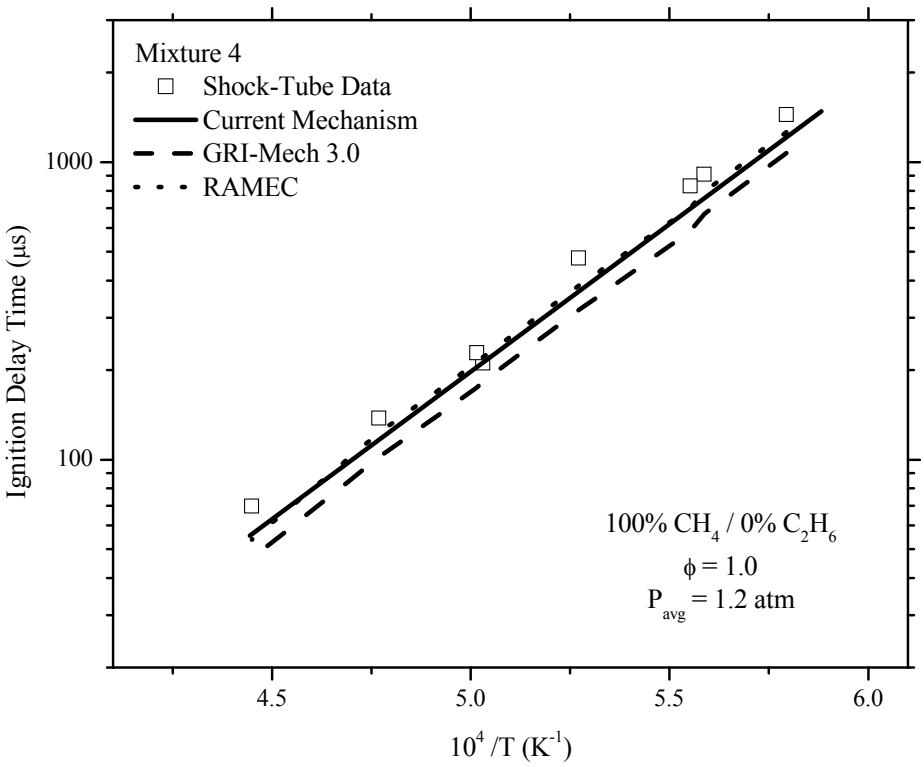

Figure 16. Experimental and modeled ignition data for mixture 4, diluted in 98% argon

Ignition delay time data for mixture 4 are presented in **Figure 16**. This mixture is 100% methane with oxygen diluted in 98% argon with an equivalence ratio of 1.0. For

this stoichiometric mixture of pure methane, there is very good agreement between the two models and the inclusion of the RAMEC model mentioned in Chapter III. Both the RAMEC model and the current mechanism have slightly better agreement when compared directly with the GRI-Mech 3.0 results, but in all cases the average error does not exceed 27% of the recorded ignition delay time data. Note that such good agreement should attributed to the formulation of the GRI mechanism and the RAMEC model, both largely based on dilute methane reacting with oxygen at pressures near 1 atm.

The ignition delay times for mixtures 1 through 4 were obtained solely through the sidewall CH* chemiluminescence, whereas the other pressure and emission data obtained for each experiment in this mixture set were used to qualitatively justify the use of sidewall emission. For all of the mixtures diluted in 98% argon, there is a distinct observation that the activation energies of the experimental data and modeled results for each mixture are generally within reasonable uncertainty.

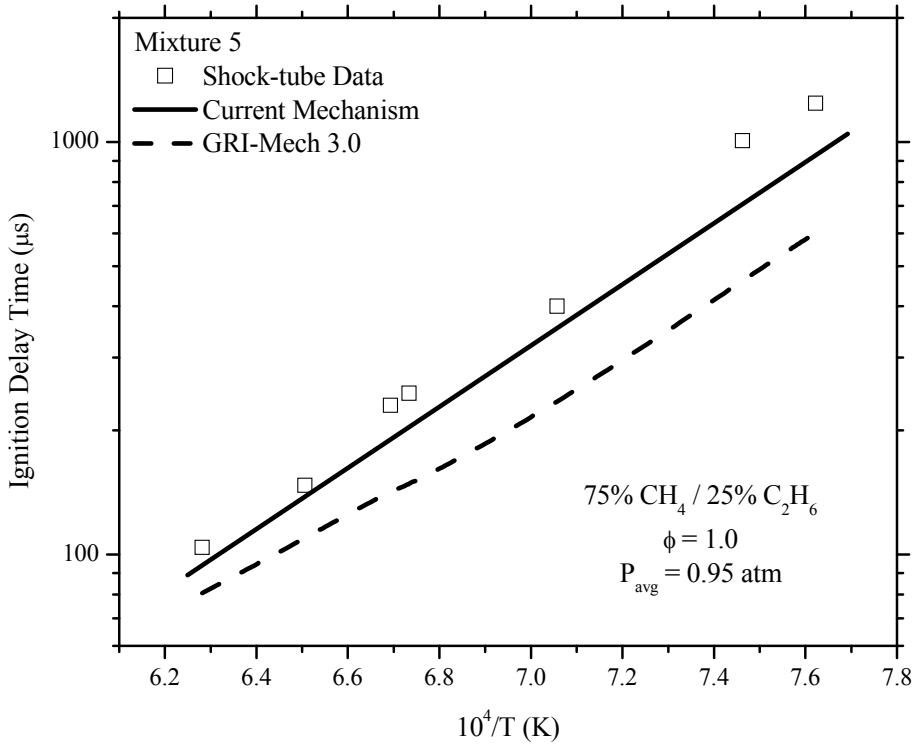

Figure 17. Experimental and modeled ignition data for mixture 5, diluted in 75% argon

Ignition delay time data for mixture 5 are presented in **Figure 17**. Mixture 5 is a stoichiometric blend of 75% methane and 25% ethane with oxygen in an overall mixture which is diluted in 75% argon. The average pressure of the data collected is 0.95 atm and, as with mixtures 6 through 8, has a lower concentration of diluent than what was recorded in the first four mixtures. Immediately noticeable is that both mechanisms tend to predict faster results then what is found in experiment. The current mechanism performs better at these conditions when compared with the GRI mechanism, which

exhibits a slight decrease in modeled slope – agreeing more so at higher temperatures. There is overall good agreement between the shock-tube data and the current model, but there is an under-prediction of ignition time from the GRI-Mech 3.0 mechanism, which is displaced by a factor of less than 0.5 at high temperatures (~ 1590 K) and worsens as the temperature decreases towards 1300 K.

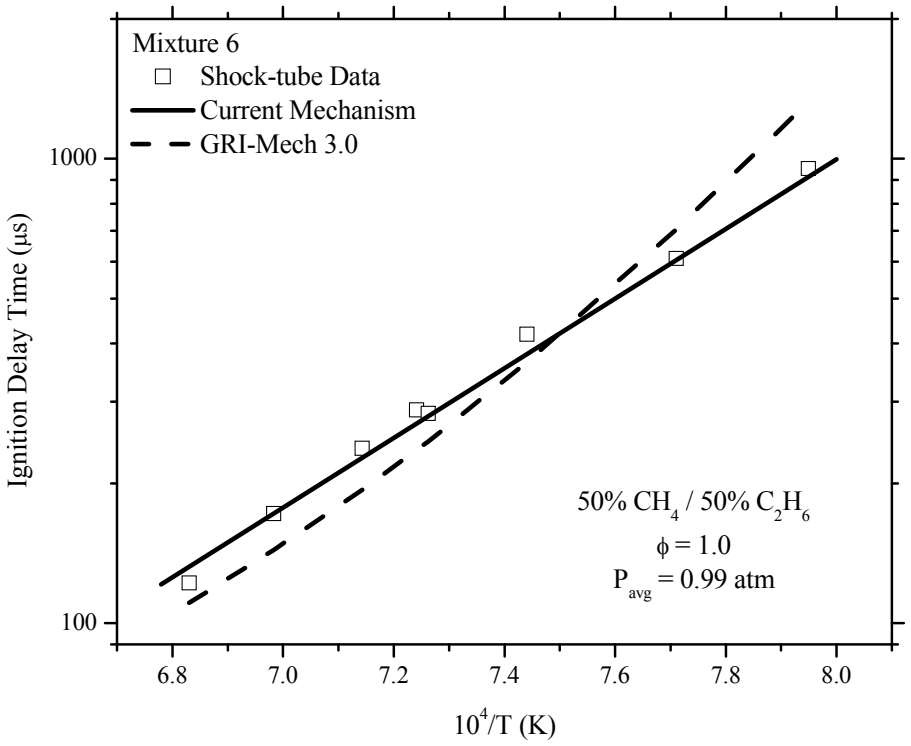

Figure 18. Experimental and modeled ignition data for mixture 6, diluted in 75% argon

Autoignition data compared with modeled results are shown for mixture 6 in **Figure 18**. Mixture 6 is a 50% methane and 50% ethane fuel blend at stoichiometric equivalence ratio with oxygen diluted in 75% argon. Modeled results for mixture 6 agree

with reasonable certainty with the current mechanism showing to be more accurate over the range of tested range of temperatures, 1258 – 1464 K. The GRI mechanism produces a distinct increase in slope at around 1375 K which is not apparent in the experimental data.

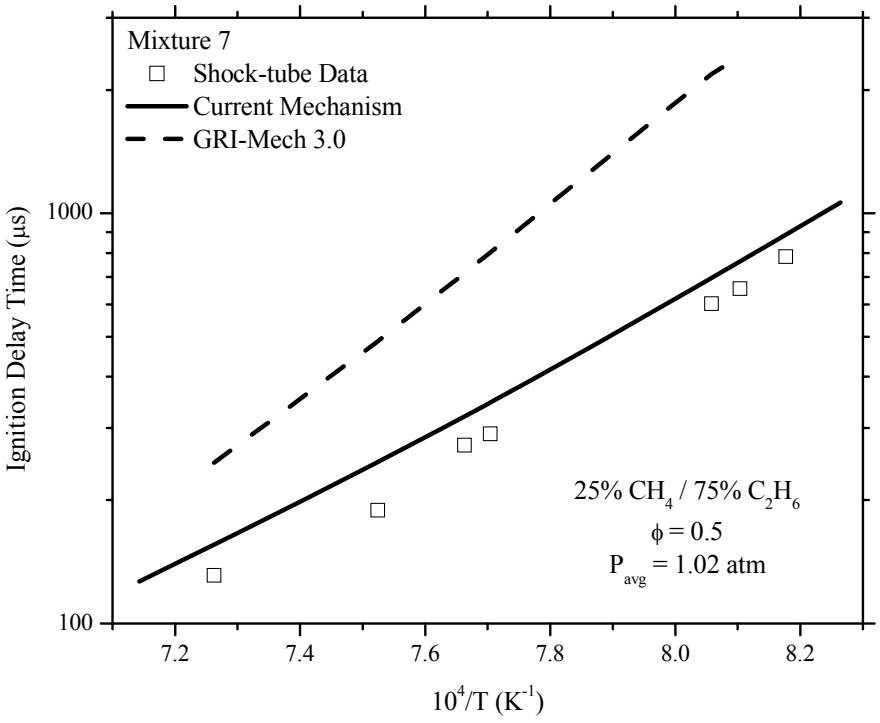

Figure 19. Experimental and modeled ignition data for mixture 7, diluted in 75% argon

Ignition data for mixture 7 are presented alongside model results in **Figure 19**. Mixture 7 is a fuel-lean ($\phi = 0.5$) blend of 25% methane and 75% ethane with oxygen diluted in 75% argon. The GRI mechanism predicts much slower ignition delay time

data over the entire range of temperatures, and has a steeper slope with much worse agreement as the temperature decreases. The current mechanism performs better but has the similar tendency to predict higher ignition delay time results. The current model also captures the slope of the data throughout for these conditions.

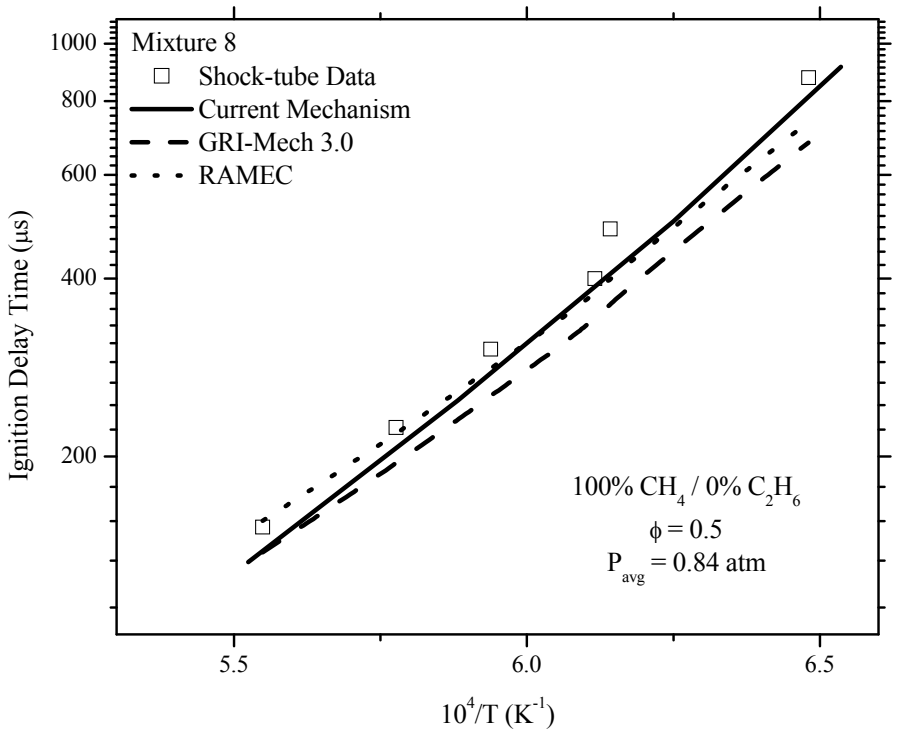

Figure 20. Experimental and modeled ignition data for mixture 8, diluted in 75% argon

Ignition delay time data are presented for mixture 8 in **Figure 20**. Similar to mixture 4, mixture 8 shows pure methane as the fuel but in this case is fuel-lean (equivalence of 0.5) and is less diluted at 75% argon. The trends shown in **Figure 16** are

again like those found in **Figure 20** with RAMEC and the current mechanism performing closer to experimental data than the GRI mechanism although all of the modeled results show good agreement. This better agreement in both mixtures 4 and 8 is mostly due to the fact that the models themselves where developed with a strong emphasis on methane oxidation.

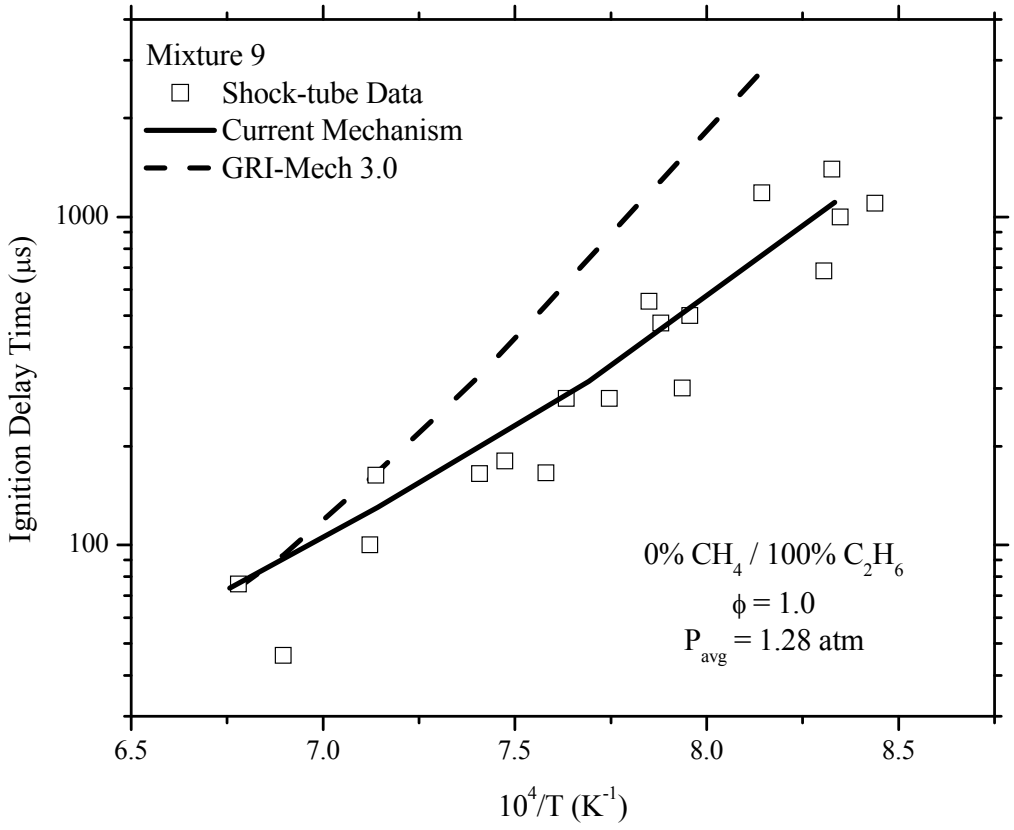

Figure 21. Experimental and modeled ignition data for mixture 9, diluted in 75% argon

The ignition delay time data obtained for mixtures 5 through 10 were all solely determined from the distinct endwall pressure increase found to be apparent at the time of ignition for more highly concentrated blends. Mixtures 5 through 10 were all diluted in 75% argon, similar to mixtures which would be representative of fuels burning in air with the replacement of nitrogen with argon.

Ignition delay time data for mixture 9 are shown in **Figure 21** compared to modeled results. Mixture 9 is a blend of pure ethane and oxygen with an equivalence ratio of unity and diluted in argon to 75%. For mixture 9, there is more scatter in the shock-tube ignition delay time data than for the other mixtures. This variation is possibly due to the chemistry involved with the decomposition of ethane, which is known to decompose much faster than methane when burned in the presence of oxygen (Cooke and Williams, 1975). The current mechanism for this mixture produces the overall trend of the scattered data. Using GRI-Mech 3.0 to simulate mixture 9 shows a change in activation energy which favors higher temperatures, a characteristic that shows that further understanding is required for ethane combustion.

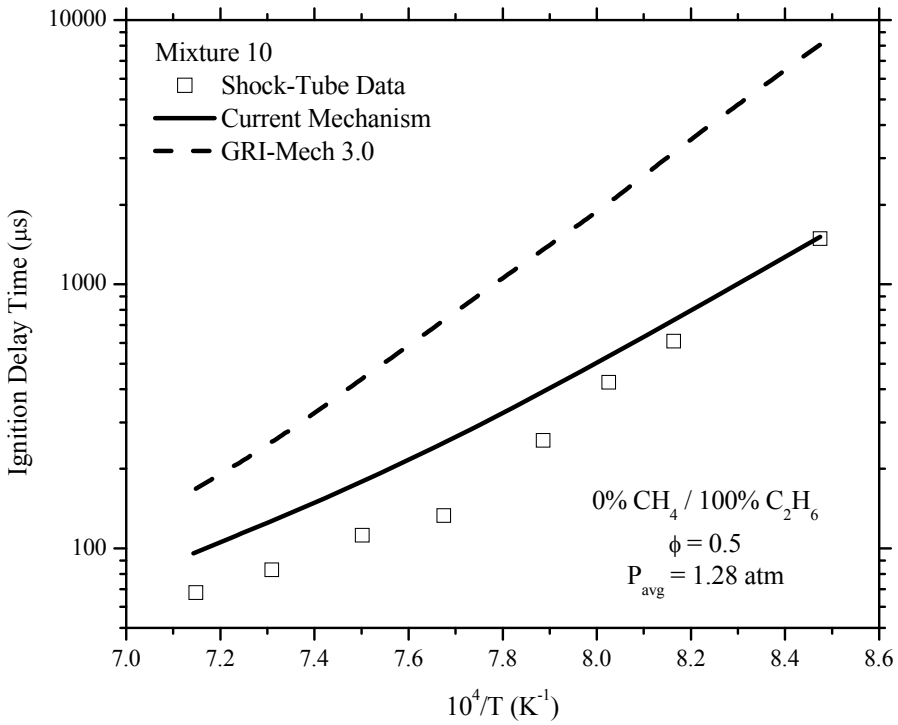

Figure 22. Experimental and modeled ignition data for mixture 10, diluted in 75% argon

Figure 22 shows ignition delay time data for mixture 10. This mixture, like mixture 9 before it, is pure ethane with oxygen in 75% argon but is fuel lean. The same scatter is not seen for the similar mixture with an equivalence ratio of 0.5, which is less reactive. Nonetheless, in both mixtures 9 and 10 it is seen that the current model shows better agreement for all of the temperatures measured when compared with the GRI-Mech 3.0 results. **Figure 22** shows for mixture 10 that there is a slight disagreement between the models and the shock-tube data. As was the case with the other mixtures with an equivalence ratio of 0.5, it is shown as a general trend that for lower equivalence

ratios, the models tend to disagree more with the experimental results. In the case for mixture 10, the current model tends to do better in predicting ignition times at lower temperatures. The GRI-Mech 3.0 mechanism further over-predicts the shock-tube data for this case by a factor of 2.5 and worsens for colder temperatures, it being almost seven times slower than experiment data at 1180 K.

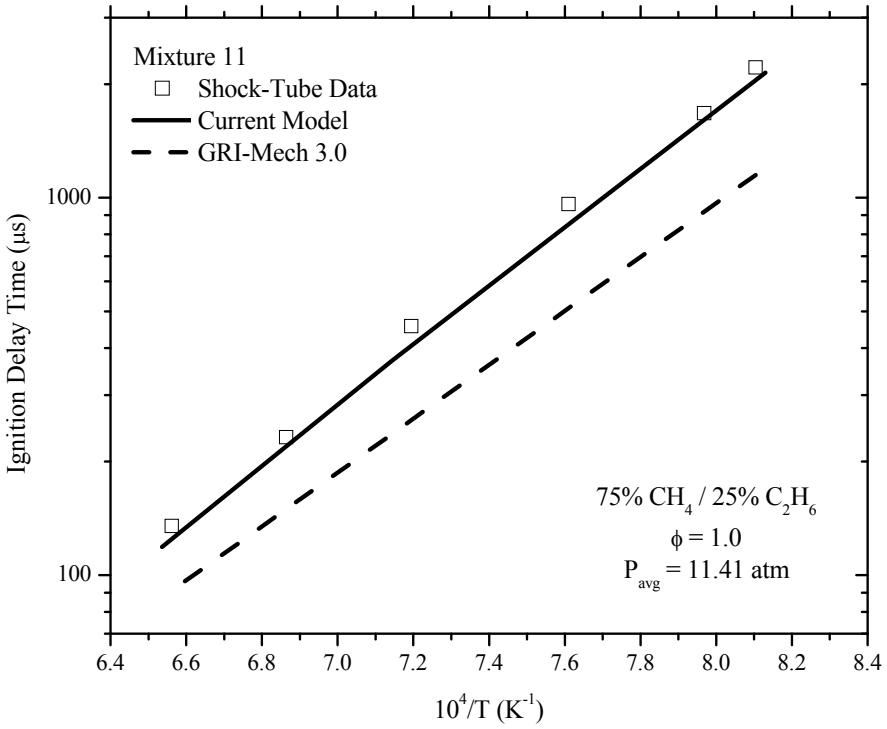

Figure 23. Experimental and modeled ignition data for mixture 11, diluted in 75% argon

Mixtures 1 through 10 were all conducted at a pressure behind the reflected shock averaging at 1 atm. Mixtures 11 through 19 were all studied at elevated pressures around 12 to 28 atm. The data presented at higher pressures show strong deviations from

the recorded data and the GRI mechanism predictions of ignition delay time. This behavior is not unexpected as the model itself was generated using data at mostly near-atmospheric conditions. However, as is shown next, the current mechanism shows rather good comparison with the shock-tube data for each of the three high-pressure mixtures. **Figure 23** looks at mixture 11 where there is 75% methane combined with 25% ethane and oxygen under sthoichiometric chemistry and diluted in 75% argon. The current model predicts very well across all of the temperatures considered in mixture 11, while GRI-Mech 3.0 shows an offset which under-predicts ignition time, being constantly approximately a factor of two faster than observed experimentally.

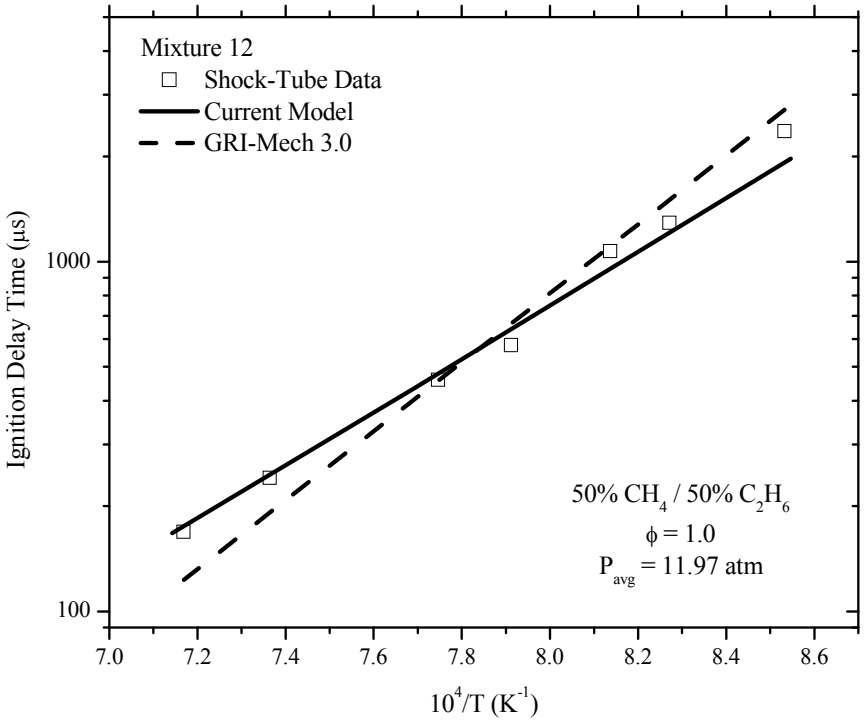

Figure 24. Experimental and modeled ignition data for mixture 12, diluted in 75% argon

Better agreement between both of the models and ignition data is shown for mixture 12 in **Figure 24** when compared with some of the other higher-pressure mixtures. This figure presents a 50% methane and 50% ethane fuel blend with oxygen with an equivalence of unity. At this particular set of conditions, GRI-Mech 3.0 models a generally steeper slope through the data, as is similar in the mixtures taken at pressures of 10 atm and above. This inability to correctly capture the activation energy of these mixtures highlights the need for better understanding of the methane and ethane chemistry in this widely used model.

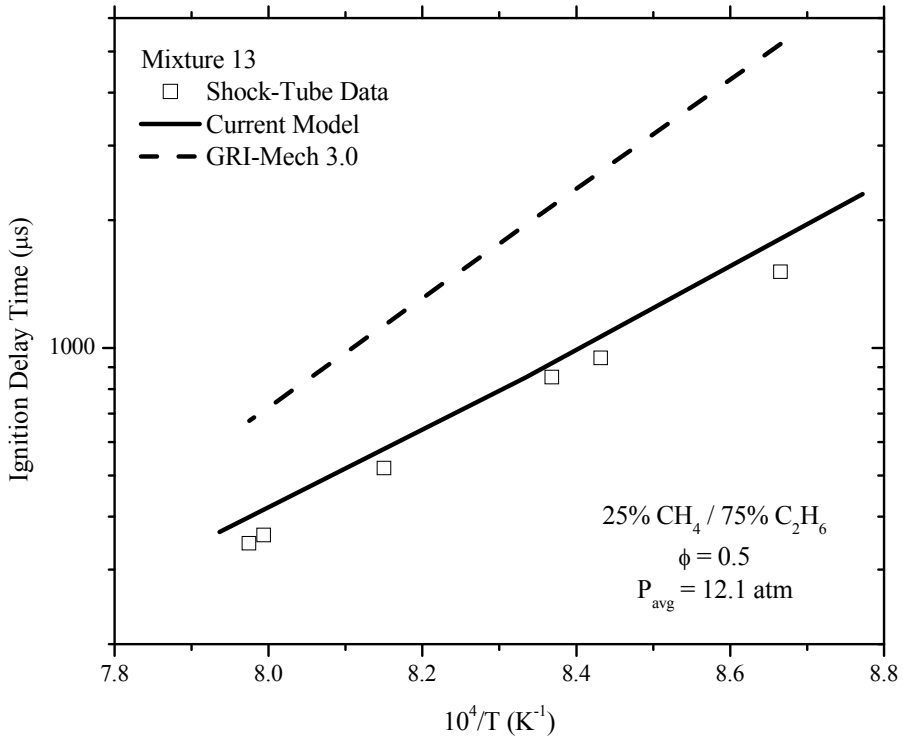

Figure 25. Experimental and modeled ignition data for mixture 13, diluted in 75% argon

Ignition delay time data for mixture 13, a 25% methane and 75% ethane fuel blend with oxygen at fuel-lean stoichiometry, are presented in **Figure 25**. This mixture shows a great difference between the current mechanism results and experimental data with the GRI mechanism. The GRI mechanism models a typical over-prediction by more than a factor of two for mixture 13 which is fuel lean and has a greater percentage of ethane.

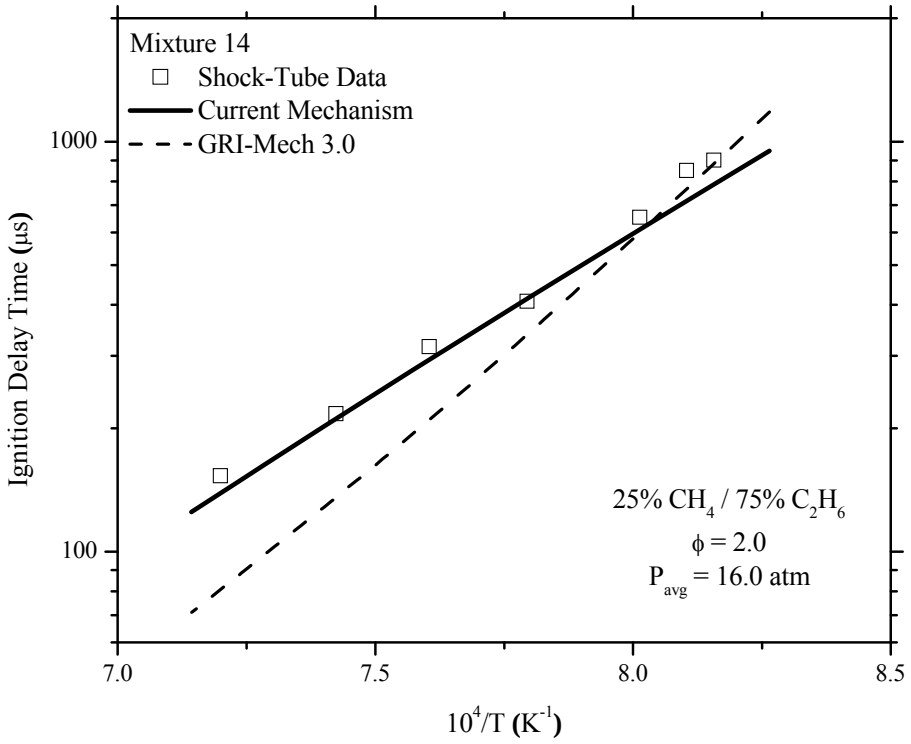

Figure 26. Experimental and modeled ignition data for mixture 14, diluted in 75% argon

Mixture 14 has a similar fuel composition as mixture 13 but is reacted at fuel-rich conditions (equivalence of 2.0). This mixture, presented in **Figure 26**, is predicted

well with the current mechanism but shows significant disagreement with the modeled results of the GRI mechanism for temperatures above 1300 K. Once again, as seen in mixtures 11 through 13, GRI-Mech 3.0 is producing a steeper slope at these high-pressure conditions. All of the high-pressure mixtures presented thus far, 11 through 14, were diluted with 95% argon and therefore provided enough of an exothermic reaction in the shock-tube experiment to determine ignition time by way of endwall pressure rise after the reflected shock.

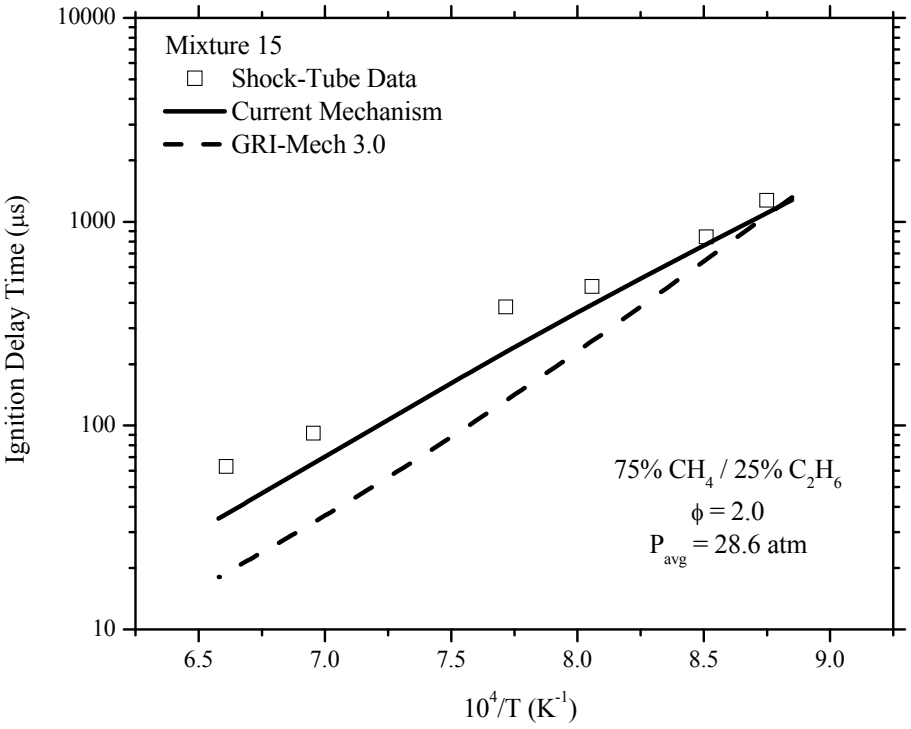

Figure 27. Experimental and modeled ignition data for mixture 15, diluted in 85% argon

Figure 27 shows ignition delay time data for mixture 15 as compared with modeled data. This mixture presents a 75% methane and 25% ethane fuel blend at fuel-rich conditions (ϕ = 2.0). The models considered for this mixture tend to under-predict ignition for temperatures higher than 1250 K with the current mechanism modeling more accurately throughout. There exists a steeper slope with the GRI-modeled results as has

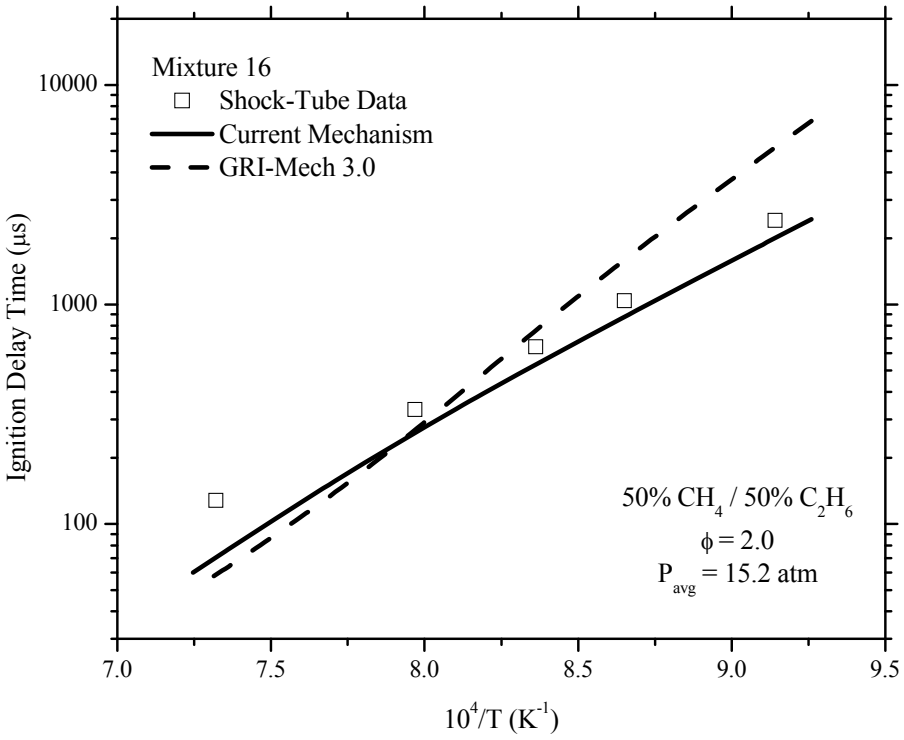

Figure 28. Experimental and modeled autoignition data for mixture 16, diluted in 85% argon

been the general trend for the past five mixtures at higher pressure. Mixture 15 is recorded at an average pressure of 28.6 atm, and a significant increase in pressure from ignition is observed owing to the largely exothermic conditions diluted in 85% argon.

The remaining mixtures were all recorded at a dilution of 85%, and ignition delay time data were recorded primarily from the large pressure rise present at the endwall of the shock tube, with the other diagnostics in place to qualitatively provide confidence in autoignition determination. Mixture 16, presented in **Figure 28**, is a 50% methane and 50% ethane fuel blend with oxygen and having an equivalence ratio of 2.0. The models under-predict the ignition delay time at temperatures above 1300 K, and then both models display oppositely shifting slopes with GRI steepening and the present mechanism conversely becoming shallower. The overall trend of the data is more accurately predicted by the current mechanism while still under-predicting the data throughout the entire temperature range.

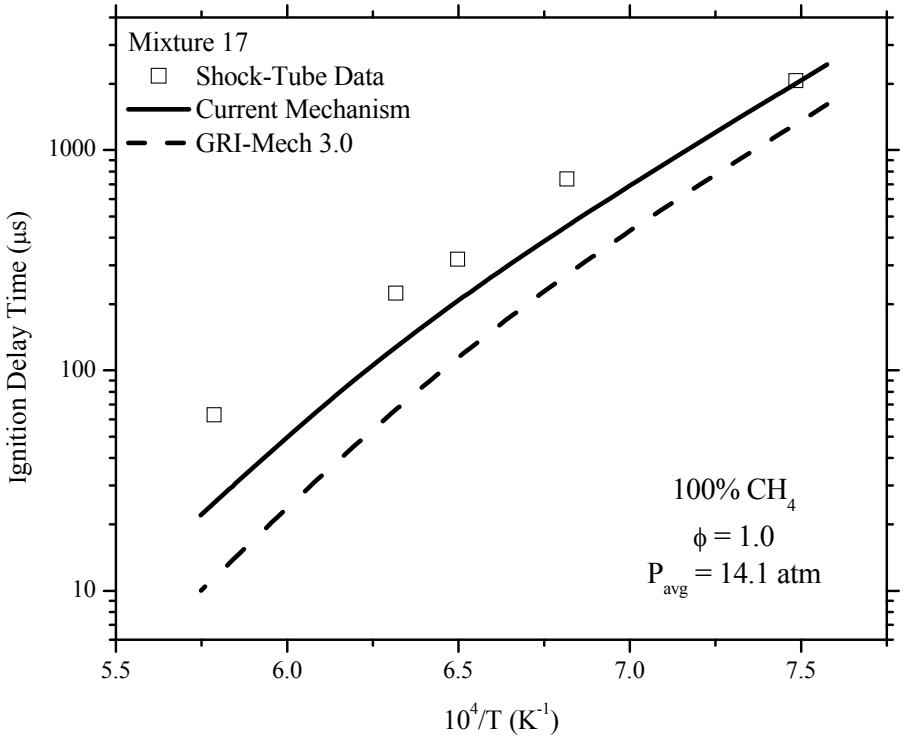

Figure 29. Experimental and modeled ignition data for mixture 17, diluted in 85% argon

Figure 29 presents data and modeled results for mixture 17 for pure methane at stoichiometric conditions diluted in 85% argon. At these conditions, the GRI mechanism predicts much faster ignition delay time data over the measured temperatures. The current mechanism does well to capture accurate ignition delay times at temperatures around 1300 K but generally becomes faster as temperature increases. The two models used in this case seem to capture the overall slope of the data with slight shifts favoring lower-temperature chemistry.

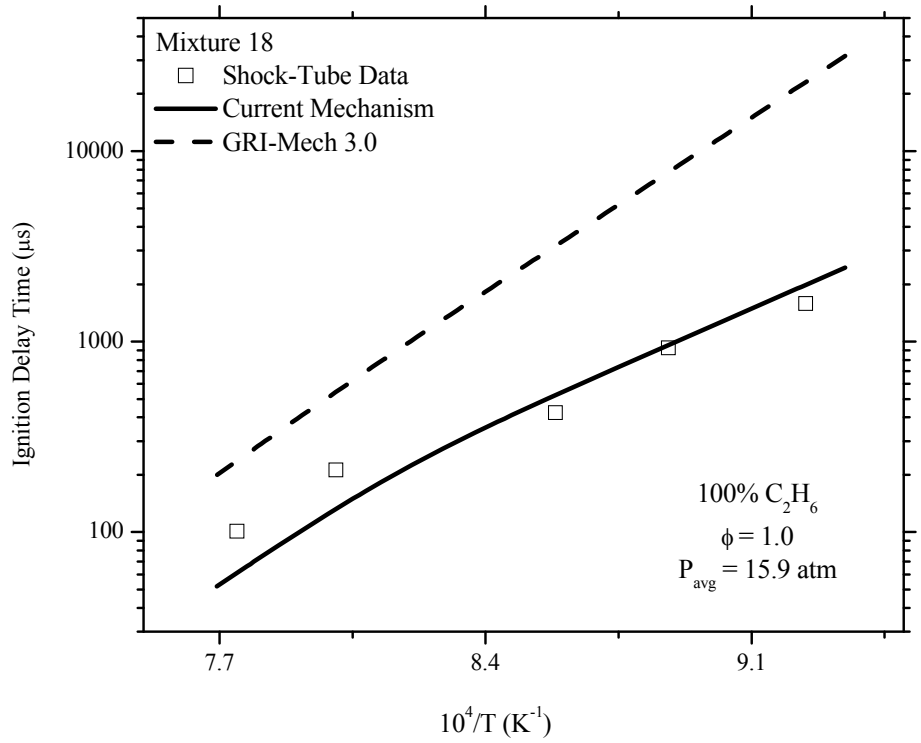

Figure 30. Experimental and modeled ignition data for mixture 18, diluted in 85% argon

Results for mixture 18 are shown in **Figure 30** with comparatively modeled ignition delay time data. This mixture, pure ethane with oxygen under stoichiometric conditions, is strongly over predicted by the GRI mechanism at relatively lower temperatures, almost an order of magnitude higher. The current mechanism shows excellent agreement at temperatures lower than 1150 K but shows a change in slope at higher temperatures that is not represented in the experimental data.

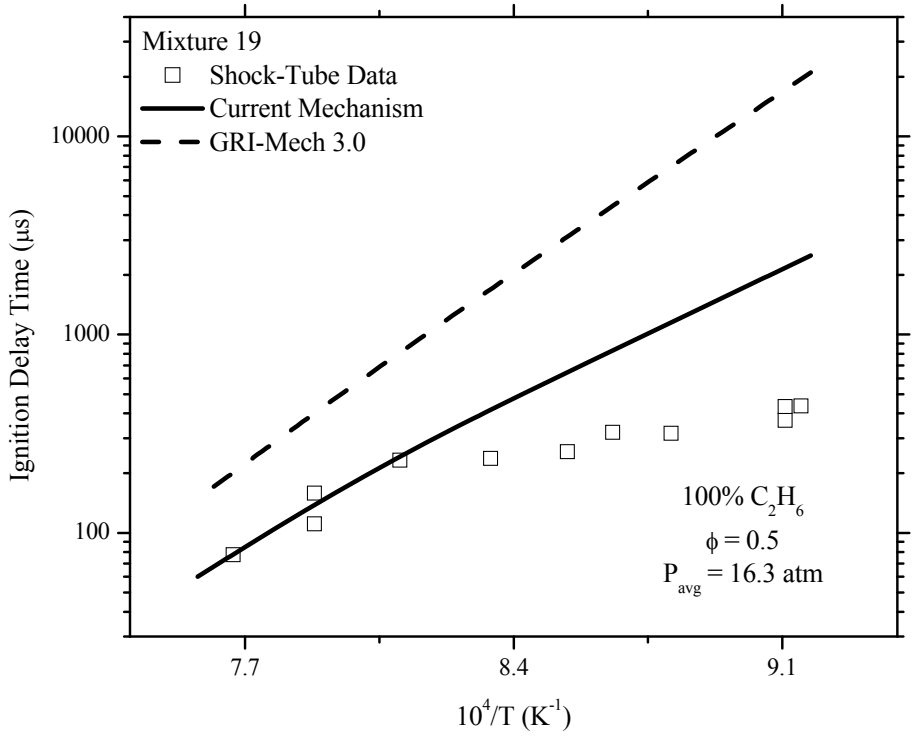

Figure 31. Experimental and modeled ignition data for mixture 19, diluted in 85% argon

Mixture 19, similar to mixture 18 with pure ethane but with an equivalence ratio of 0.5, is presented in **Figure 31** with modeled results. The same over prediction noted in mixture 18 with the GRI mechanism is apparent for mixture 19 with worse agreement at lower temperatures. The current mechanism shows to have better agreement at higher temperatures and predicts slower ignition at temperatures lower than 1240 K. This behavior is in contrast with the trend presented for mixture 18 in **Figure 30** which has the current mechanism agreeing at lower temperatures.

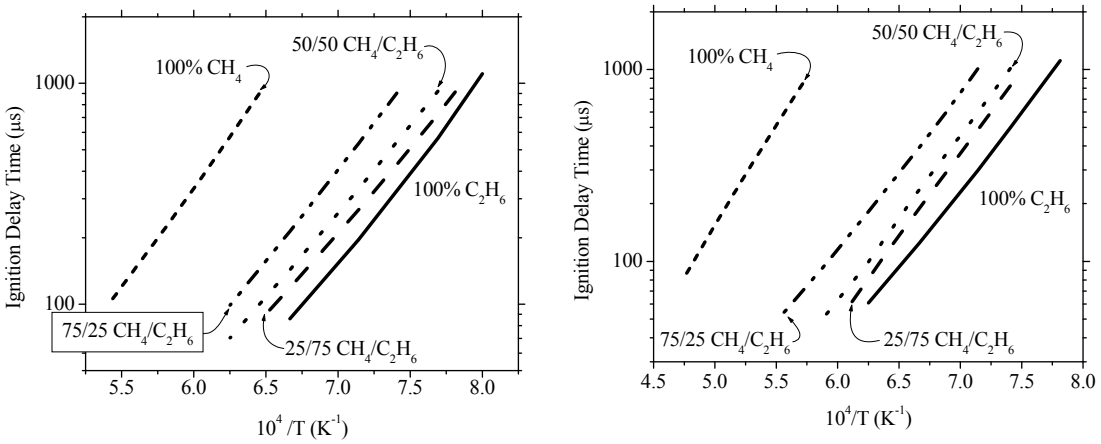

Figure 32. C4 model results for blends of methane and ethane diluted in 75% argon at 1 atm that are (a) stoichiometric and (b) fuel lean

Although improvements can be made in the current mechanism for certain mixtures and stiochiometries, it performs well enough to be able to use it for a parametric comparison on the impact of ethane on methane-ethane ignition. **Figure 32**a shows simulated results for the same equivalence ratio, stoichiometry, and dilution (75% in argon) over the range from 100% methane to 100% ethane. As expected, pure methane reacts the slowest in comparison. The addition of ethane with methane, as shown in experimental results, tends to increase the reaction rate and decrease the ignition delay time. **Figure 32** shows that there is a large change in ignition delay time by adding only 25% ethane, but the relative effect of increasing levels of ethane diminishes when more ethane is introduced.

Figure 32b shows the case for fuel-lean, $\phi = 0.5$, blends of methane and ethane diluted in 75% argon. The results in **Figure 32**b are very similar to those presented in

Figure 32a in that there exists a large change in reaction rate with the initial introduction of ethane, but this effect diminishes as more ethane is added. The difference between reaction times with addition of ethane provides an excellent test of a kinetics mechanism and can impact the selection of fuels with large percentages of ethane. It is recommended that an in-depth sensitivity analysis be performed to gain greater insight as to which reactions hold more importance at the points where experimental data and current models disagree the most.

Correlation Results

A correlation of the entire dataset presented in this work was performed to predict ignition delay times as a function of fuel blend, temperature, pressure and mixture concentration. The basic form of such a correlation is as follows:

$$\tau_{ign} = A[Fuel]^x[O_2]^y \exp\left(\frac{E_a}{RT}\right)$$

Where τ_{ign} is the ignition delay time in μs, [Fuel] is the fuel blend concentration in mol/cm^3, [O_2] is the oxygen concentration in mol/cm^3, A, x, y, z are constants, and E_a is termed the ignition activation energy and is given in the units kcal/mol. R is the gas constant given in kcal/mol-K units, and T is the temperature. This equation shows that ignition delay time depends on the exponential of inverse temperature and the mixture concentration to some power. Considering four of the five fuel blend ratios involved in this study (100/0, 75/25, 50/50, 25/75, of methane and ethane) a series of four correlations was generated for each specific fuel blend without the inclusion of pure ethane. As has been shown for mixtures 9, 10, 18 and 19 containing only ethane as a fuel

there exists slight shifts in slope that change temperature dependence and make correlation cumbersome and will not be considered here.

For the whole of the dataset considered for correlating, there is minimal presence of distinct shifts in slopes within the data as the temperatures investigated do not extend into the negative temperature coefficient (NTC) regions often seen in alkanes at temperatures lower than 1000 K. Due to the absence of any temperature dependence shift, it is adequate to generate one correlation per fuel blend ratio with the exception of pure ethane.

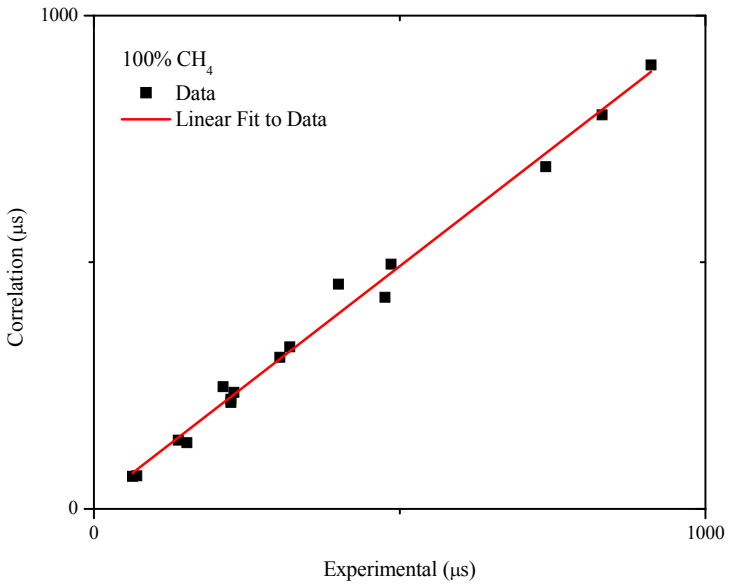

Figure 33. Correlation results derived from mixtures 4, 8, and 7

A correlation for a fuel blend of 100% methane is given as follows:

$$\tau_{ign} = 1.21 \times 10^{-5}[Fuel]^{0.36}[O_2]^{-1.05}\exp\left(\frac{40.4}{RT}\right)$$

and results for each experimental result are compared in **Figure 33**. This plot shows a goodness of fit, or R^2 value, of 0.99 and shows good representation over the range of data used to generate the temperature and pressure dependence. Mixtures 4, 8, and 7 were used and cover temperatures between 1223 – 2248 K and pressures up to 1.2 atm.

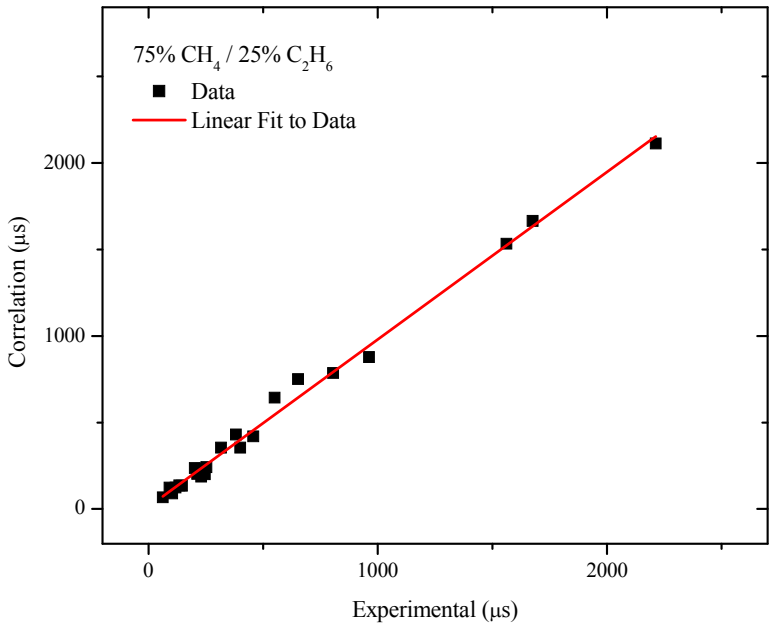

Figure 34. Correlation results derived from mixtures 1, 5, 11, and 15

A correlation for 75% methane and 25% ethane fuel blends is given in the following form:

$$\tau_{ign} = 1.304 \times 10^{-4}[Fuel]^{-0.90}[O_2]^{0.80}\exp\left(\frac{35.7}{RT}\right)$$

and is plotted against experimental results in **Figure 34** with an R^2 value of 0.993. This relation was formulated from mixtures 1, 5, 11, and 15 and is valid over the conditions

covered by the experimental data at temperatures of 1143 – 1670 K and pressures up to 28 atm.

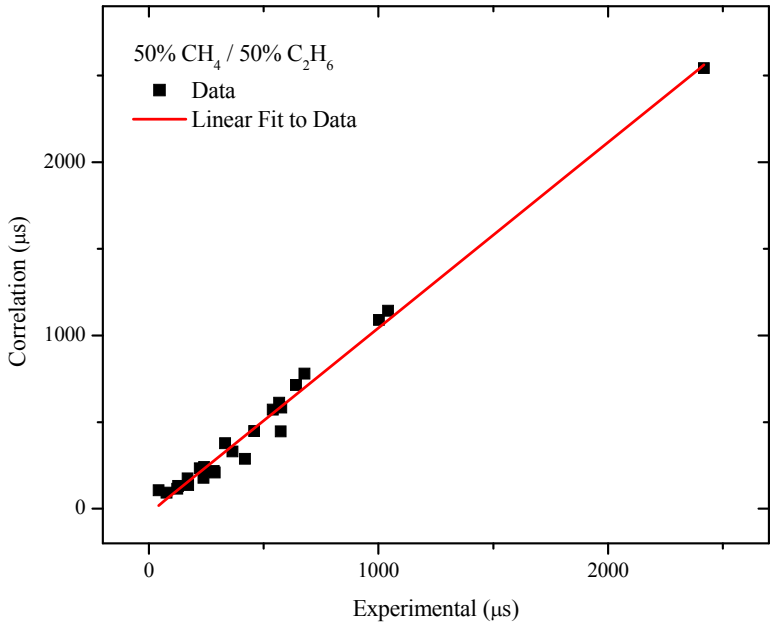

Figure 35. Correlation results derived from mixtures 2, 6, 12, and 16

For the fuel blend of 50% methane and 50% ethane, the following correlation has been developed:

$$\tau_{ign} = 2.83 \times 10^{-4}[Fuel]^{-0.65}[O_2]^{0.58}\exp\left(\frac{32.6}{RT}\right)$$

and is represented in **Figure 35** with an R^2 value of 0.987 when comparing experimental to correlated values. This correlation is valid for the conditions covered in mixtures 2, 6, 12, and 16, which are temperatures from 1094 – 1571 K and pressures up to 15.2 atm.

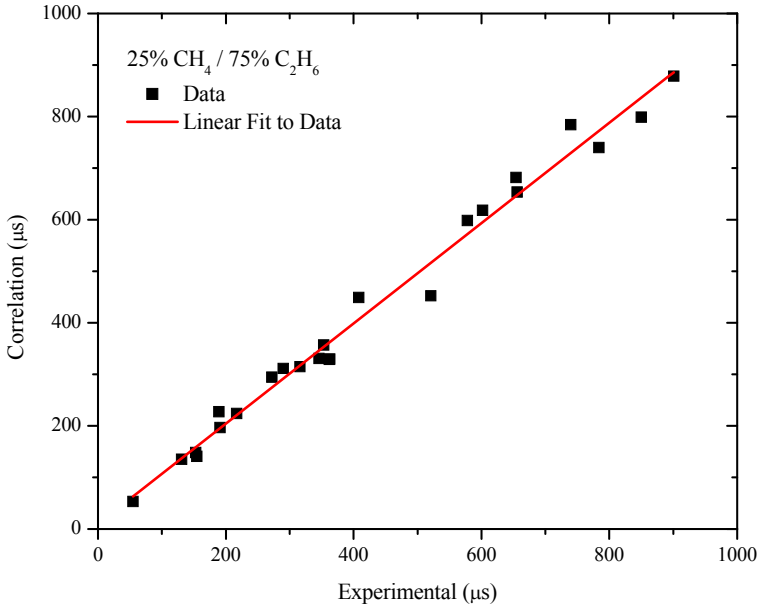

Figure 36. Correlation results derived from mixtures 3, 7, 13, and 14

Figure 36 shows results for a correlation of mixtures involving 25% methane and 75% ethane as a fuel source and is defined by the following:

$$\tau_{ign} = 8.82 \times 10^{-8}[Fuel]^{0.47}[O_2]^{-1.04}\exp\left(\frac{39.6}{RT}\right)$$

and has an R^2 value of 0.985 when plotted with experimental results. This correlation is only considered to be valid over the conditions involved with mixtures 3, 7, 13, and 14 for temperatures between 1154 and 1700 K and pressures up to 16 atm.

CHAPTER V

CONCLUSIONS AND RECOMMENDATIONS

Summary

Shock tubes are useful for studying reaction chemistry at a wide variety of temperatures and pressures. A new shock-tube facility has been built to investigate post-reflected shock pressures up to 100 atm and temperatures between 600 and 4000 K with applicability to gas-phase, vaporization, atomization, and solid particulate studies. The shock tube has a large-diameter driven section (15.24 cm) which limits boundary layer effects that can lead to uncertainty in determination of experimental conditions. Stainless steel 304 was used for construction of the shock tube because of its high strength and generally inert nature when in the presence of media typical of combustion research. A large number of access ports, 25 in all, have been built into the side of the shock tube test section to facilitate the implementation of optical and sensor diagnostics.

A smart gas delivery system was designed to help reduce turnaround time between experiments. Advanced vacuum staging is utilized to obtain pressures as low as 10^{-6} Torr before diaphragm rupture. Further reducing experiment run time is the unique diaphragm replacement breech loader that can support the use of lexan diaphragms and pre-scored aluminum discs at varying thicknesses. Diaphragm versatility allows for the wide range of pressures obtainable in this facility. Shock-tube wall perturbations are minimized by way of port design and weldless flange interfaces between portions of the modular driven section. The interior of the shock tube is polished to a 1-μm RMS or

better surface finish to limit any fluid mechanic disturbances during shock formation and travel leading to non-ideal gas dynamic effects.

An extensive ignition delay time study was performed in this new facility on a comprehensive set of methane and ethane fuel blends. Varying mixtures of 100/0, 75/25, 50/50, 25/75, and 0/100 concentration percentages of methane and ethane were reacted with oxygen at varying stoichiometries, ϕ = 0.5, 1.0, and 2.0, diluted in 98%, 95%, 85%, and 75% argon. Pressures of the mixtures ranged from 1 to 28 atm and temperatures between 1082 and 2248 K. The data set is comprised of 19 mixtures which have varying levels of fuel-blend ratio, stoichiometry, dilution, and pressure; and was chosen in such a way to sample the entire parameter space without choosing every possible iteration.

It was found in this study that models perform reasonably well for mixtures of methane and ethane at highly dilute conditions. For mixtures where dilution reflects that of real fuel-air conditions, results between the models investigated are mixed. The GRI-Mech 3.0 model tends to perform poorly over the range of low-dilution cases, with varying severity as levels of ethane increase when compared to methane. The current model performs better at higher fuel-oxidizer concentrations although there still exist areas for needed improvement.

Recommendations

It is recommended that more mixtures at varying levels of fuel blend ratio and stoichiometry be performed at higher pressure levels, around 25 atm, to balance the range of low- and high-pressure data. Also of considerable interest would be a complete and thorough sensitivity analysis to highlight important reactions at dilution and pressure

ranges not previously well studied before this work. An all-encompassing master correlation of the entire data set presented, including pure ethane chemistry, in this work would be beneficial. Species time histories of the radicals important in combustion, such as OH* and CH* at varying conditions and with different mixtures would be helpful to validate kinetics models and is recommended.

REFERENCES

Amadio, A.R., Crofton, M.W., and Petersen, E.L. 2006. Test-time extension behind reflected shock waves using CO_2-He and C_3H_8-He driver mixtures. *Shock Waves*, **16**, 157.

Bourque, G., Healy, D., Curran, H., Zinner, C., Kalitan, D., de Vries, J., Aul, C., and Petersen, E. 2008. Ignition and flame speed kinetics of two natural gas blends with high levels of heavier hydrocarbons. ASME Paper GT2008-51344.

Ciezki, H.K., and Adomeit, G. 1993. Shock-tube investigation of self-ignition of *n*-heptane-air mixtures under engine relevant conditions. *Combust. Flame*, **93**, 421

Cooke, D.F., and Williams, A. 1975. Shock tube studies of methane and ethane oxidation. *Combust. Flame*, **24**, 245.

de Vries, J., Hall, J.M., Simmons, S.L., Rickard, M.J.A., Kalitan, D.M., and Petersen, E.L. 2007. Ethane ignition and oxidation behind reflected shock waves. *Combust. Flame*, **150**, 137.

de Vries, J., and Petersen, E.L. 2007. Autoignition of methane-based fuel blends under gas turbine conditions. *Proc. Combust. Inst.*, **31**, 3163.

Energy Information Administration. 2008. *2008 Annual Energy Review*. DOE/EIA-0384(2008), Washington, DC. http://www.eia.doe.gov/emeu/aer.

Fieweger, K., Blumenthal, R., and Adomeit, G. 1997. Self-ignition of S.I. engine model fuels: A shock tube investigation at high pressure. *Combust. Flame*, **109**, 599.

Gayden, A.G., and Hurle, I.R. 1963. *The Shock Tube in High Tmperature Chemical Physics*, Reinhold, New York, NY.

Goy, C.J., Moran, A.J., and Thomas, G.O. 2001. Autoignition characteristics of gaseous fuels at representative gas turbine conditions. ASME Paper GT-0051.

Healy D., Curran H.J., Simmie J.M., Kalitan D.M., Zinner C.M., Barrett A.B., Petersen E.L., and Bourque G. 2008. Methane/ethane/propane mixture oxidation at high pressures and at high, intermediate and low temperatures. *Combust. Flame*, **155**, 441.

Herzler, J., Jerig, L., and Roth, P. 2005. Shock-tube study of the ignition of lean *n*-heptane/air mixtures at intermediate temperatures and high pressures. *Proc. Combust. Inst.*, **30**, 147.

Herzler, J., Jerig, L., and Roth, P. 2004. Shock-tube study of the ignition of propane at intermediate temperatures and high pressures. *Combust. Sci. Technol.*, **176**, 1627.

Huang, J., and Bushe, W.K. 2006. Experimental and kinetic study of autoignition in methane/ethane/air and methane/propane/air mixtures under engine-relevant conditions. *Combust. Flame*, **144**, 74.

Kee, R.J., Rupley, F.M., Miller, J.A., Coltrin, M.E., Grcar, J.F., Meeks, E., Moffat, H.K., Lutz, A.E., Dixon-Lewis, G., Smooke, M.D., Warnatz, J., Evans, G.H., Larson, R.S., Mitchell, R.E., Petzold, L.R., Reynolds, W.C., Caracotsios, M., Stewart, W.E., Glarborg, P., Wang, C. and Adigun, O. 2004. *Chemkin Collection, Release 4.1.1*, Reaction Design, Inc., San Diego, CA.

Lamoureux, N., and Paillard, C.–E. 2003. Natural gas ignition delay times behind reflected shock waves: Application to modeling and safety. *Shock Waves*, **13**, 57

Lefebvre, A.H. 1999. *Gas Turbine Combustion*, 2nd Ed., Taylor and Francis, Philadelphia, PA.

Lieuwen, T., McDonell, V., Petersen, E.L., and Santavicca, D. 2006. Fuel flexibility influences on pre-mixed combustor blowout, flashback, autoignition, and stability. ASME Paper GT2006-90770.

Lund, C.M., and Chase, L. 1995. HCT-A general computer program for calculating time-dependent phenomena involving one-dimensional hydrodynamics, detailed chemical kinetics and transport. Rep. UCRL-52504, Lawrence Livermore National Laboratory, Livermore, CA.

Petersen, E.L. 2009. Interpreting endwall and sidewall measurements in shock-tube ignition studies. *Combust. Sci. Technol.*, **181**, 1123.

Petersen, E.L., Davidson, D.F., and Hanson, R.K. 1999. Kinetics modeling of shock-induced ignition in low-dilution CH_4/O_2 mixtures at high pressures and intermediate temperatures. *Combust. Flame*, **117**, 272.

Petersen, E.L., Hall, J.M., Smith, S.D., de Vries, J., Amadio, A.R., and Crofton, M.W. 2007a. Ignition of lean methane-based fuel blends at gas turbine pressures. *ASME JEGTP*, **129**, 937.

Petersen, E.L., Kalitan, D.M., Simmons, S., Bourque, G., Curran, H.J., and Simmie, J.M. 2007b. Methane/Propane oxidation at high pressures: Experimental and detailed chemical kinetic modeling. *Proc. Combust. Inst.*, **31**, 447.

Petersen, E. L., Lamnaouer, M., de Vries, J., Curran, H., Simmie, J., Fikri, M., Schulz, C., and Bourque, G. 2009. Discrepancies between shock tube and rapid compression machine ignition at low temperatures and high pressures. In Hannemann, K., and Seiler, F. eds. *Shock Waves: 26th International Symposium on Shock Waves*, 1st Ed., Springer-Verlag Berlin Heidelberg, Berlin, Germany.

Petersen, E.L., Rickard, M.J.A., Crofton, M.W., Abbey, E.D., Traum, M.J., and Kalitan D.M. 2005. A facility for gas- and condensed-phase measurements behind shock waves. *Meas. Sci. Technol.*, **16**, 1716.

Petersen, E.L., and de Vries, J. 2005. Measuring the ignition of fuel blends using a design of experiments approach. AIAA Paper 2005-1165.

Rotavera, B., and Petersen, E.L. 2007. Shock-tube combustion studies of atomized fuels in the reflected-shock region. AIAA Paper 2007-5687.

Smith, G.P., Golden, D.M., Frenklach, M., Moriarty, N.W., Eiteneer, B., Goldenberg, M., Bowman, C.T., Hanson, R.K., Song, S., Gardiner, Jr., W.C., Lissianski, V.V., Qin, Z., *GRI-Mechanism 3.0*, http://www.me.berkeley.edu/gri_mech/ [Cited June 25, 2008].

Spadaccini, L.J., and Colket III, M.B. 1994. Ignition delay characteristics of methane fuels. *Prog. Energy Combust. Sci.*, **20**, 431.

Walker, B. 2007. *Shock-Tube Investigation of Ignition Delay Times of Blends of Methane and Ethane with Oxygen*. M.S. Thesis. University of Central Florida, Orlando.

Zhukov, V.P., Sechenov, V.A., and Starikovskii, A.Yu. 2005. Self-ignition of a lean mixture of n-pentane and air over a wide range of pressures. *Combust. Flame*, **140**, 196.

APPENDIX A

The shock tube experiment was designed completely in house with both detailed custom parts and equipment from commercial manufacturers. Parts fabricated for use in this facility are detailed herein with shop-ready drawings for reference. The application for each part as well as how each part interacts with the whole is described with further detail in Chapter II.

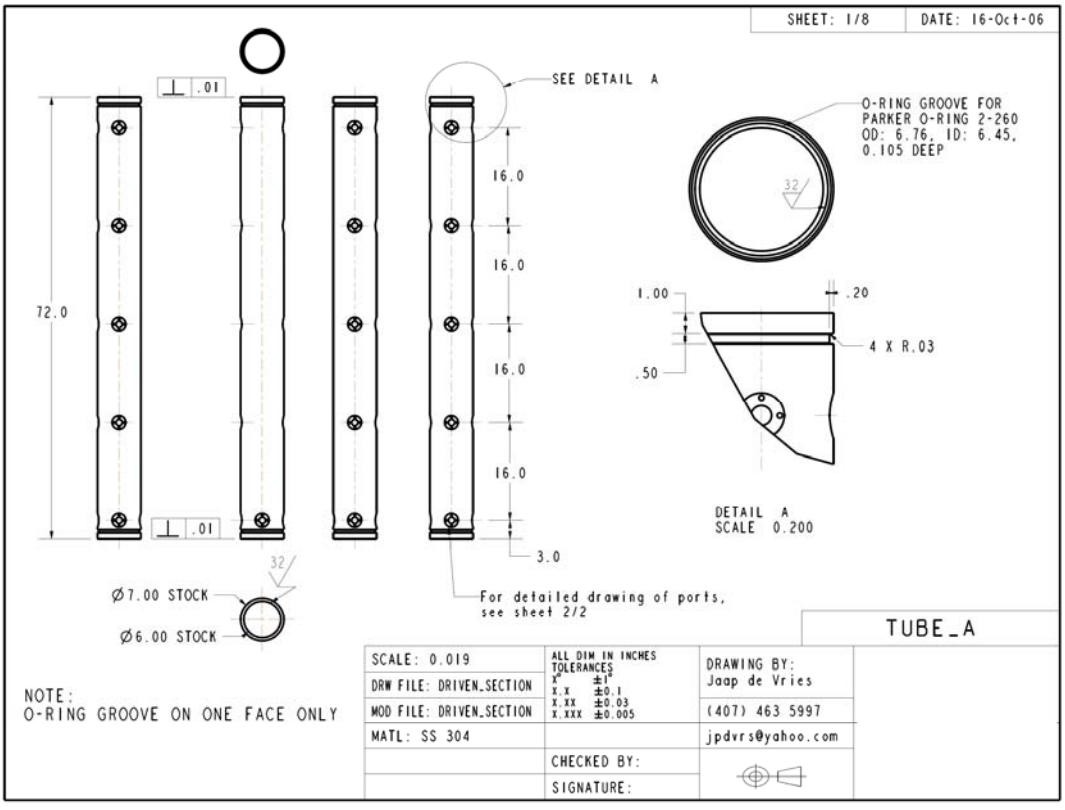

Figure A1. Test section of the shock tube located at the end of the driven side with multiple ports located across from each other for sensor and optical access

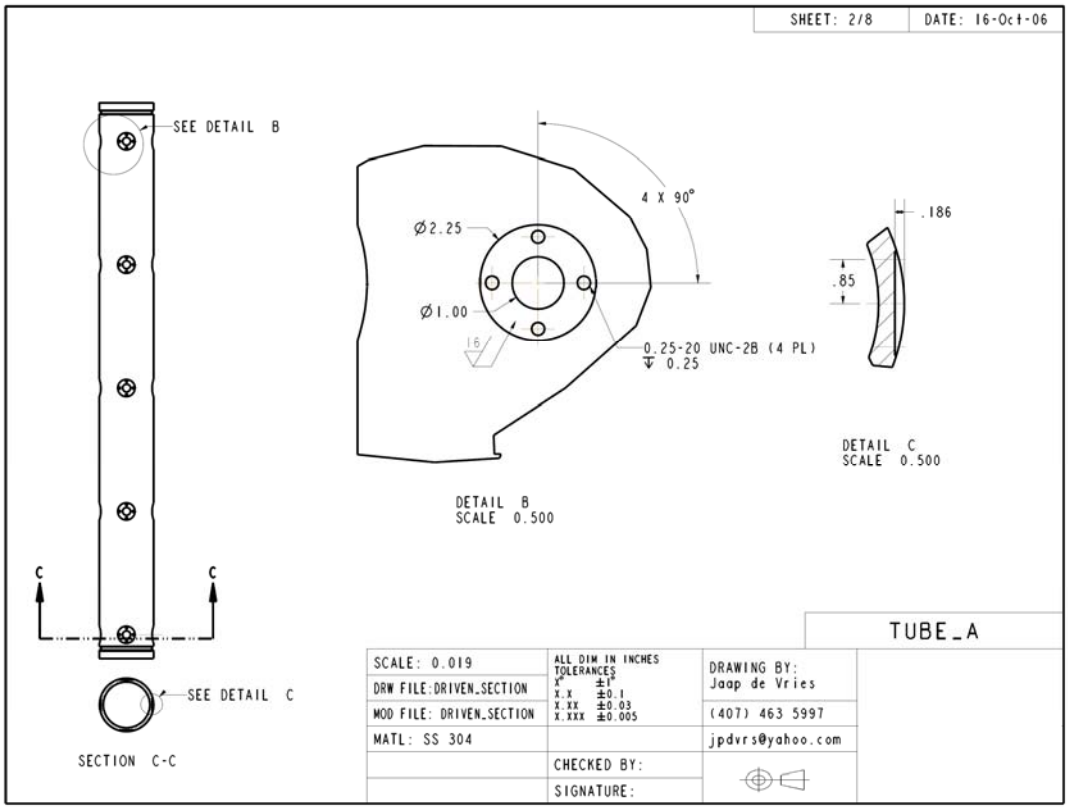

Figure A2. Detail of port locations at side of driven section portion of the shock tube

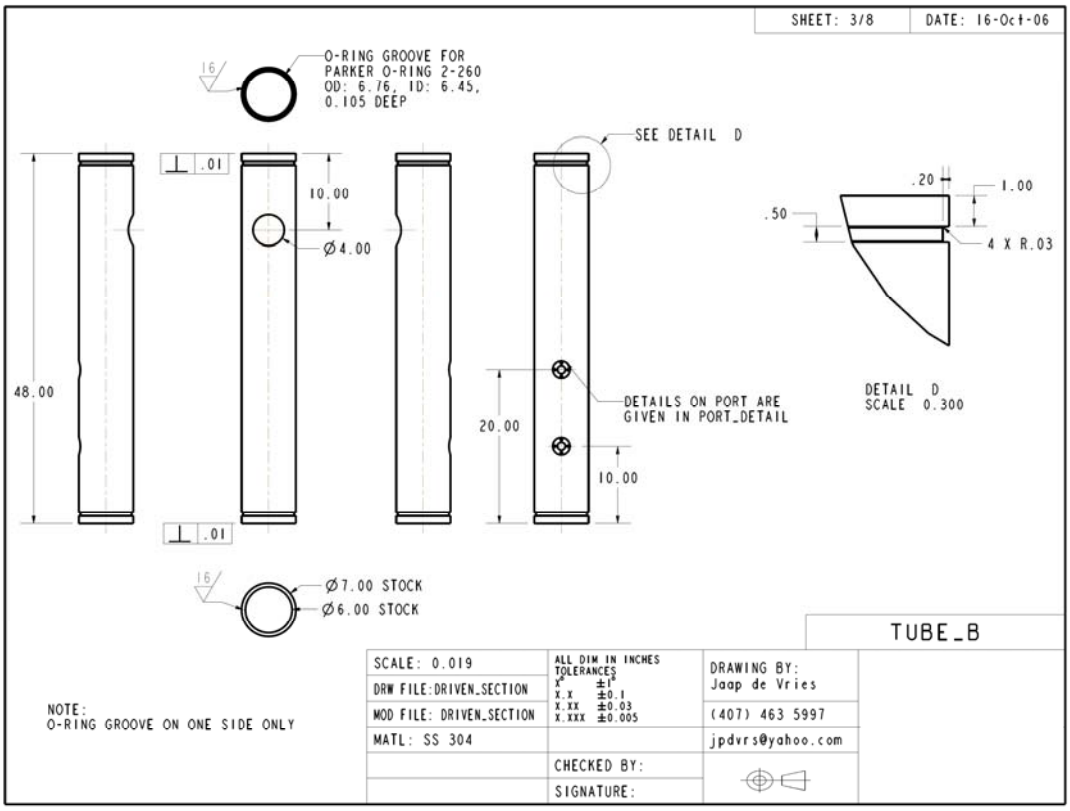

Figure A3. Portion of driven section which is located closest to the diaphragm loader. Note large diameter access for branch to vacuum manifold section via the Tube Branch detailed in Figure A4

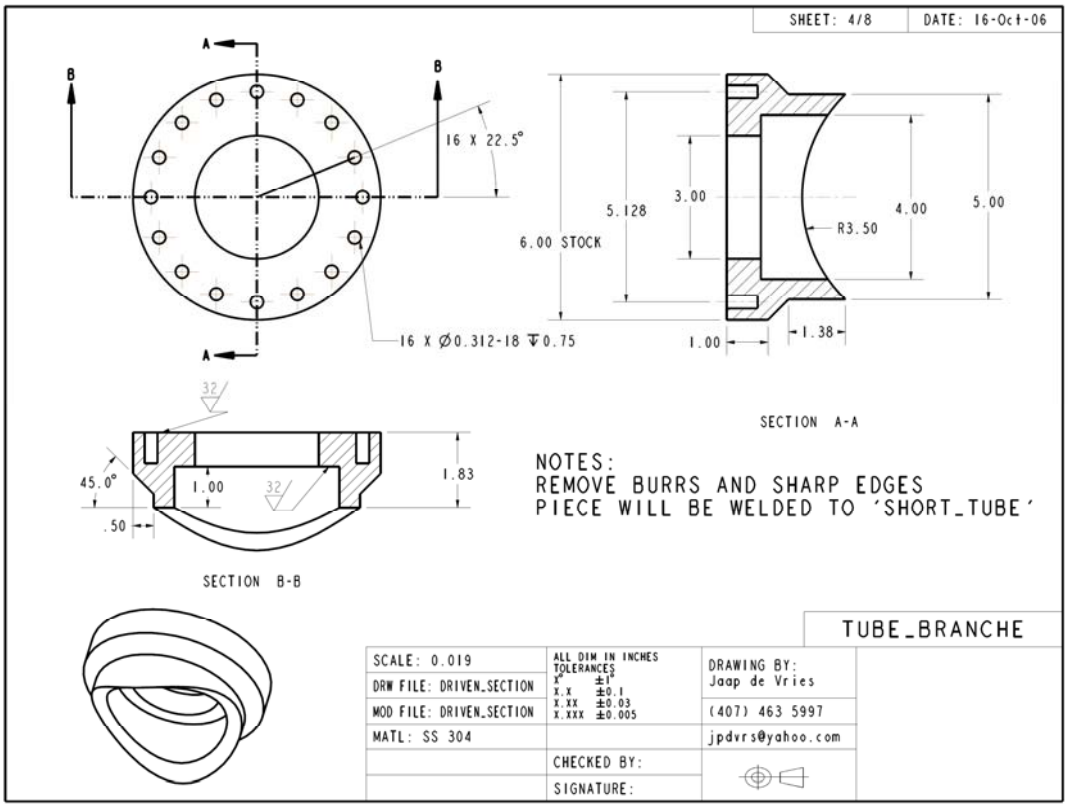

Figure A4. Tube branch interface that extends from Tube B in Fig. A3 into the vacuum manifold

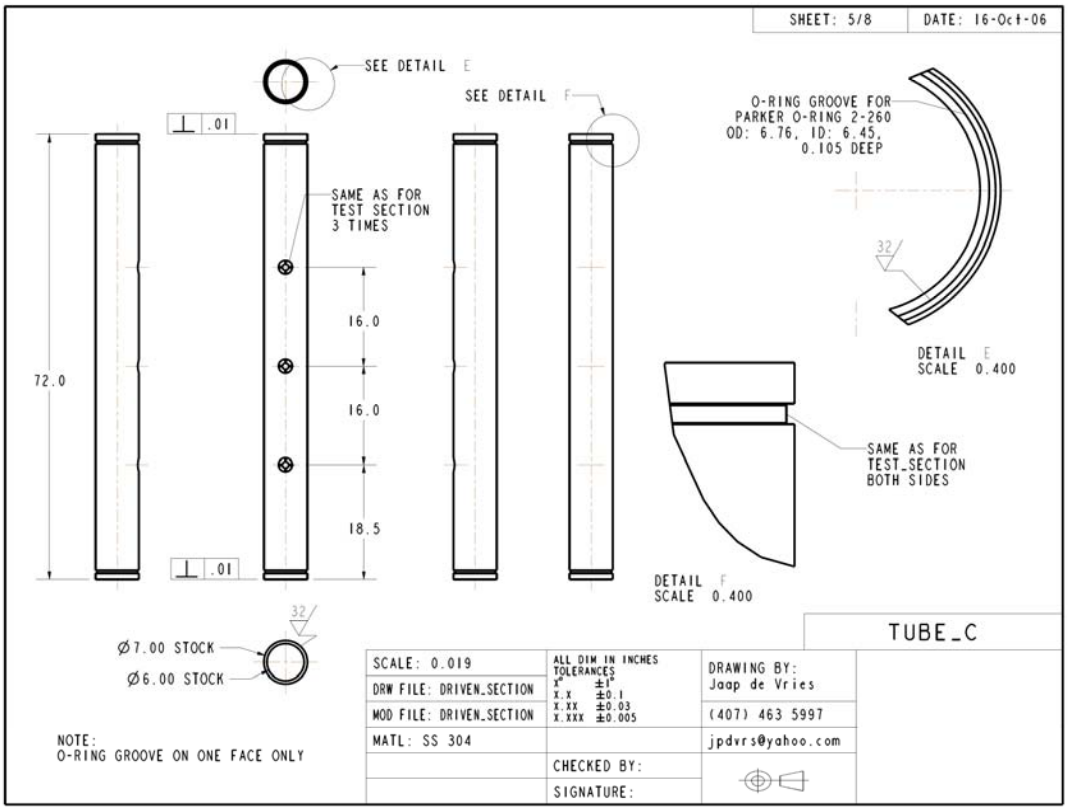

Figure A5. Intermediate tube section that is located between Tube A and Tube B, detailed in Figs. A1 and A3, with several access ports for diagnostics

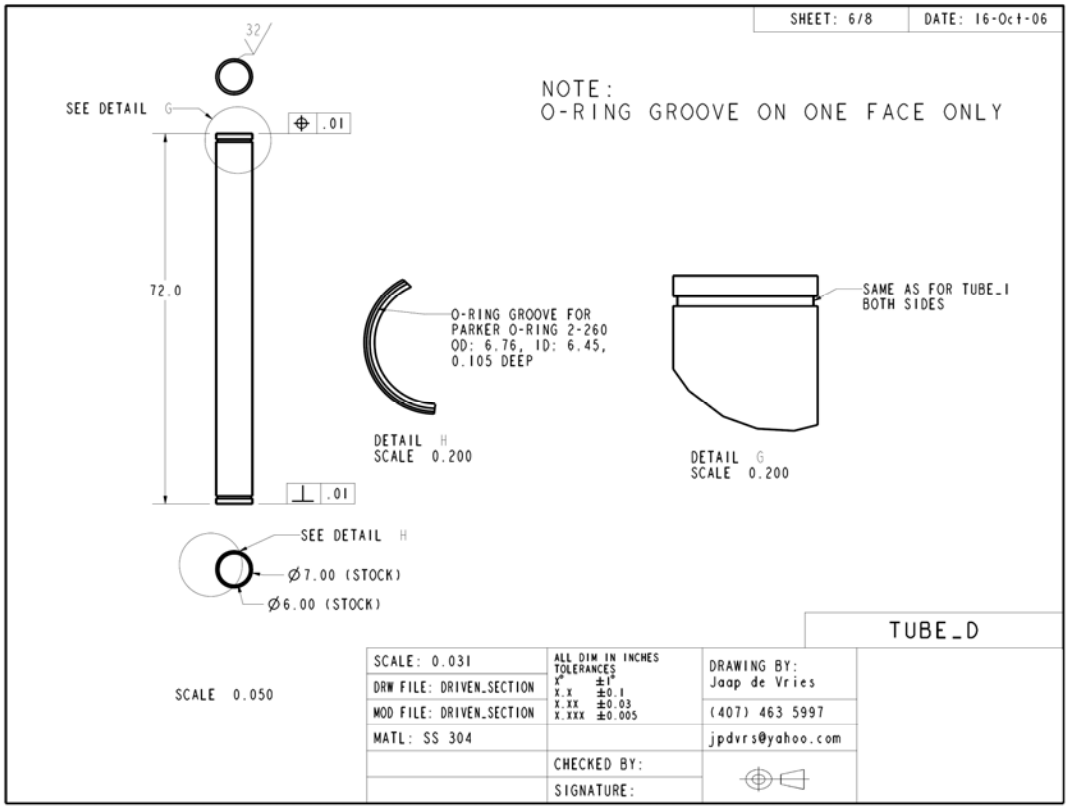

Figure A6. Six foot tube section similar to others located in the driven section for use as separate volume, i.e. mixing tank, or optional interface with shock tube experiment

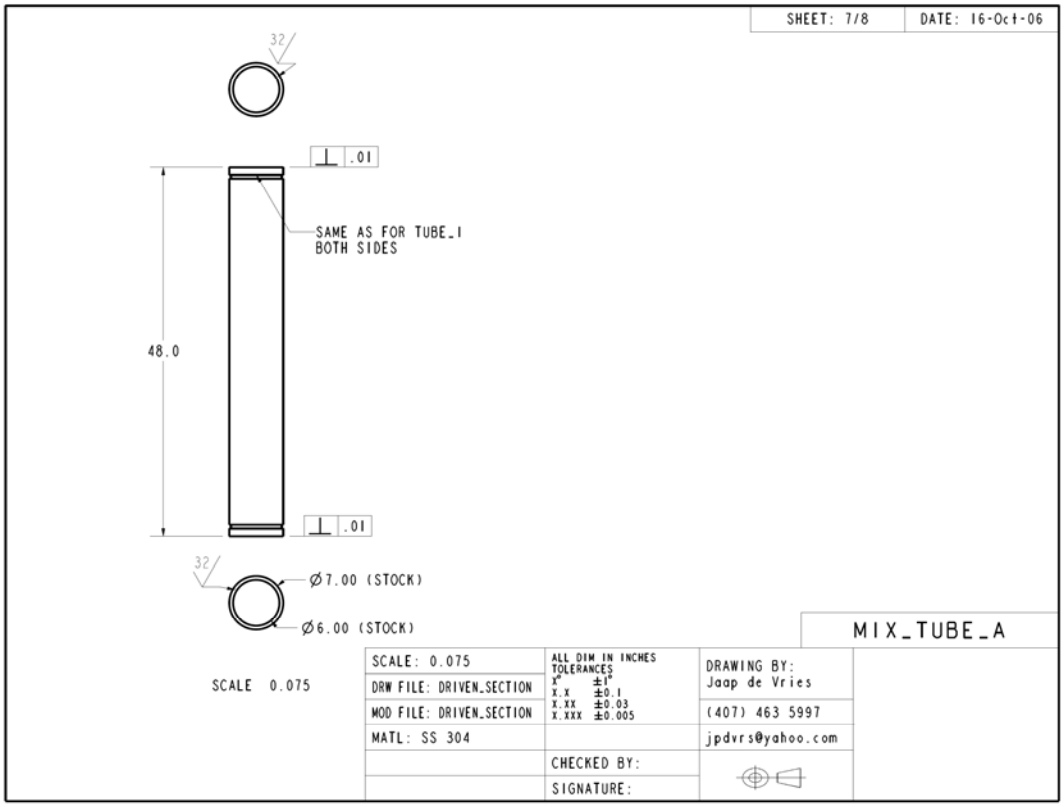

Figure A7. Tube similar to driven section of shock tube for use as a mixing volume for fuel and oxidizer mixtures

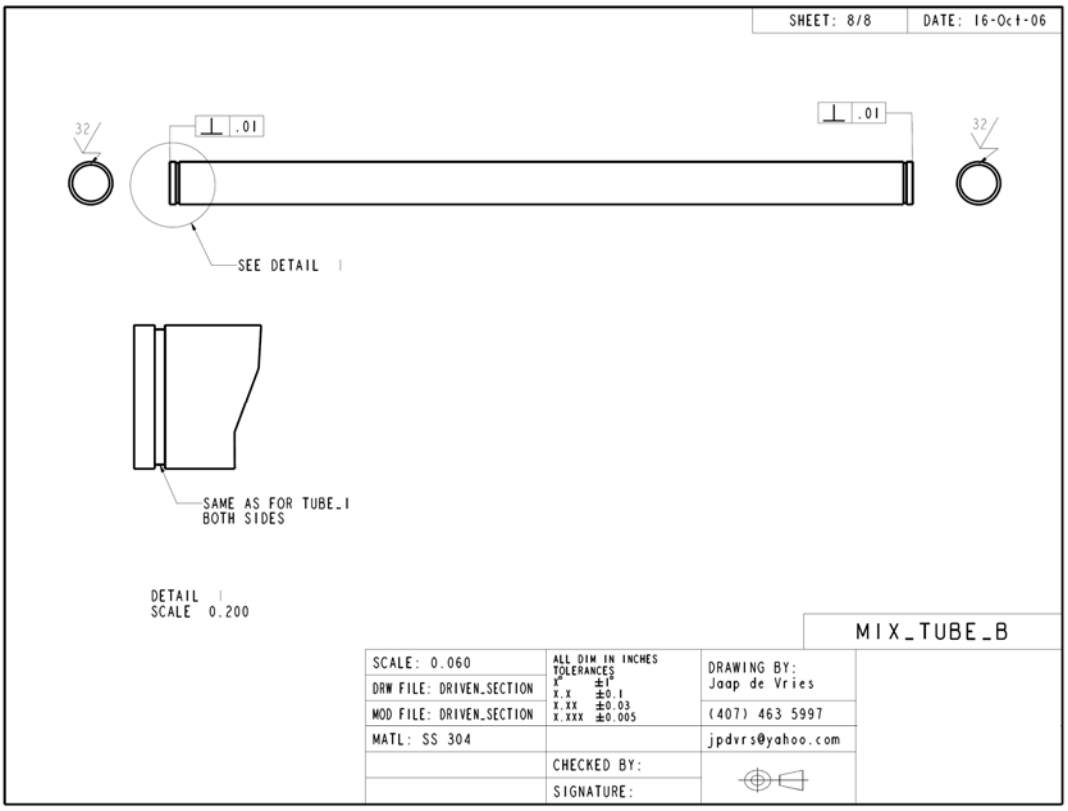

Figure A8. Mixing vessel similar to that shown in Fig A7 with a length of 10 ft

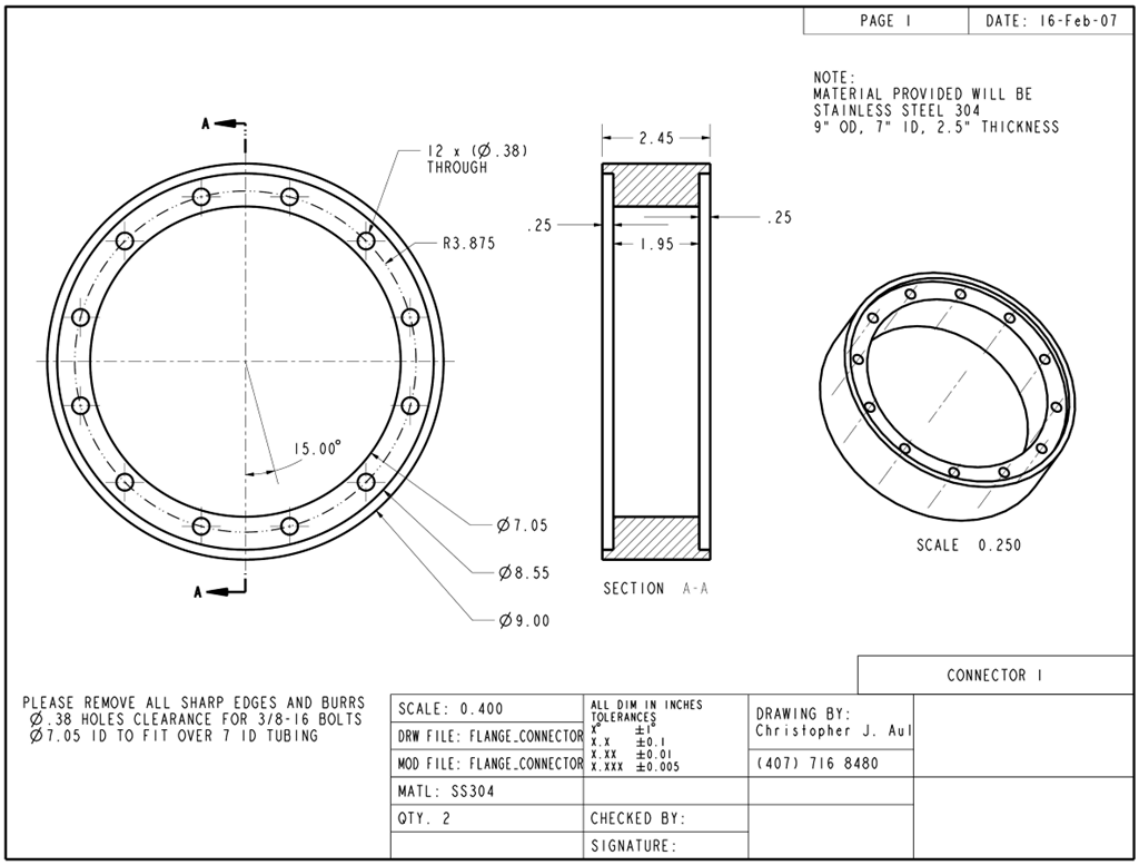

Figure A9. Connector piece that fits in between weldless flange design employed in shock tube

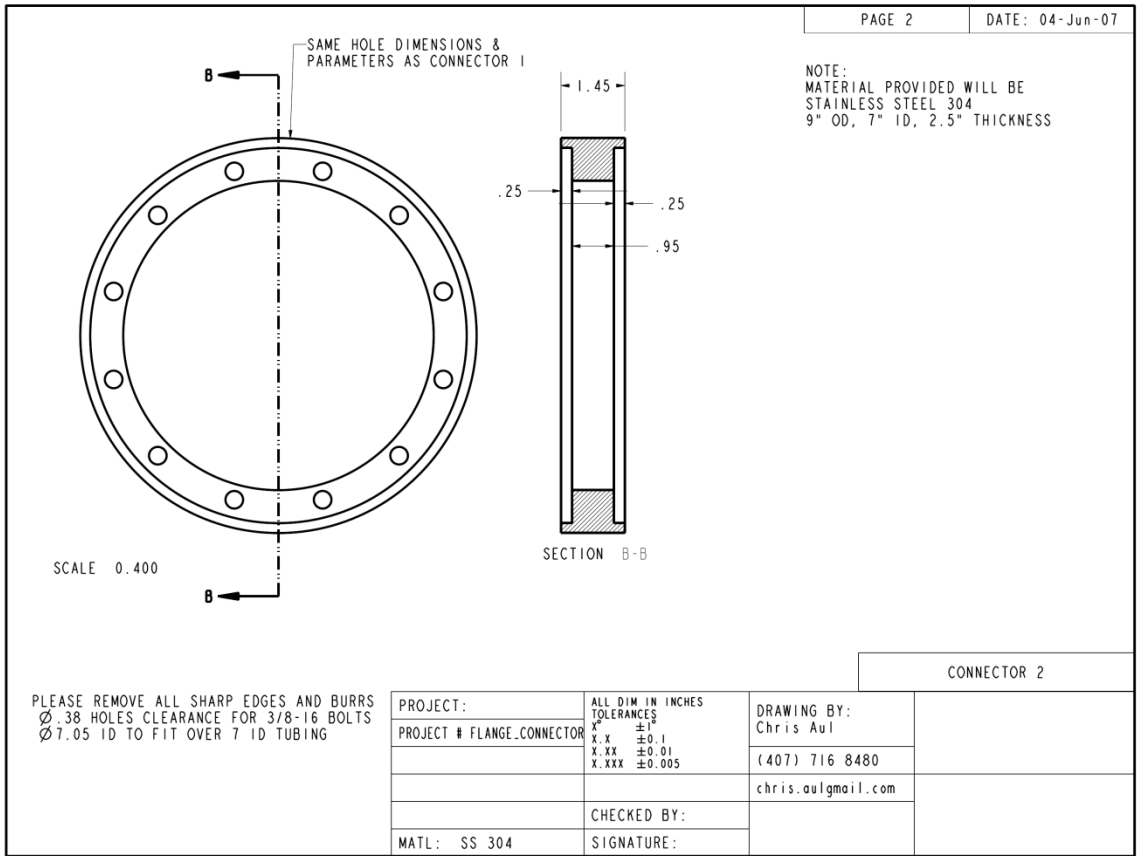

Figure A10. Connector similar to one shown in Figure A9 with shorter length for use on end pieces of both the shock tube and mixing tanks

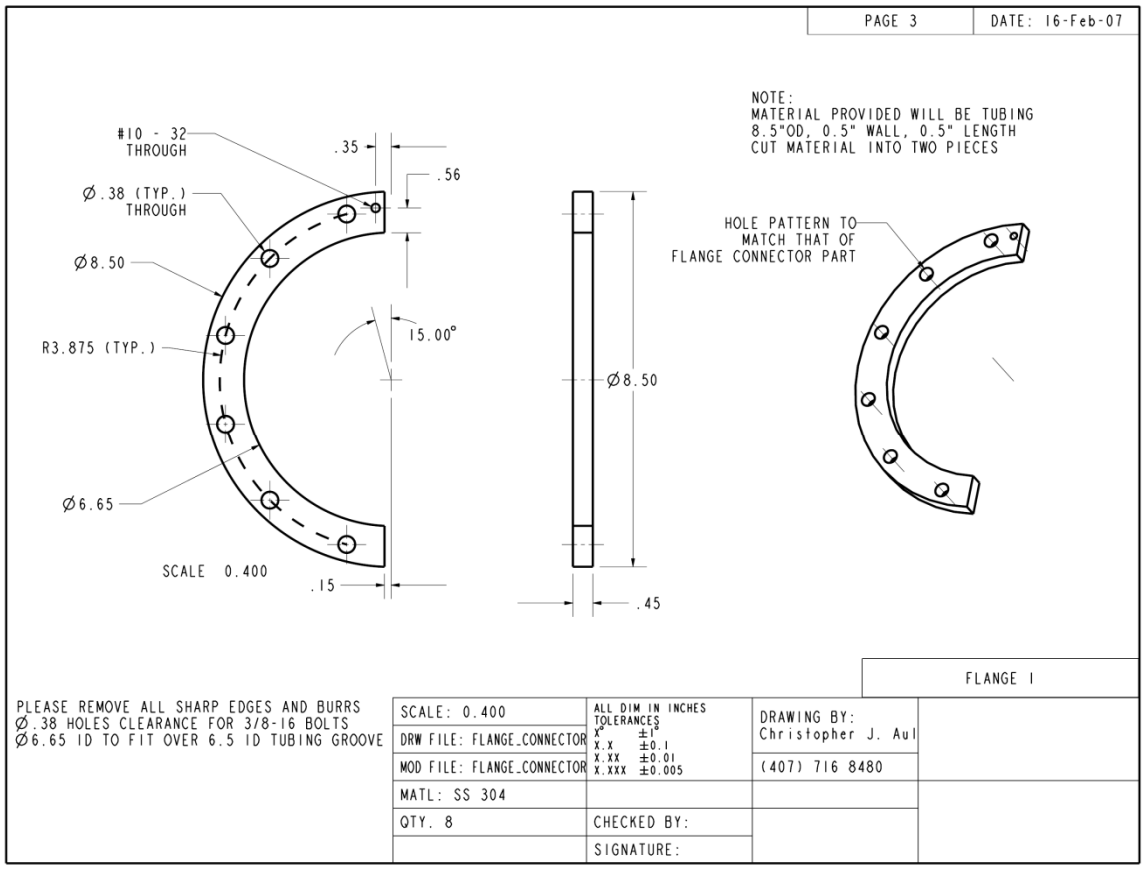

Figure A11. Flange portion that fits into groove detailed in Figs A1 through A8 in order to complete compression style fitting between two adjoining sections. Shown here is the style with through holes as opposed to design found in Fig A12 with threaded holes

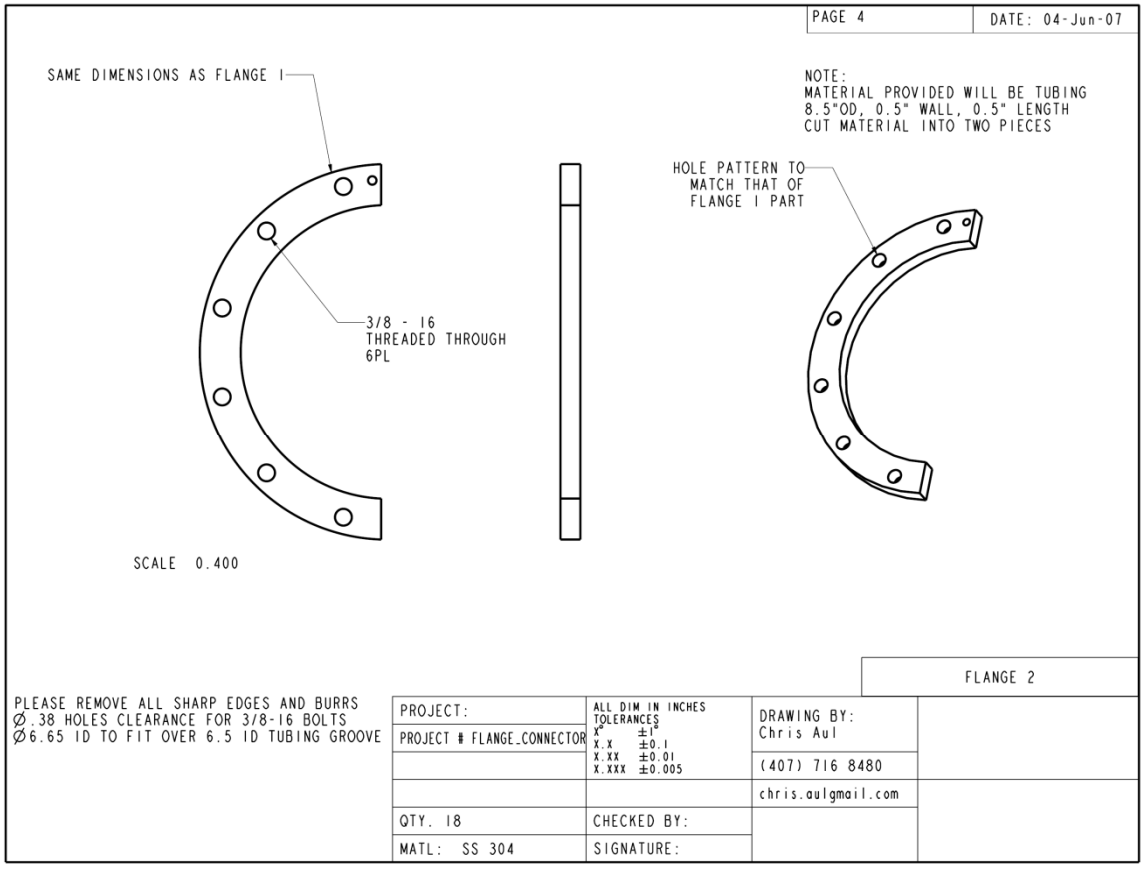

Figure A12. Flange similar to Figure A11 with 3/8-16 threaded holes for bolts used to adjoin weldless connection

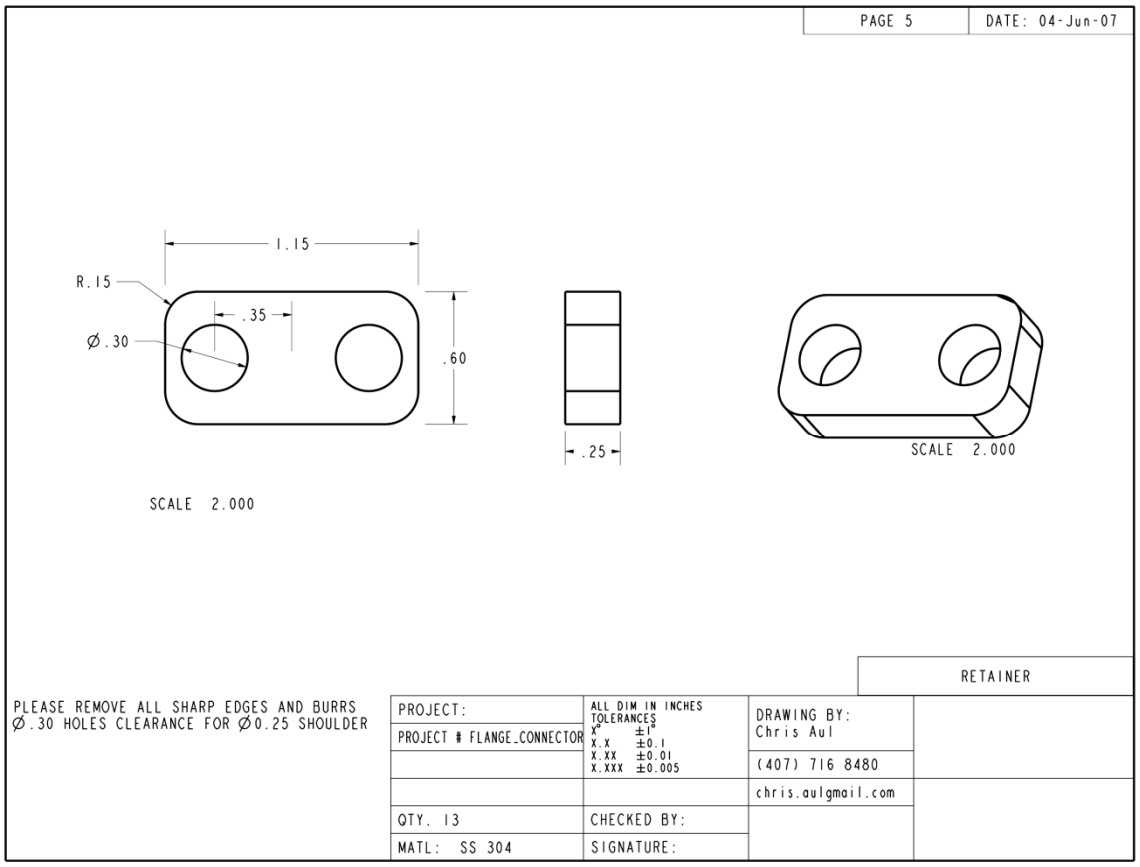

Figure A13. Retainer designed to simply keep two similar semi-circle flange pieces detailed in Figs A11 and A12 together when changing flange pieces or removing endwall sections for inspection and/or diagnostic implementation

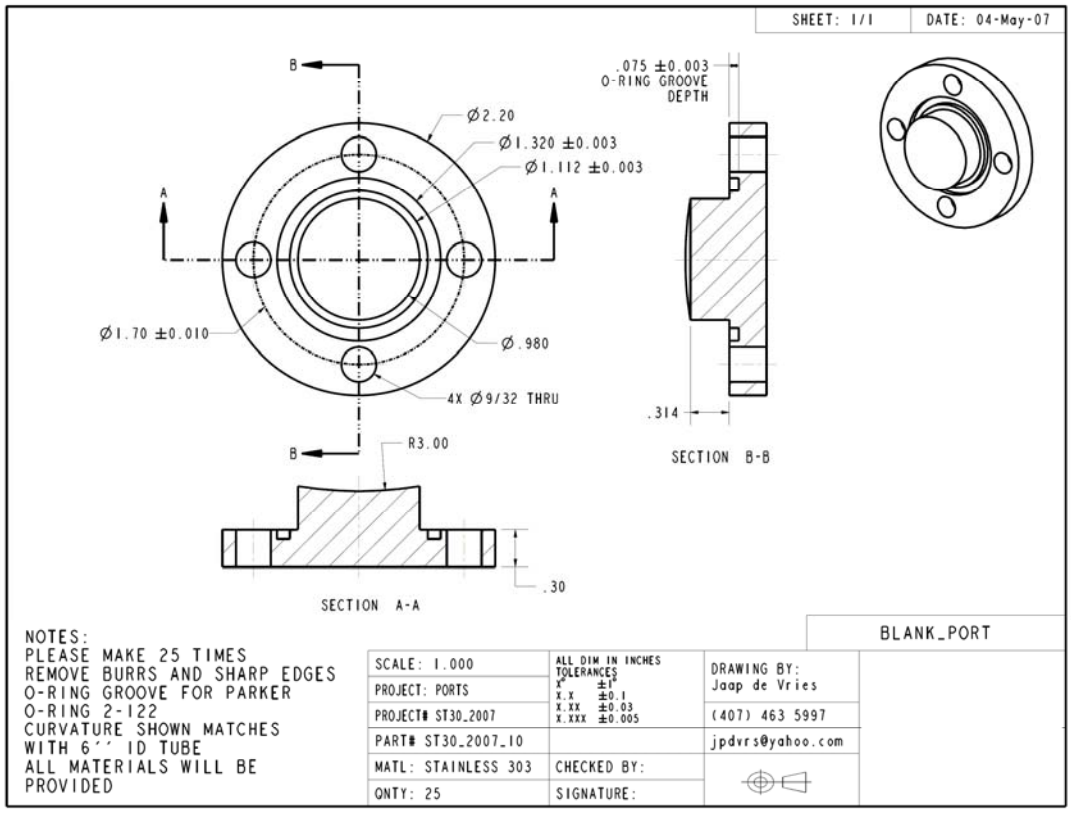

Figure A14. Sidewall port for use on parts detailed in Figs A1 through A5. Shown as blank version to be fitted with various sensors, inlets, or optical media

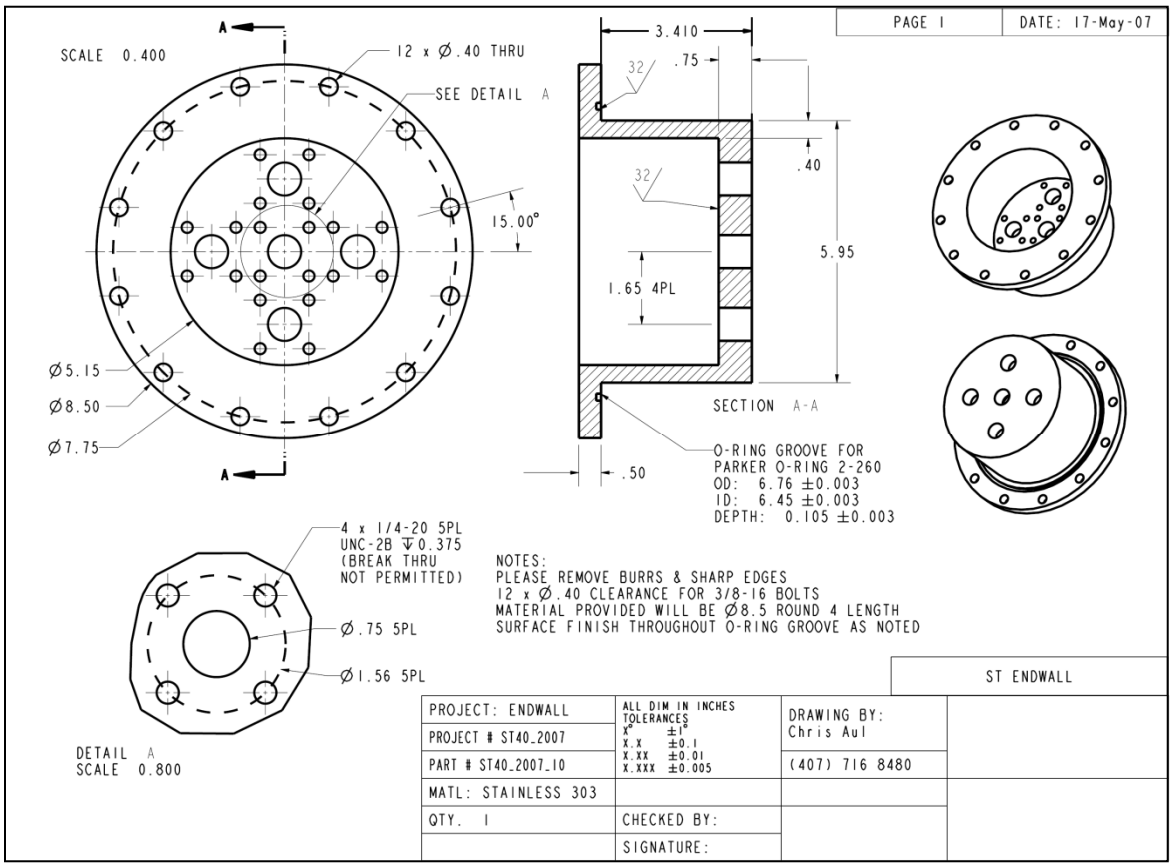

Figure A15. Endwall of driven section of the shock tube. Available to the experiment are five port locations designed to fit in item shown in Figure A18. This part is designed to extend inside the end of the shock tube for precise sidewall diagnostics 1.6 cm away from fitted endwall location

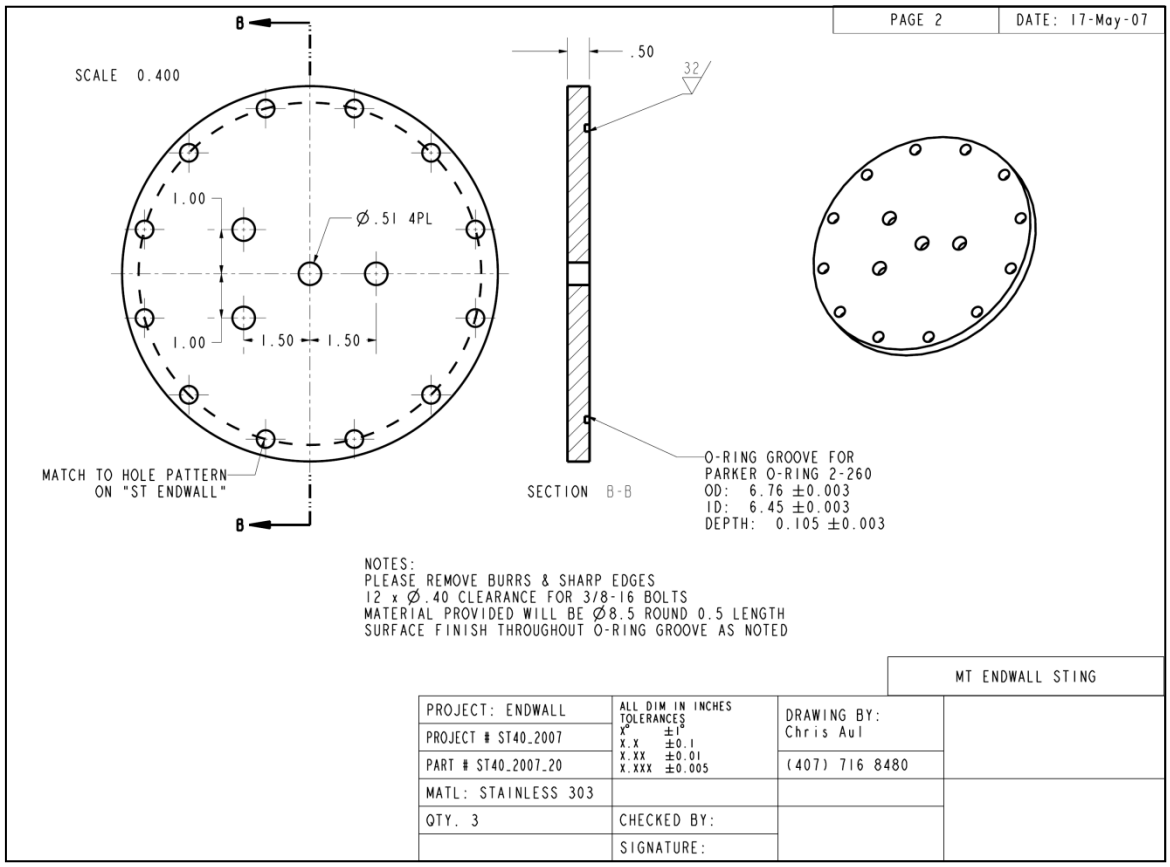

Figure A16. Endwall for mixing tank with hole locations for access. Center location hole designed to fit appropriately sized "stinger" – tubing which extends into the tank volume with multiple holes throughout designed to induce turbulent mixing during fill

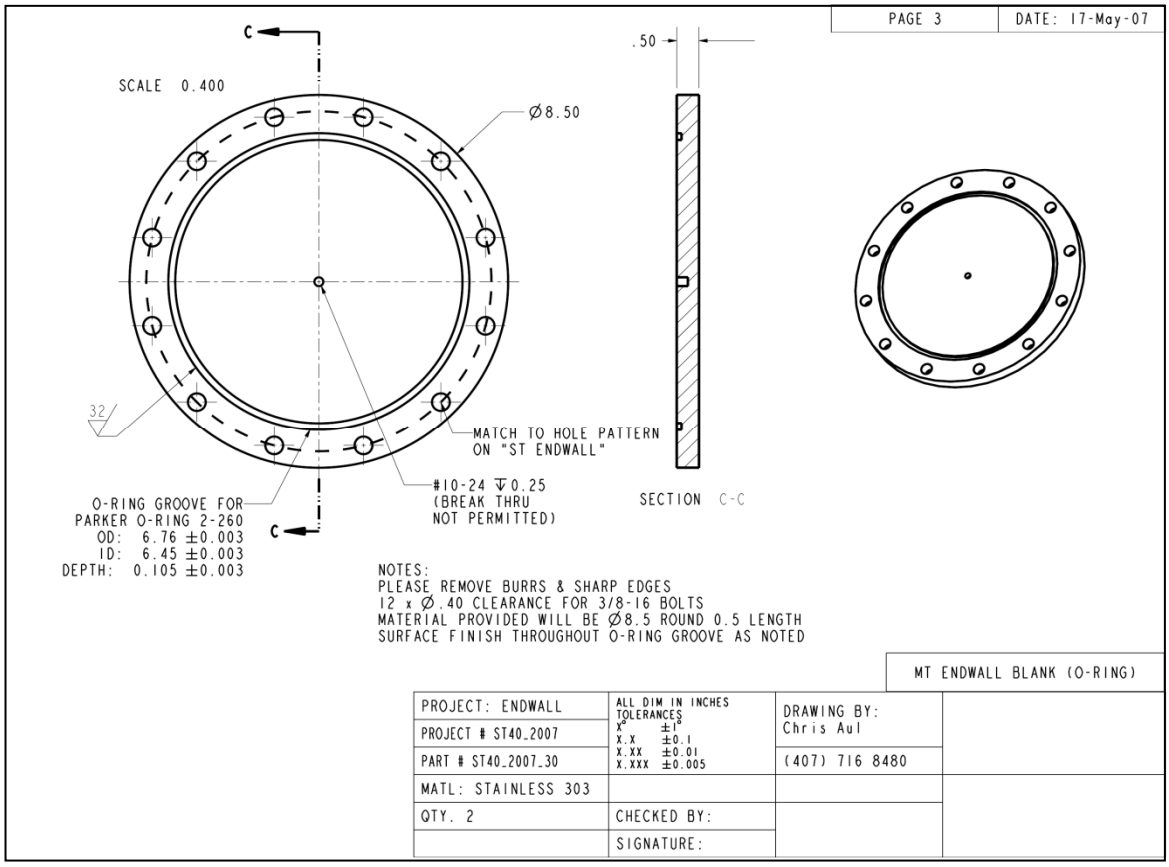

Figure A17. Endwall for mixing tank to stand opposite piece described in Figure A16

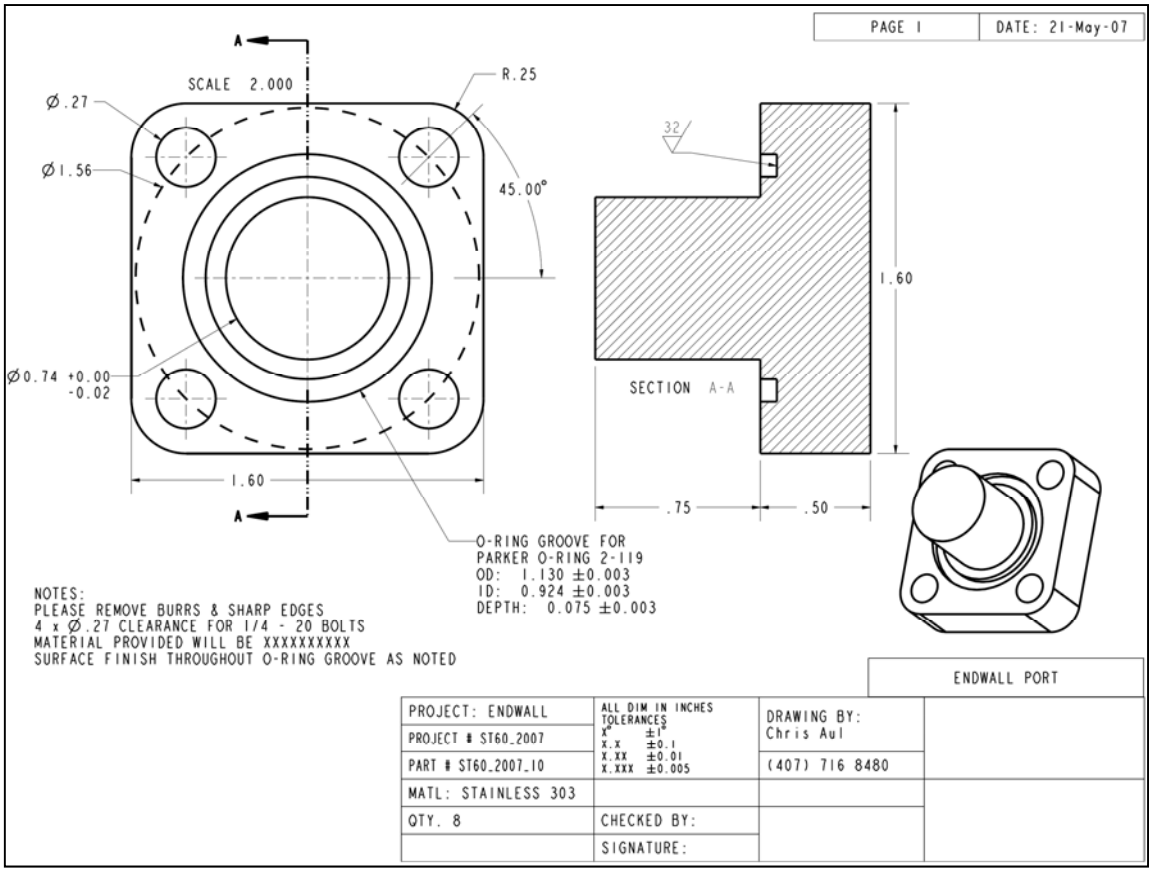

Figure A18. Endwall port designed to fit with part outlined in Figure A15. Allows for removable access of various sensing equipment at the endwall of the shock tube

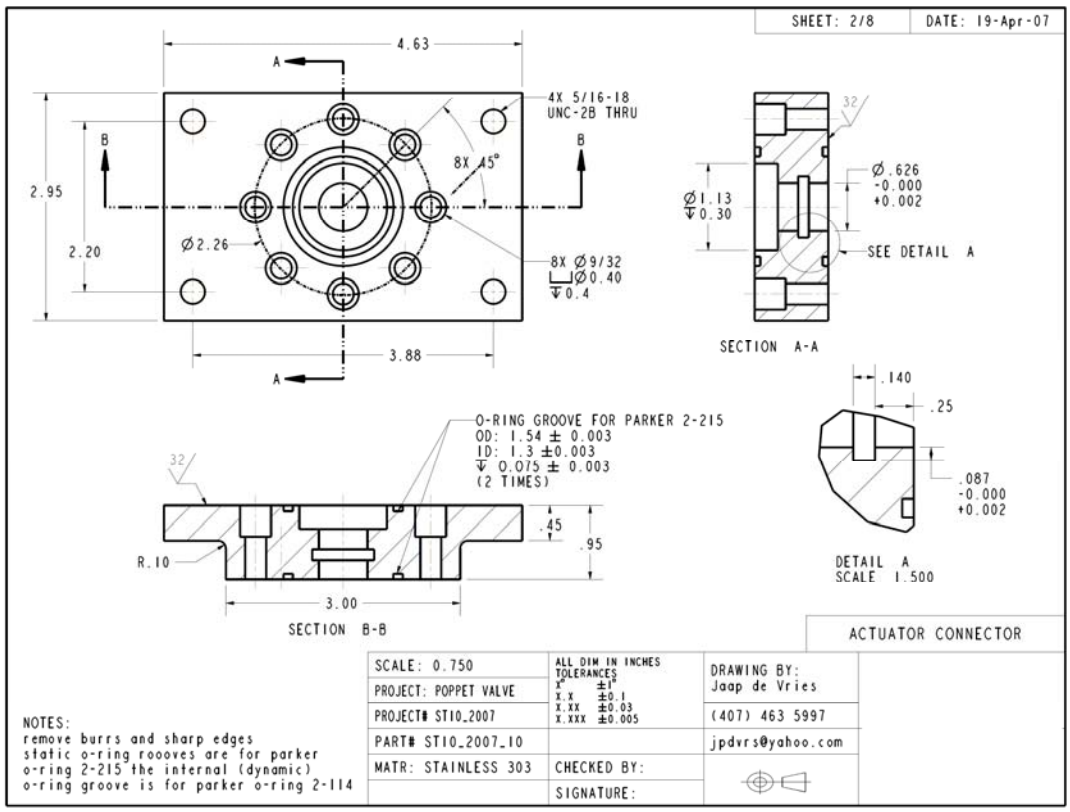

Figure A19. Interface part designed for placement between pneumatic piston actuator and the vacuum manifold. Actuator shaft, shown in Figure A23, extends through center through hole to poppet piston detailed in Figure A22

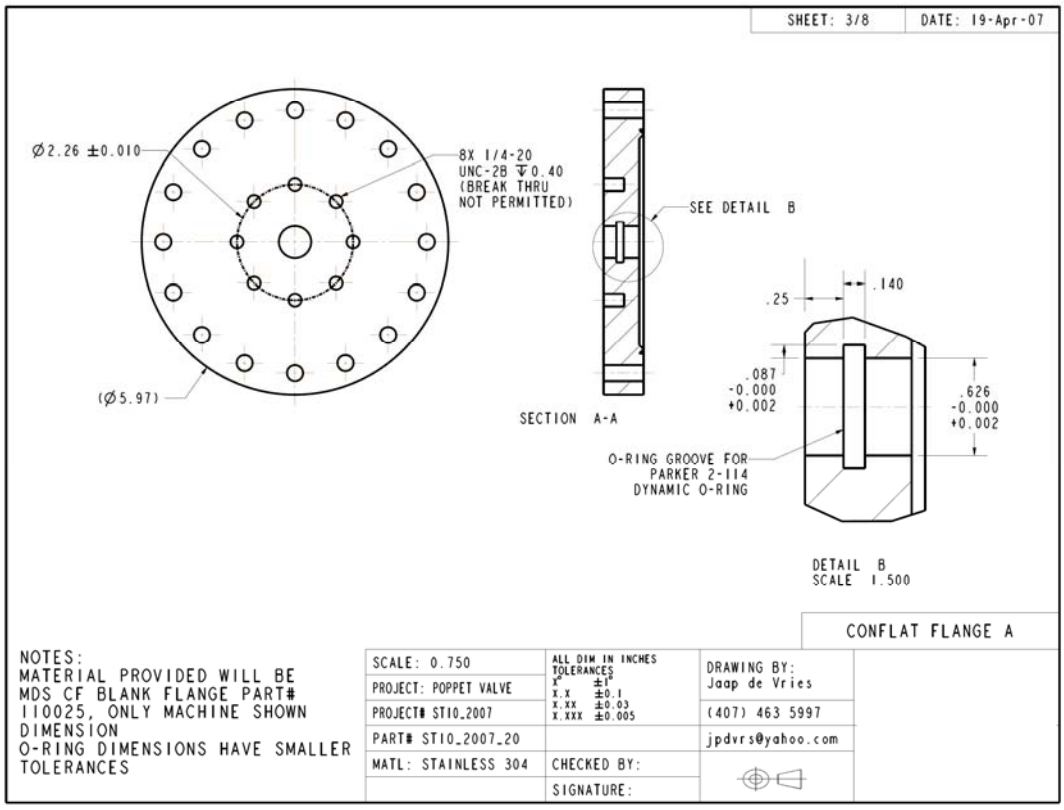

Figure A20. Conflat interface flange designed to accept actuator connector in Figure A19 and bolt directly onto main vacuum manifold

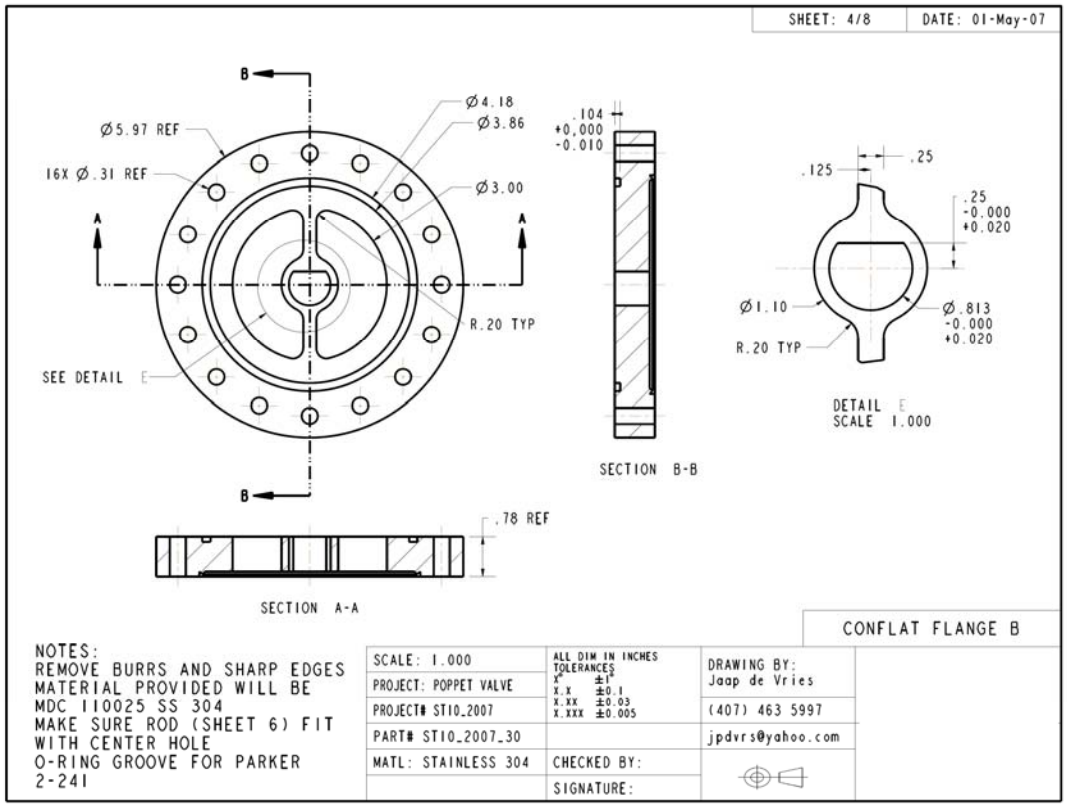

Figure A21. Conflat flange with alignment hole for accurate movement of the actuating rod without rotation. Designed to fit onto shock tube driven branch section detailed in Figure A4

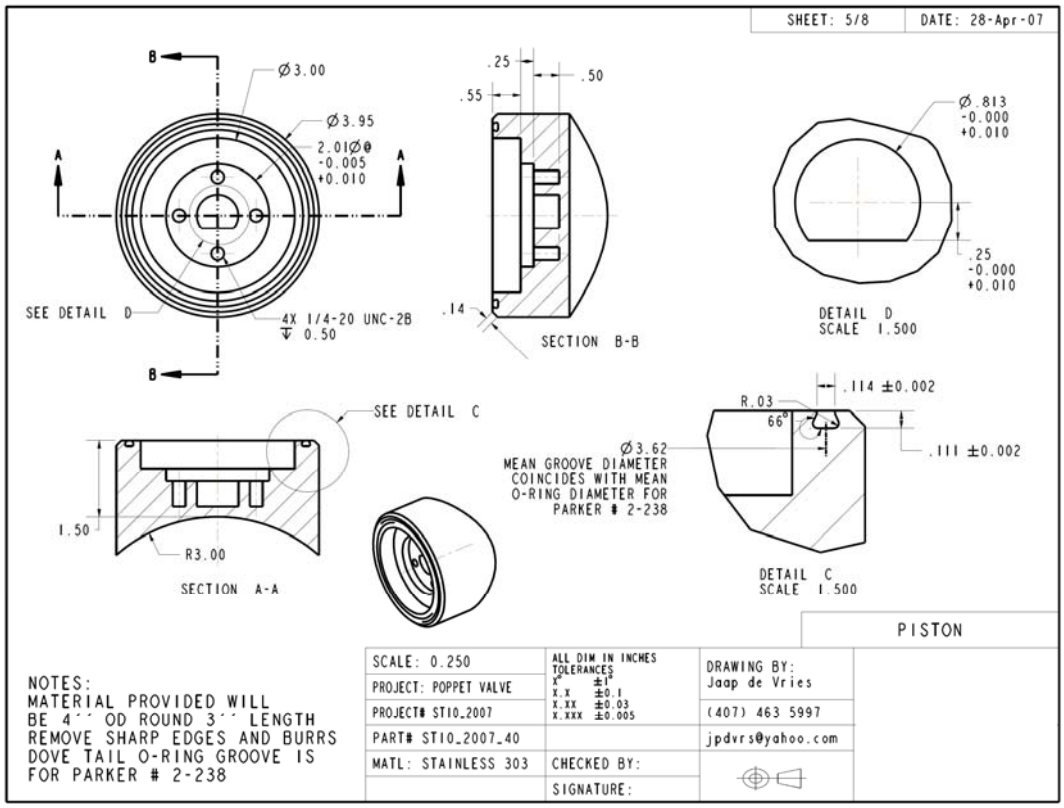

Figure A22. Piston head with matching radius to that found in the driven section of the shock-tube. Actuating rod in Figure A23 fits into this piece and is secured by two overlapping connectors outlined in Figures A24 and A25. Dove tail groove along the outside of the piston is beveled to restrict movement or eventual dislodgement of the noted O-ring

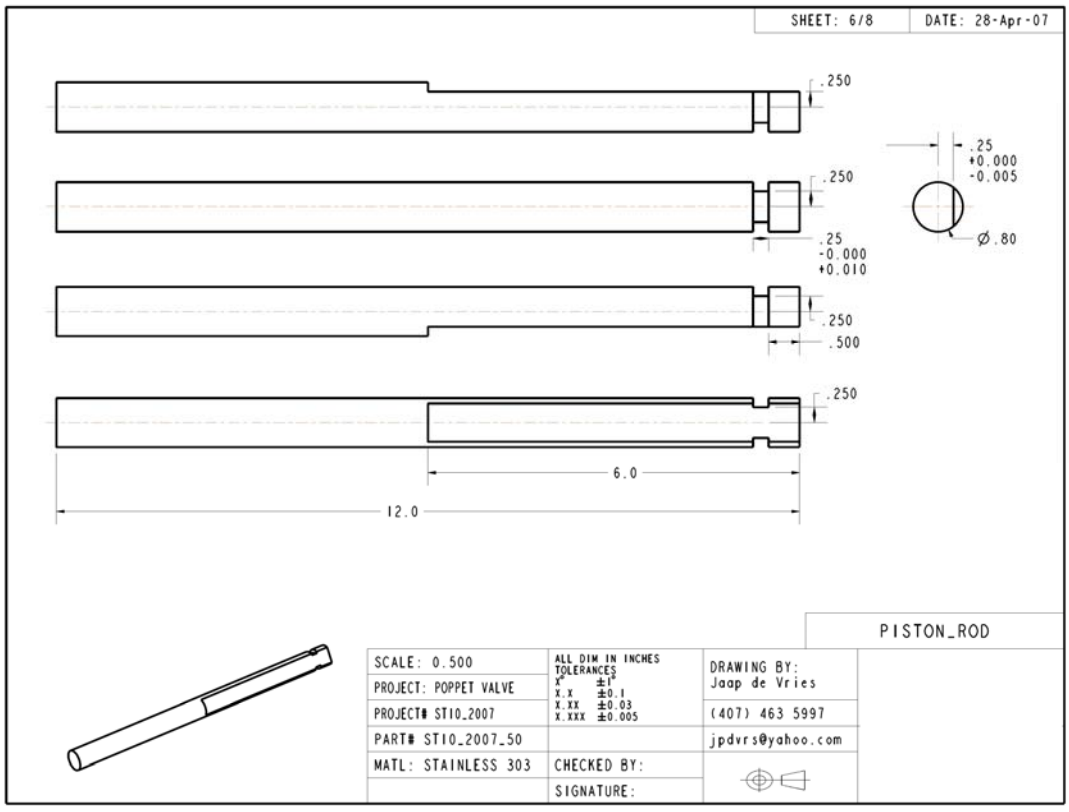

Figure A23. Piston rod to extend down through vacuum manifold and actuate piston shown in Figure A22 for gas handling access into the shock tube between experiments

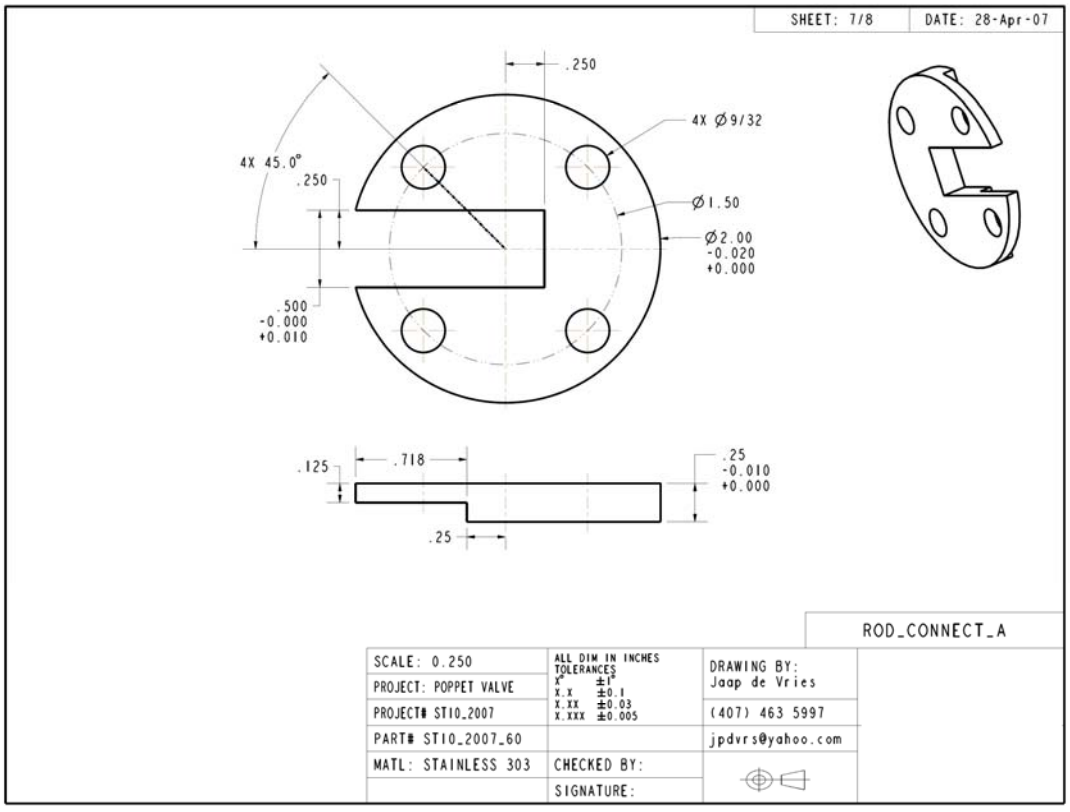

Figure A24. Simple connecting piece meant to adjoin actuating rod (Figure A23) into piston head (Figure A22). Matches bolt pattern with opposite connector part in Figure A25

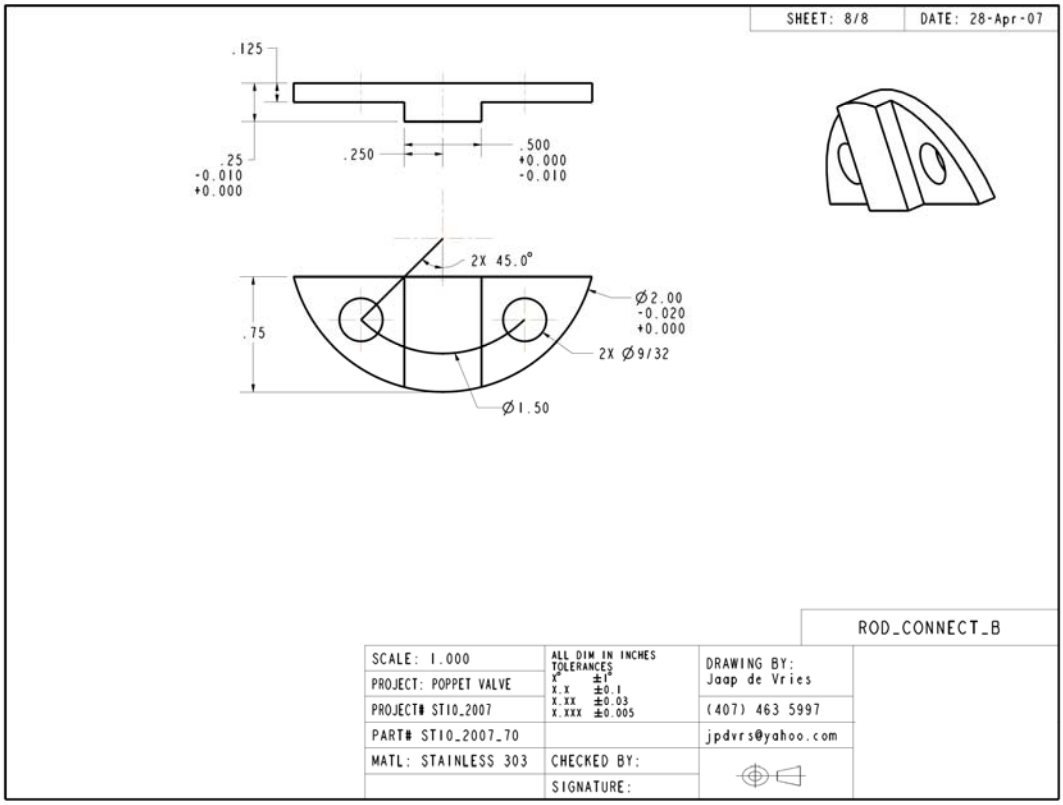

Figure A25. Opposite connecting piece fitting for part described in Figure A24

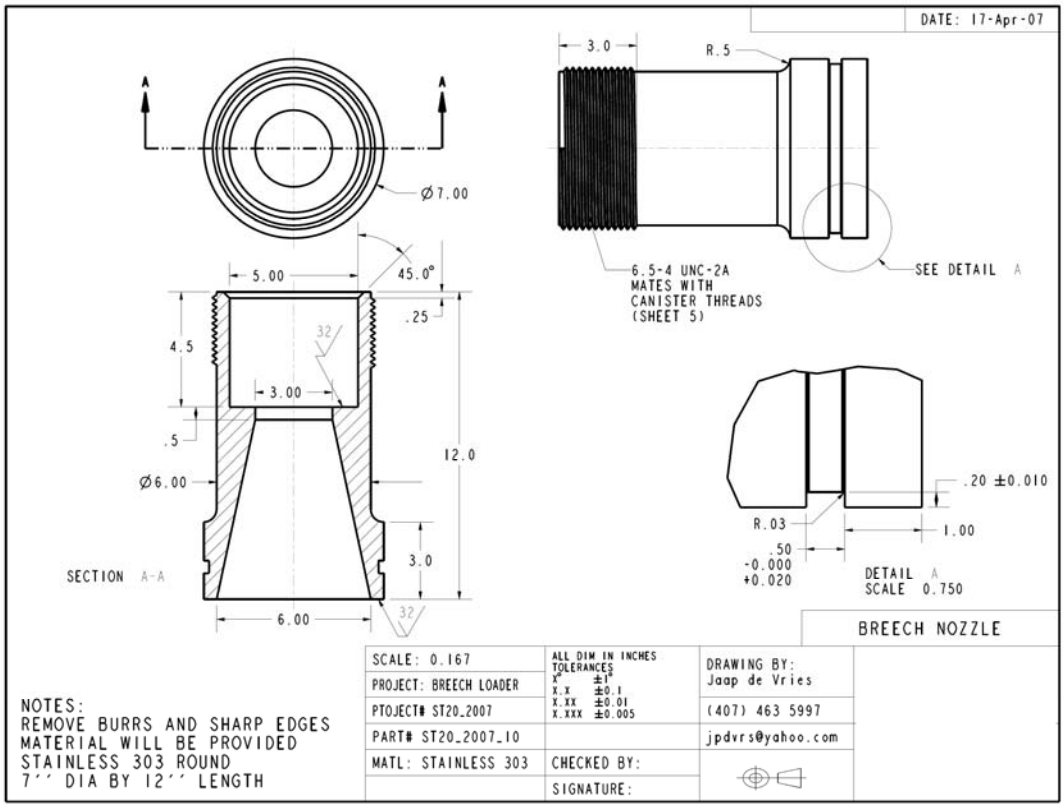

Figure A26. Breech nozzle that interfaces the driver section with the driven section of the shock tube. The large volume opposite the nozzle portion of this part houses the breech loading assembly that delivers the diaphragm per each experiment. The nozzle geometry is designed to allow for the area change between the outlet of the driver tube and the interior profile of the driven section

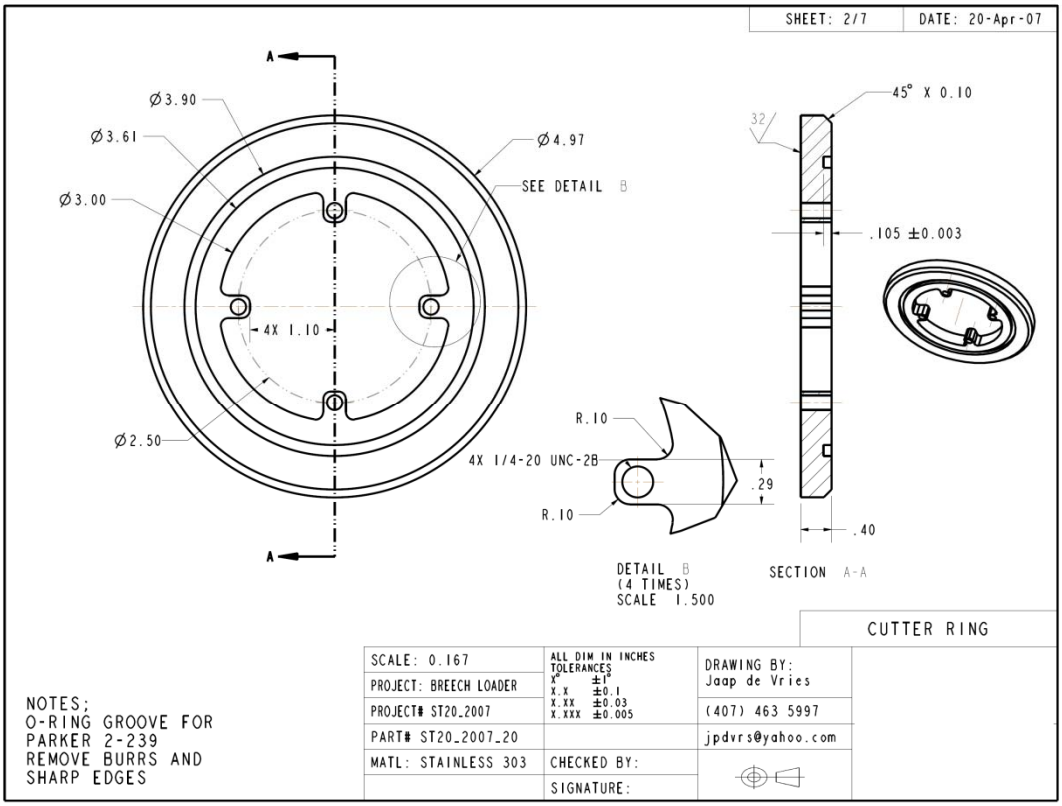

Figure A27. This part is placed in the housing described in Figure A26 and has an extruded bolt pattern designed to hold a blade which ruptures polycarbonate, or any other type of appropriate plastic, diaphragms at specific pressures with high repeatability. O-ring grooves for this and the following parts are aligned in a specific manner to allow for proper sealing

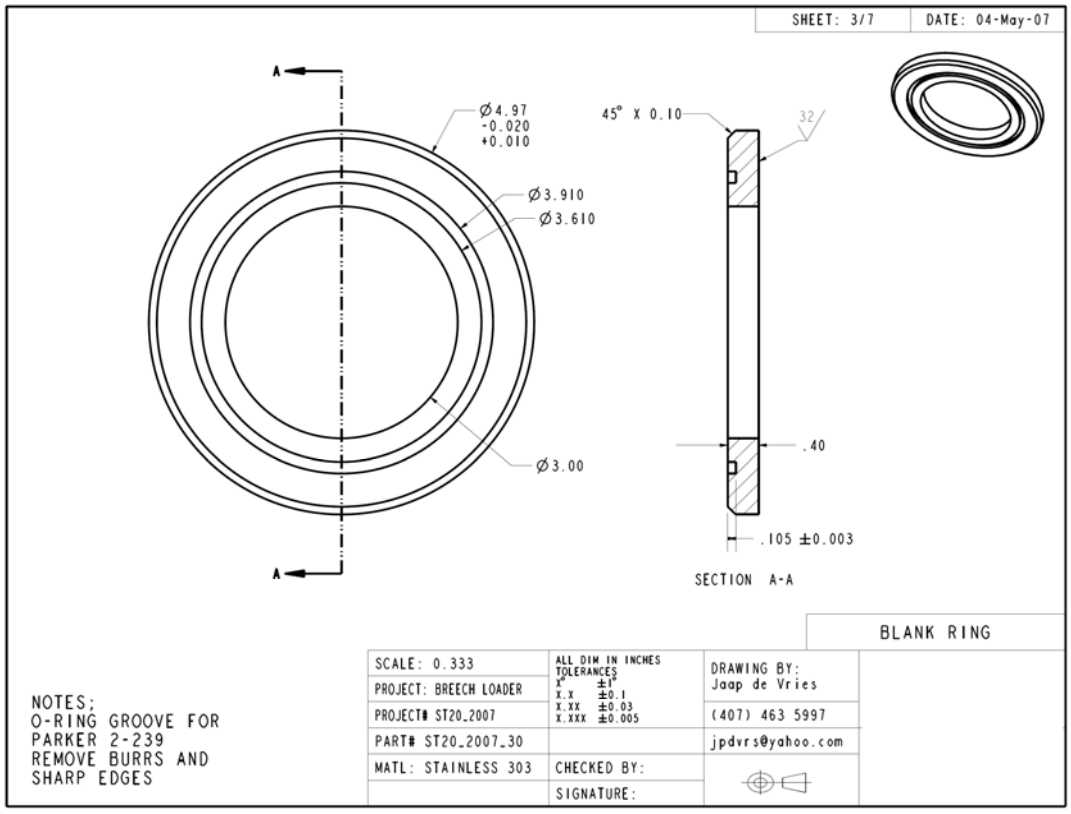

Figure A28. For higher pressures behind the reflected shock it is necessary to use larger or more robust diaphragm materials. For the use of pre-scored aluminum diaphragms the part described in Figure A29 is replaced with a spacing piece as described above

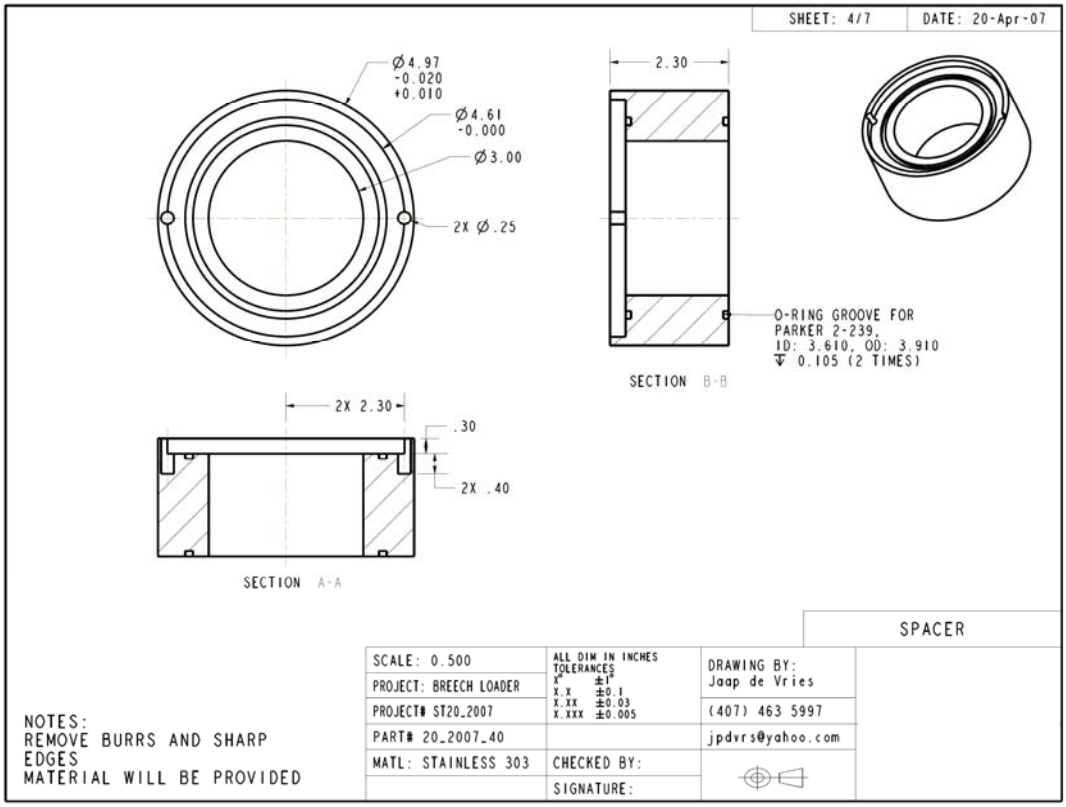

Figure A29. Large end of the breech loader housing meant to fit into part described in Figure A26. This piece interfaces directly with part shown in Figure A30 to hold a wide assortment of diaphragms

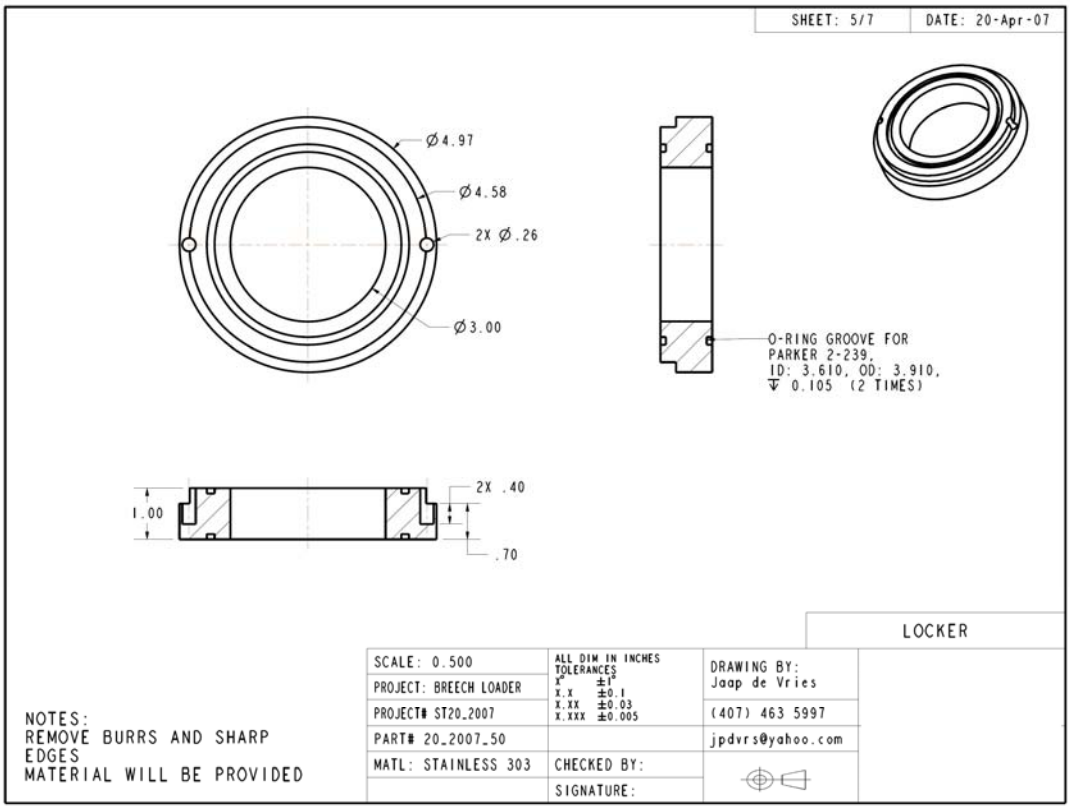

Figure A30. Part fitting opposite that of what is shown in Figure A29. Locks into place with pins that fit in 0.26” diameter holes on both ends of this piece

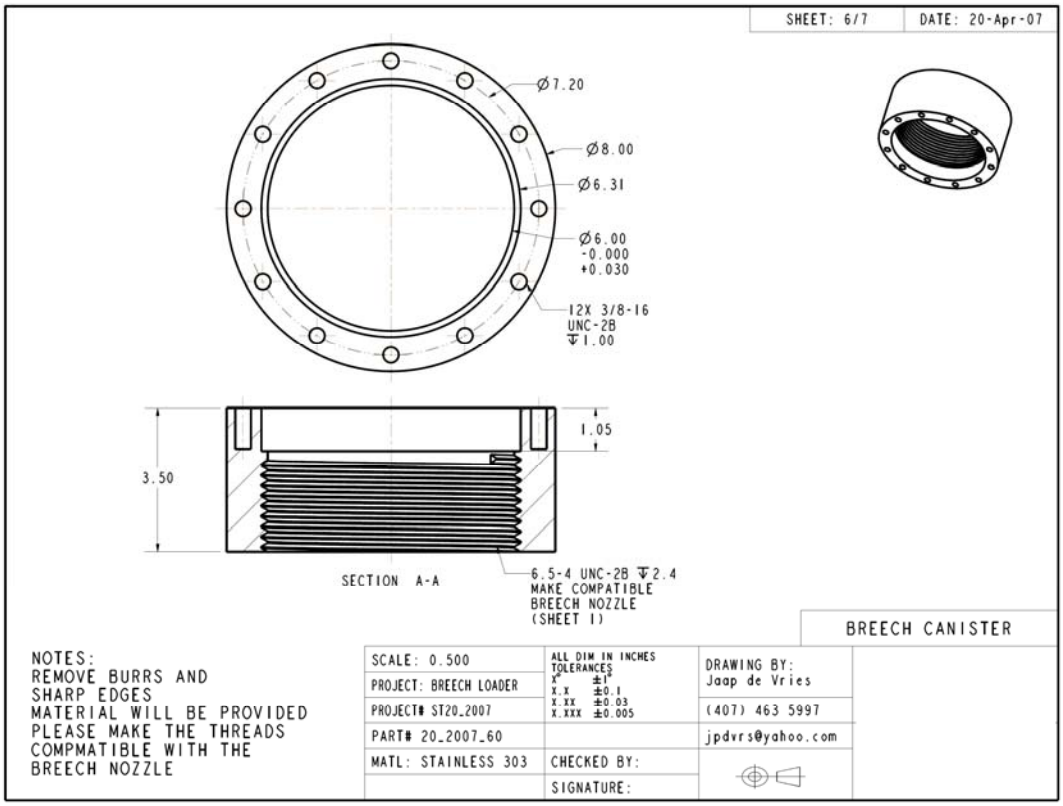

Figure A31. Piece that is meant to accept threading on part in Figure A26 and secure the entire diaphragm section together. This particular part is also fitted with large handle rods which allow for quick replacement of the diaphragm

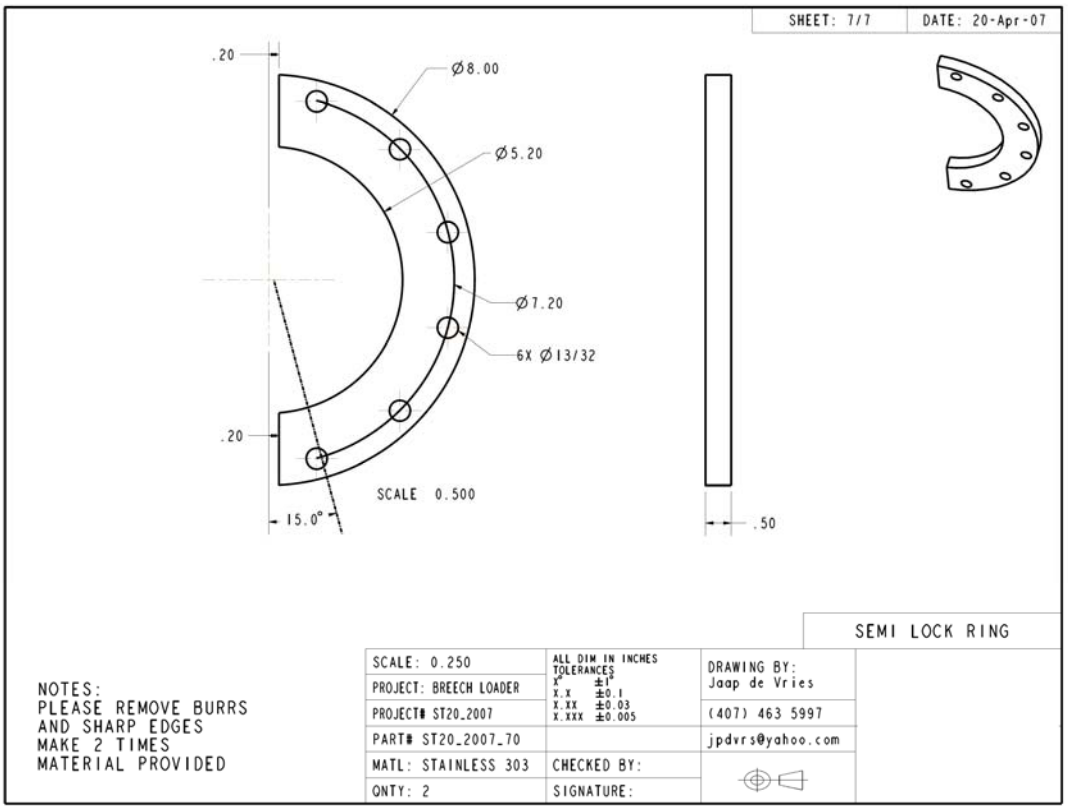

Figure A32. Ring, quantity of 2, that fits directly to the hole pattern on part detailed in Figure A31. This part encases the end of the driver tube and makes the compression style seal of the diaphragm breech loader

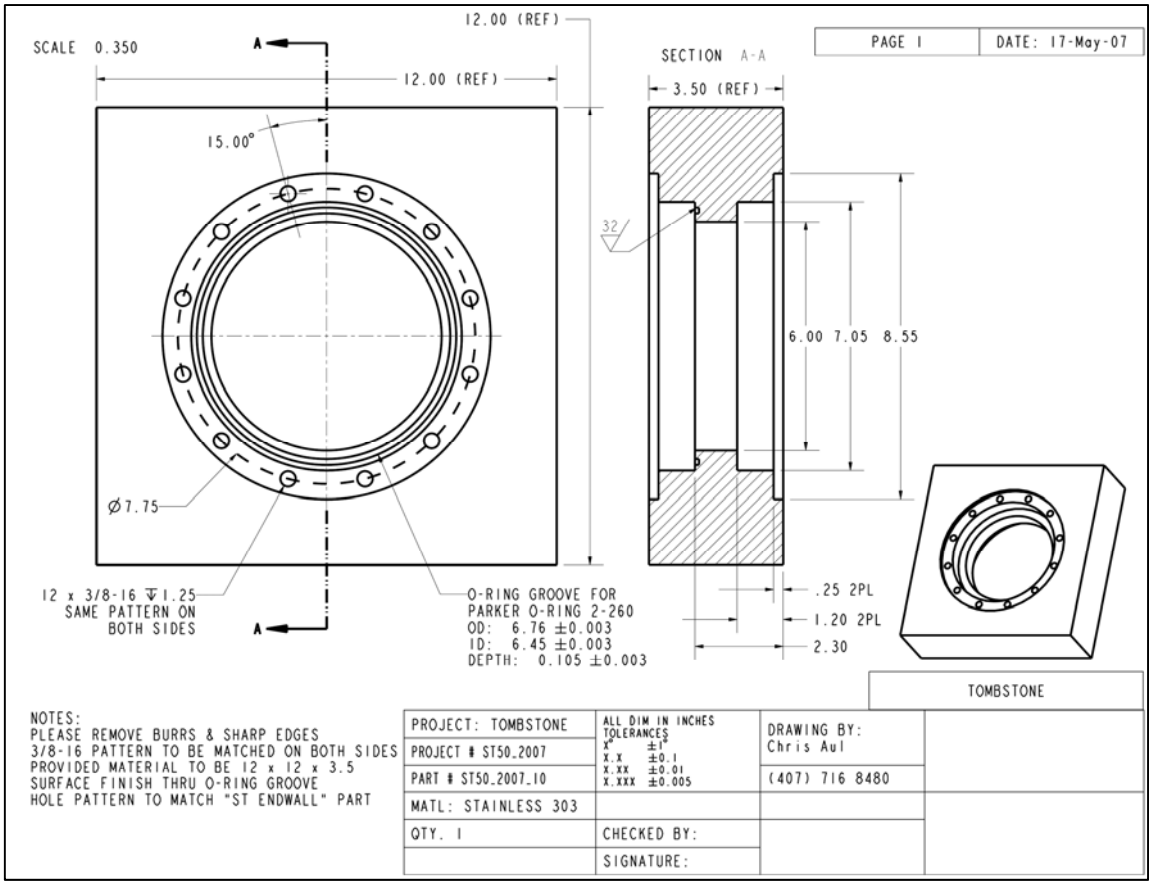

Figure A33. Interface part that fits in between breech loader shown in Figure A26 and the driven section of the shock tube. This part is what accepts the axial force resulting from each shock and is attached directly to the inertial mass

VITA

Name:	Christopher Joseph Erik Aul
Address:	Department of Mechanical Engineering
	Texas A&M University
	3123 TAMU
	College Station, TX 77843-3123
Email Address:	caul@tamu.edu
Education:	B.S., Mechanical Engineering, University of Central Florida, 2006
	M.S., Mechanical Engineering, Texas A&M University, 2009